

THE UNIVERSITY OF MANITOBA

INFILTRATION, HEAT TRANSFER, AND PHASE CHANGE

IN SNOW AND OTHER POROUS MEDIA

by

T. MURRAY WILSON

A THESIS

SUBMITTED TO THE FACULTY OF GRADUATE STUDIES
IN PARTIAL FULFILLMENT OF THE REQUIREMENTS FOR THE DEGREE
OF MASTER OF SCIENCE

DEPARTMENT OF CIVIL ENGINEERING

WINNIPEG, MANITOBA

APRIL, 1975

INFILTRATION, HEAT TRANSFER, AND PHASE CHANGE
IN SNOW AND OTHER POROUS MEDIA

by

T. MURRAY WILSON

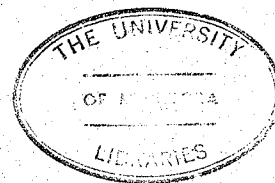
A dissertation submitted to the Faculty of Graduate Studies of
the University of Manitoba in partial fulfillment of the requirements
of the degree of

MASTER OF SCIENCE

© 1975

Permission has been granted to the LIBRARY OF THE UNIVERSITY OF MANITOBA to lend or sell copies of this dissertation, to the NATIONAL LIBRARY OF CANADA to microfilm this dissertation and to lend or sell copies of the film, and UNIVERSITY MICROFILMS to publish an abstract of this dissertation.

The author reserves other publication rights, and neither the dissertation nor extensive extracts from it may be printed or otherwise reproduced without the author's written permission.



ABSTRACT

This study is an investigation of ice-capping; the infiltration and freezing of water, applied to an artificially compacted snow road surface. Infiltration theory is reviewed; the treatment of snow as a porous medium is summarized and further analyzed. The overall process is empirically studied, linear least-squares regression analysis identifies the controlling parameters for one-dimensional infiltration. Two zones of infiltration are observed; a zone of uniform penetration is normally well defined by a freezing front. This zone may be desaturated by a second zone of further penetrating discrete channels. High speed measurement of thermocouple strings during infiltration tests illustrate freezing at the wetting front, the results indicate heat transfer is convection dominated. Scintillation measurements of the ice-capped zone after re-freezing suggest that residual air saturation is quite low for the imbibition cycle. Drainage of the ice-capped zone is also identified by the scintillation measurements. One-dimensional finite-difference simulation of the infiltration process indicates that permeability of the snow is critical to the rate of infiltration, but the shape of the infiltration profile is not changed significantly by changes in the flow properties. The infiltration simulation further illustrates the rate of freezing of the penetrating water. One-dimensional finite-difference simulation of the ice-cap re-freezing gives approximate times required for complete phase change.

ACKNOWLEDGEMENTS

The author wishes to gratefully acknowledge his advisor, Dr. K.M. Adam for his advice and guidance during the author's graduate program.

The prompt and valuable assistance of Dr. G.E. Laliberte, Head, Department of Agricultural Engineering, and Dr. A.H. Shah, Associate Professor, Department of Civil Engineering, members of the graduate committee, is sincerely appreciated.

Introduction to, and assistance with the Hewlett Packard Data Acquisition System, by Dr. K.R. McLachlan, Associate Professor, Department of Civil Engineering, is gratefully noted.

Special thanks are extended to Janet Gourlay and Diane Walton for their patience and excellent typing.

Without the support and encouragement of the author's wife, Deb, this endeavour would not have been successful.

Financial assistance for the project was provided by Canadian Arctic Gas Study Limited and the National Research Council of Canada.

TABLE OF CONTENTS

<u>Chapter</u>		<u>Page</u>
	ABSTRACT	i.
	ACKNOWLEDGEMENTS	ii.
	TABLE OF CONTENTS	iii.
	LIST OF TABLES	vii.
	LIST OF FIGURES	viii.
	LIST OF SYMBOLS	xi.
I	INTRODUCTION	1.
II	THEORY AND BACKGROUND	3.
	INFILTRATION	3.
	General Equations of Flow	4.
	Approaches for Solution of Infiltration	
	Problems	7.
	Hysteresis	11.
	Conceptual Differences of Infiltration	
	Models	13.
	WATER FLOW THROUGH SNOW	17.
	Flow of Water Through Wet Isothermal Snow	17.
	Flow of Water in Snow Below 0°C	22.
	SNOW AS A POROUS MEDIUM	24.
	Capillary Pressure - Saturation Relationships	24.
	Pore-size Distribution Index	25.
	Bubbling Pressure	26.
	Saturation - Relative Permeability Relationships	26.
	Permeability - Porosity Relationships	28.

<u>Chapter</u>		<u>Page</u>
	HEAT TRANSFER	30.
	THERMAL PROPERTIES OF SNOW	33.
III	EXPERIMENTAL TECHNIQUES	36.
	Infiltration into Sand	36.
	Infiltration into Compacted Snow	37.
	Continuous Temperature Measurement Tests	38.
	Scintillation Tests	39.
	Re-Freezing Test	40.
	Simulations	40.
IV	RESULTS AND DISCUSSION	41.
	INFILTRATION INTO SAND	41.
	Linear Regression Models for Sand Infiltration	43.
	Summary of Infiltration into Sand	44.
	INFILTRATION INTO SNOW	45.
	Linear Regression Models for Snow Infiltration	48.
	Models MSN 1 to MSN 9	49.
	Models MSN 10 to MSN 15	50.
	Models MTS 1 to MTS 11	51.
	Penetration of Water	52.
	Two-Phase Infiltration into Snow	52.
	Delayed Water Application	53.
	Ice-Capped Densities	54.
	Results with Implanted Thermocouples	55.
	SIMULATION OF INFILTRATION	58.
	Infiltration Without Phase Change	59.

<u>Chapter</u>	<u>Page</u>
Pseudo Freezing	62.
Summary of Infiltration Simulation	64.
OVERVIEW OF INFILTRATION INTO SNOW	65.
Validity of One-Phase Approach	65.
Channeling/Fingering	65.
Laminar Flow	67.
Significance of Snow Permeability	68.
Effect of Age Hardening of Snow	69.
THERMAL EFFECTS	70.
Freezing of Water	70.
Pore Changes	70.
Evaporation	70.
Heat Loss in the Radial Direction	71.
Freezing at the Front	72.
RE-FREEZING TEST AND SIMULATION	74.
PRACTICAL IMPLICATIONS	76.
V CONCLUSIONS AND RECOMMENDATIONS	79.
BIBLIOGRAPHY	82.
APPENDIX A	89.
EXPERIMENTAL DATA AND PHOTOGRAPHS OF INFILTRATION TESTS	
APPENDIX B	106.
EXPERIMENTAL RESULTS FROM SCINTILLATION AND THERMOCOUPLE MEASUREMENTS	
APPENDIX C	129.
ANALYSIS OF INFILTRATION DATA	

ChapterPage

APPENDIX D

FINITE-DIFFERENCE MODELS

138.

APPENDIX E

INFILTRATION SIMULATION

145.

APPENDIX F

ICE-CAP RE-FREEZING

155.

LIST OF TABLES

<u>Table</u>		<u>Page</u>
A-1	Selkirk Silica Sand (35-50) Tests:	
	Water Temperature 0°C	90.
A-2	Selkirk Silica Sand (35-50) Tests	92.
A-3	Selkirk Silica Sand Tests: Water	
	Temperature 0°C, 1 Phase Flow	93.
A-4	Snow Tests	94.
A-5	Snow Tests with Temperature Measurement	98.
B-1	Scintillation Results	107.
B-2	Front Penetration Summary	109.
C-1	Empirically Fitted Linear Models	130.
C-2	Model Fitting Results for Sand	133.
C-3	Model Fitting Results for Snow Tests	134.
C-4	Model Fitting Results for Snow Tests with $(\rho_s T_s)$ as a Variable	135.
C-5	Model Fitting Results for Snow Tests with Temperature Measurement	136.
E-1	Summary of Infiltration Simulation	146.
E-2	Simulation of Infiltration with Phase Change	147.
F-1	Re-Freezing Simulation Tests	157.

LIST OF FIGURES

<u>Figure</u>		<u>Page</u>
A-1	Photographs of Sand Infiltration Tests	100.
A-2	Photographs of Snow Infiltration Tests	101.
A-3	Photographs of Snow Infiltration Tests	102.
A-4	Photographs of Snow Infiltration Tests	103.
A-5	Photographs of Snow Infiltration Tests	104.
A-6	Photographs of Snow Infiltration Tests	105.
B-1	Temperature Measurements During Water Infiltration into Snow (Test TS 1)	111.
B-2	Temperature Measurements During Water Infiltration into Snow (Test TS 2)	112.
B-3	Temperature Measurements During Water Infiltration into Snow (Test TS 3)	113.
B-4	Temperature Measurements During Water Infiltration into Snow (Test TS 4)	114.
B-5	Temperature Measurements During Water Infiltration into Snow (Test TS 5)	115.
B-6	Temperature Measurements During Water Infiltration into Snow (Test TS 6)	116.
B-7	Temperature Measurements During Water Infiltration into Snow (Test TS 7)	117.
B-8	Temperature Measurements During Water Infiltration into Snow (Test TS 8)	118.
B-9	Temperature Measurements During Water Infiltration into Snow (Test TS 9)	119.

<u>Figure</u>		<u>Page</u>
B-10	Temperature Measurements During Water Infiltration into Snow (Test TS 10)	120.
B-11	Temperature Measurements During Water Infiltration into Snow (Test TS 11)	121.
B-12	Temperature Measurements During Water Infiltration into Snow (Test TS 12)	122.
B-13	Temperature Measurements During Water Infiltration into Snow (Test TS 13)	123.
B-14	Temperature Measurements During Water Infiltration into Snow (Test TS 14)	124.
B-15	Temperature Measurements During Water Infiltration into Snow (Test TS 15)	125.
B-16	Temperature Measurements During Water Infiltration into Snow (Test TS 16)	126.
B-17	Temperature Measurements During Water Infiltration into Snow (Test TS 17)	127.
B-18	Temperature Measurements During Water Infiltration into Snow (Test TS 18)	128.
C-1	Incidents of Full Penetration	137.
E-1	Infiltration with Drainage and Imbibition Capillary Pressure Curves	148.
E-2	Capillary Pressure - Water Saturation Curve	149.
E-3	Water Saturation Profiles	150.
E-4	Water Saturation Profiles	151.
E-5	Water Saturation Profiles	152.
E-6	Water Saturation Profiles	153.

Figure

Page

E-7	Water Saturation Profiles	154.
F-1	Re-Freezing Temperatures: Test and Simulation	156.

LIST OF SYMBOLS

<u>Symbol</u>		<u>Dimensions</u> [†]
a	Subscript indicating "air"	none
a	Subscript indicating "apparent"	none
a	Constant in equation for effective thermal conductivity	
a	Constant in equation for hydraulic conductivity	
A	Empirical constant for infiltration equations	
A	Surface area for heat transfer	L^2
b	Subscript indicating "bubbling"	none
b	Constant in equation for effective thermal conductivity	
B	Empirical constant for infiltration equation	
c	Subscript indicating "capillary"	none
C	Hydraulic conductivity	L/τ
C	Specific heat capacity	H/MT
C	Volumetric heat capacity	H/L^3T
C	Correction factor for thermal conductivity	none
d	Grain diameter	L
\bar{d}	Average grain diameter	L
D	Diffusivity; $C(\partial h/\partial \theta)$	L^2/τ
D	Depth of penetration	L
e	Subscript indicating "effective"	none
f	Subscript indicating "wetting front"	none
f_p''	Liquid water holding capacity	none

<u>Symbol</u>		<u>Dimensions</u> ⁺
FP	Depth of uniform front penetration	L
g	Gravitational acceleration	L^2/τ
gr	Grain sieve size	none
grav	Subscript indicating "gravity"	none
Gr_L	Grashof number; $\beta g \rho^2 L^3 \Delta T / \mu^2$	none
h	Pressure head in height of liquid	L
h	Convective heat transfer coefficient	$H/LT\tau$
H	Pressure head in height of liquid	L
i	Subscript indicating "lower bound"	none
i	Subscript indicating "saturated"	none
i	Subscript indicating "ice"	none
i	Subscript indicating finite-difference "spatial interval"	none
i_r	Rain intensity	L/τ
I	Infiltration rate	L/τ
IT	Infiltration time	τ
j	Superscript indicating finite-difference "temporal interval"	none
k	Permeability	L^2
k	Thermal conductivity	$H/LT\tau$
k	$\partial\theta/\partial h$	$1/L$
l	Subscript indicating "liquid"	none
L	Latent heat of fusion	H/M
L	Characteristic heat transfer length	L
max	Superscript indicating "upper bound"	none
m	Melt intensity	L/τ

<u>Symbol</u>		<u>Dimensions</u> [†]
MP	Maximum liquid penetration	L
n	Exponent in relative permeability equation	none
N	Constant in equation for hydraulic conductivity	
o	Subscript indicating "original"	none
o	Subscript indicating "saturated"	none
o	Subscript indicating "saturated permeability"	none
p	Subscript indicating "constant pressure"	none
p	Pressure	F/L^2
Pr	Prandtl number; $\mu C_p/k$	none
q	Heat flux	H/τ
q	Volumetric flow	L^3/τ
qi	Volumetric flow into finite-difference interval	L^3/τ
qo	Volumetric flow out of finite-difference interval	L^3/τ
r	Subscript indicating "residual"	none
r	Subscript indicating "relative permeability"	none
Re	Reynolds number; $\bar{u}d/\nu$	none
s	Subscript indicating "snow"	none
s	Specific surface	L^2/L^3
sa	Subscript indicating "sand"	none
S	Sorptivity	$L/\tau^{1/2}$
S	Saturation	none
t	Time	t
t	Age hardening time	t
T	Temperature	T
\bar{u}	Bulk flow	$L^3/L^2/\tau$

<u>Symbol</u>		<u>Dimensions</u> [†]
v	Fluid flux	L/τ
\bar{v}	Average velocity	L/τ
w	Subscript indicating "water"	none
W	Applied water	L ³ /L ²
x	Spatial co-ordinate	L
z	Spatial co-ordinate	L
α	Thermal diffusivity; $k/\rho C_p$	L ² /τ
β	Coefficient of thermal expansion	T ⁻¹
Δ	Denotes a difference	none
θ	Volumetric water contents	none
λ	Pore-size distribution index; $-d(\log S^*)/d(\log p_c)$	none
μ	Dynamic viscosity	M/Lτ
ν	Kinematic viscosity	L ² /τ
ρ	Mass density	M/L ³
∑	Summation	none
τ	Dimensionless time	none
φ	Porosity	none
∇	Gradient operator	L ⁻¹
*	Superscript indicating "effective saturation"	none
1	Subscript indicating "thawed thermal conductivity"	none
2	Subscript indicating "frozen thermal conductivity"	none

† Fundamental dimensions chosen:

force	- F
heat	- H
length	- L
mass	- M
temperature	- T
time	- τ

CHAPTER I

INTRODUCTION

Resource development in arctic and sub-arctic regions of Canada, in recent years, has resulted in a series of new engineering and multi-disciplinary problems.

A study by Adam [1] indicates the importance of ice and compacted snow roads for transportation purposes in remote northern regions during the winter season. The main thrust of the study was towards defining a winter road capable of withstanding the high intensity of traffic along a proposed pipeline route during the construction phase. The implications associated with such a study are very far ranging, and reach from the logistics of materials transport to environmental protection. It was concluded that an ice-capped snow road will have the most important advantages of both a snow road and an ice road. The ice-capped snow road is a processed and compacted snowbed which has water applied to the surface to increase its density and strengthen the road. The results of tests performed by Adam indicate the final densities of the ice-cap should be in the range of 0.85 g/cm^3 ; pure ice has a density of 0.917 g/cm^3 .

This study is a response to the general lack of conceptual and predictive information available for the ice-capping process. The objectives of this study include: the identification of general relationships and controlling parameters of the process, the development of guidelines for practical use in the ice-capping of snow roads, and to further the understanding of the mechanisms of water flow in snow.

Penetration of water into snow below 0°C is governed by the linked effects of fluid flow, heat transfer and phase change. Most investigations of water flow in snow have related to hydrological studies, in particular spring snowmelt, and consider the snow to be isothermal at 0°C .

Colbeck [7 - 13] has performed a comprehensive series of physically based studies of water flow in snow that were instrumental to this investigation. This series of studies deals with a Darcian approach to water flow in snow during snowmelt situations.

A dual approach to the ice-capping problem is used in this study. A empirically based investigation to identify overall trends is supplemented and complemented by a physically based analysis to yield a more mechanistic understanding of the complex process. The water movement is treated as one-dimensional infiltration into a porous medium with associated one-dimensional heat transfer. Although the major part of the study considers the flow to be one-phase in nature, two-phase flow effects are considered.

Infiltration tests for this research were conducted with compacted snow samples and Selkirk Silica Sand. A high speed data gathering system and a scintillation scaler were used to investigate details of the coupled fluid flow and heat transfer processes. Physically based numerical simulation models were developed to study the infiltration and re-freezing of the ice-capped zone.

Results of this research are discussed in both practical and more conceptual manners.

CHAPTER II

THEORY AND BACKGROUND

In this chapter, the theoretical background relating to the penetration of water into a packed snowbed as well as the results of pertinent studies are summarized. The scope of this study limits itself to a one-dimensional treatment of the problem. Infiltration, water flow through snow, snow as a porous medium, heat transfer, and thermal properties of snow will be discussed.

INFILTRATION

The movement of water into a flooded, compacted snow surface may be likened to infiltration phenomena important to hydrologists and soil scientists.

"Infiltration is the entry into the soil of water made available at the ground surface, together with the associated downward flow."¹

In this section, infiltration will be considered as an isothermal process so as not to obscure the results obtained by previous studies.

Until the past six or seven years, infiltration has been treated as a one-phase problem. The assumption was made that the water influx and subsequent redistribution in the soil was unaffected by the dynamics of the air phase. Viscous forces of flowing air and pressure build-up in the air phase were considered negligible. Recently, more complete treatments of infiltration have included these considerations. Comparisons between the two approaches indicate when the more complete

¹ Freeze, A.R. Water Resources Research, Vol. 5, No. 1, 153-171, 1969, p. 153.

model is needed.

General Equations of Flow

One-phase flow of water in isotropic porous media is characterized by Darcy's equation.

$$\bar{u}_w = - \frac{k_{rw} k_{ow}}{\mu_w} \nabla(p_w - \rho_w gz) \quad (1)$$

where:

\bar{u}_w = bulk water flow, $\text{cm}^3/\text{cm}^2/\text{sec}$

k_{ow} = water permeability, cm^2

k_{rw} = relative permeability of water, a function
of water saturation, dimensionless

μ_w = water viscosity, $\text{g}/\text{cm}\text{-sec}$

p_w = water pressure, dynes/cm^2

ρ_w = water density, g/cm^3

g = gravitational constant, cm/sec^2

z = relative vertical position, positive downwards, cm .

The associated continuity equation for the unsaturated flow is:

$$\text{div}(\bar{u}_w \rho_w) = - \frac{\phi \partial (\rho_w S_w)}{\partial t} \quad (2)$$

where:

ϕ = porosity, dimensionless

S_w = water saturation (fraction of voids filled), dimensionless

t = time, sec .

If water is assumed to be incompressible ($\rho_w = \text{constant}$),
equations (1) and (2) combine to give

$$\text{div} \left[\frac{k_{rw} k_{ow}}{\mu_w} \nabla (p_w - \rho_w g z) \right] = \phi \frac{\partial S_w}{\partial t} \quad (3)$$

Capillary pressure for the air-water system is defined as the pressure difference across the interface of the two immiscible fluids.

$$p_c = p_a - p_w \quad (4)$$

where:

p_c = capillary pressure, dynes/cm²

p_a = air phase pressure, dynes/cm².

Thus

$$p_w = p_a - p_c \quad (5)$$

Substituting equation (5) into equation (3) and considering one-dimensional vertical flow:

$$\frac{\partial S_w}{\partial t} = \frac{1}{\phi \mu_w} \frac{\partial}{\partial z} \left[k_{rw} k_{ow} \frac{\partial}{\partial z} (p_a - p_c - \rho_w g z) \right] \quad (6)$$

The air phase will be assumed to have a constant pressure throughout the system ($\partial p_a / \partial z = 0$). Therefore

$$\frac{\partial S_w}{\partial t} = - \frac{1}{\phi \mu_w} \frac{\partial}{\partial z} \left[k_{rw} k_{ow} \left(\frac{\partial p_c}{\partial z} \right) + \rho_w g \right] \quad (7)$$

The more common form of the vertical, one-dimensional Richards equation is given by McWhorter [35].

$$\frac{\partial \theta}{\partial t} = \frac{\partial}{\partial z} \left(C(h) \left(\frac{\partial h}{\partial z} - 1 \right) \right) \quad (8)$$

where:

h = pressure head, cm of water

$$C(h) = \frac{\rho_w g k_{rw} k_{ro}}{\mu_w}, \text{ hydraulic conductivity, cm/sec}$$

θ = volumetric water content, dimensionless.

If the two-phase approach to infiltration is pursued, equation (7) is rewritten as

$$\frac{\partial S_w}{\partial t} = - \frac{1}{\phi \mu_w} \frac{\partial}{\partial z} [k_{rw} k_{ow} (- \frac{\partial p_a}{\partial z} + \frac{\partial p_c}{\partial z} + \rho_w g)] \quad (9)$$

that is, $\partial p_a / \partial z \neq 0$.

The general Darcy and continuity equations for the air phase are similar to equation (1) and (2) for the water phase.

$$\bar{u}_w = - \frac{k_{ra} k_{oa}}{\mu_a} \nabla (p_a - \rho_a g z) \quad (10)$$

and

$$\text{div} (\bar{u}_a \rho_a) = - \phi \frac{\partial (\rho_a S_a)}{\partial t} \quad (11)$$

where:

\bar{u}_a = bulk air flow, $\text{cm}^3/\text{cm}^2/\text{sec}$

k_{oa} = air permeability, cm^2

k_{ra} = relative permeability of air, a function
of air saturation

μ_a = air viscosity, g/cm-sec

p_a = air pressure, dynes/cm^2

ρ_a = air density, g/cm^3 .

Combining (10) and (11) and simplifying for one-dimensional vertical flow yields:

$$\frac{\partial(S_w \rho_a)}{\partial t} = - \frac{1}{\phi} \frac{\partial}{\partial z} \left(\frac{k_{ra} k_{oa}}{\mu_a} \left(- \frac{\partial p_a}{\partial z} + \rho_a g \right) \right). \quad (12)$$

The identity

$$S_w + S_a = 1.0 \quad (13)$$

will hold if air and water are the only phases present in the pores. Thus S_a can be expressed as $1 - S_w$. Relative permeability and capillary pressure may also be expressed as functions of water saturation, or each other, for a particular porous medium.

Approaches for Solution of Infiltration Problems

Early investigators of infiltration, such as Green and Ampt (Hillel [28]) derived largely empirical equations to predict the rate of infiltration and cumulative infiltration into soils from a ponded surface. In early treatments of the infiltration process a distinct saturation front was assumed to move through the porous medium, behind the front, wetting phase saturation was assumed to be uniform at the value corresponding to the residual air content. The rest of the soil water saturation profile, deeper than the front, was assumed to be uniform at an initial water saturation. Although the saturation profile is controlled by the assumptions made, the Green and Ampt approach does yield reasonable results for coarse-grained soils with relatively low initial water saturations.

Recently, Morel-Seytoux and Khanji [39], and Mein and Larson [36]

have shown that the two constants in the Green and Ampt equation

$$I = C (H + Z_f + H_f) / Z_f = A + (B/Z_f) \quad (14)$$

where:

I = infiltration rate

C = fully saturated water conductivity

H = depth of ponded water

Z_f = vertical extent of saturation zone

H_f = capillary pressure at wetting front

A, B = empirical constants .

do actually have a physical basis although the assumptions made will limit the equations validity in many practical situations.

Philip [41] presents a complete summary of the one-phase approach to infiltration. Using the one-dimensional, horizontal (neglecting the gravity term), one-phase flow equation in the form

$$\frac{\partial \theta}{\partial t} = \frac{\partial}{\partial x} \left(D \frac{\partial \theta}{\partial x} \right) \quad (15)$$

where:

$$D = C(h) \frac{\partial h}{\partial \theta}$$

and applying the Boltzman transformation, $\phi = xt^{-1/2}$, results in a solution for infiltration rate being proportional to $t^{1/2}$. This would hold for the vertical case when t is small, the effects of gravity are negligible compared with capillarity. Philip [41] presents his own series solution for the saturation profile in the infiltration problem as well as an approximate form:

$$I = 1/2 St^{-1/2} + At \quad (16)$$

S = sorptivity, a function defining the influence of capillarity over a step change in saturation for a particular porous medium, $\text{cm-sec}^{-1/2}$

A = constant embodying effects of gravity.

As Philip [41] points out, "A" is a fraction of saturated conductivity depending on which development model is used. Brutsaert [6] solves the gravity term by transformations that employ the use of Bessel functions. At large times, it is usually assumed for the one-phase approach that the infiltration rate from a ponded surface will asymptotically approach a low value equal to the conductivity at saturation, (De Wiest [16]). That is, only gravity effects are significant. From Philip [41], the time at which gravity effects are as great as capillarity is equal to

$$t_{\text{grav}} = \left(\frac{S}{C_i - C_o} \right)^2 \quad (17)$$

where:

t_{grav} = time when gravity and capillarity effects are equal, sec

S = sorptivity, $\text{cm-sec}^{-1/2}$

C_i = hydraulic conductivity at saturation, cm/sec

C_o = hydraulic conductivity at initial saturation, cm/sec.

Whisler and Klute [59], Hanks and Bowers [26], Freeze [18], Giesel [21] and Pikul et al. [42] use finite-difference techniques to solve the one-dimensional, one-phase infiltration equation of the general form:

$$K(h) \frac{\partial h}{\partial t} = \frac{\partial}{\partial z} (C(h) \frac{\partial h}{\partial z}) - \frac{\partial C(h)}{\partial z} \quad (18)$$

where:

$$K(h) = \frac{\partial \theta}{\partial h}$$

Rubin and Steinhardt [48] use the diffusivity form of the one-phase equation for their finite-difference solution,

$$\frac{\partial \theta}{\partial t} = \frac{\partial}{\partial z} (D(\theta) \frac{\partial \theta}{\partial z}) - \frac{\partial C(\theta)}{\partial z} \quad (19)$$

where the diffusivity is defined by:

$$D(\theta) = C(\theta) \frac{\partial h(\theta)}{\partial z}$$

Bruch [4] solves the same equation by finite-element techniques.

More recently, Rubin [46] has used another transformation to solve the infiltration problem. Rubin defines

$$v = v(h) = \frac{1}{V} \int_{h_{\max}}^h C(h) dh \quad (20)$$

and

$$v = \int_{h_{\max}}^{h_i} C(h) dh \quad (21)$$

where:

h_{\max} = upper bound of pressure head in the porous medium

h_i = lower bound of pressure head in the porous medium .

Then, using equations (20) and (21) along with the Richards equation (8), results in

$$Y(v) \frac{\partial v}{\partial t} = \frac{\partial^2 v}{\partial z^2} - Z(v) \frac{\partial v}{\partial z} \quad (22)$$

where

$$Y(v) = \frac{1}{V} \frac{\partial \theta}{\partial z}$$

$$Z(v) = \frac{1}{V} \frac{\partial C}{\partial v}$$

The solution of equation (22) is then obtained by finite-difference approximations.

Morel-Seytoux [37],[38] summarizes the two-phase flow theory and approached the solution of infiltration problems on this basis. Phuc [43], Green [23], and Vachaud et al. [56], base finite-difference solutions for two-phase flow on combinations of equations (1), (2), (4), (9), (10), (11), (12), and (13). McWhorter [35] summarizes the theoretical approach to two-phase flow and develops scaling factors applicable to infiltration problems based on the two-phase approach. Brustkern and Morel-Seytoux [5] develop a semi-analytical method for solving the two-phase infiltration problem. Noblanc and Morel-Seytoux [40] describe a perturbation technique (semi-analytical) with assumptions that are not as restrictive as the Brustkern method. This technique yields results that are not significantly better for infiltration rate prediction but the water saturation profile is better defined.

Hysteresis

The overall infiltration process is characterized by two distinct stages. A wetting stage (imbibition) at any point in the porous medium will normally be followed by a drying stage (drainage) while the wetting fluid saturation decreases. These two stages will most often

occur near the surface with imbibition being followed by drainage after the amount of water available at the surface is decreased. This redistribution will be accompanied by hysteretic effects that may or may not be significant depending on the particular system and its boundary conditions.

The discussion of hysteretic effects will be limited to saturation-capillary pressure relationships. Relative permeability hysteresis may also occur but this phenomenon will not be discussed here.

Rubin [47] used a finite-difference model to simulate hysteretic effects of post-infiltration redistribution in Rehovot sand. The results obtained from this study indicate that the redistribution from the higher saturated soil nearer the surface to the dryer soil below is slower when hysteresis is considered. Whisler and Klute [59] investigated hysteretic effects at the wetting front during infiltration. Using the main drainage saturation-capillary pressure curve resulted in an over-estimation of front advancement in comparison with the advancement predicted when hysteretic effects were modeled. Estimation of front advancement using the main wetting curve underestimated the rate compared with the hysteresis case, but was much closer to the hysteresis-effected movement than the results obtained from the drainage curve.

Ibrahim and Brutsaert [29] analyzed intermittent infiltration, and found that neglecting hysteresis during redistribution after infiltration wetting has a negligible effect on the saturation profile up to a dimensionless time $\tau = 0.10$, where

$$\tau = tC_o/[(\theta_o - \theta_r)] \Delta Z \quad , \text{ and} \quad (23)$$

where:

t = time , sec

θ_o = saturated volumetric water content, dimensionless

θ_r = residual volumetric water content, dimensionless

ΔZ = finite difference interval, cm

C_o = capillary conductivity at θ_o , cm/sec.

Hysteresis considered in the two-phase approach of Phuc [43.] slowed the infiltration rate by 2.5% with an impermeable boundary at a depth of 495 cm. During redistribution stages, the more saturated zone near the surface dried more slowly and the drier two areas at greater depths wetted more slowly when hysteresis was considered. The significance at larger times is not great, but no information was available for distribution effects immediately after infiltration at the surface stops.

Experimental work by Vachaud and Thony [55] indicates that once the water saturation in the upper zones reaches saturated conditions, the redistribution for these zones will take place along the main drainage curve.

Conceptual Differences of Infiltration Models

Philip [41] and Hillel [28] both offer qualitative descriptions of the saturation profile during infiltration under a constant depth of ponded surface water, assuming air phase effects are negligible. Four saturation regions exist from the surface downward; saturation zone, transmission zone, wetting zone, and wetting front, are used to characterize

the profile. The saturation zone near the surface is presumed to be saturated to $S_w = 1 - S_{ra}$ where S_{ra} is the residual air saturation. Under shallow ponding conditions this saturation zone could be present to a depth of one centimetre. The transmission zone is characterized by a saturation profile that changes very little with time and position, but is lengthening. Next follows the wetting zone that is characterized by a saturation profile with increasing gradient with respect to depth until the wetting front is reached. Here the saturation gradient is steep enough to define a clear boundary between the wetting zone and the soil still at initial water saturation below the front.

The initial saturation of the porous medium will affect the infiltration rate and the rate of front advancement, (Philip [41]). Lower initial saturations will increase the influx of the wetting phase through the surface, at larger times the effect will disappear. The saturation front will advance at a faster rate through porous media with a higher initial saturation. Decreasing the unsaturated fraction, (higher initial saturation) has much more influence on the wetting front advancement than the associated decreased capillary potential.

Rubin [46] investigated numerically the results of different rainfall intensities on infiltration into air-dried Rehovat sands. At an intensity of 30 times the saturated conductivity the sand at 0.5 cm was saturated within 25 seconds and surface ponding began by 90 seconds. Decreasing the intensity to 1.5 times the saturated conductivity resulted in saturation at 0.5 cm after 110 seconds; ponding did not occur until approximately 580 seconds. Rubin [46] also indicated that the depth of front advancement at ponding time, decreases as the intensity of rainfall

increases. Saturation gradients are steeper in the unsaturated zone at the wetting front when higher rain intensities are experienced.

In the two-phase treatment of infiltration, air is considered in a dynamic sense. Phuc and Morel-Seytoux [44] indicate that implicit in the one-phase approach are assumptions that the viscous resistance to airflow is negligible and that there is no compression of the air below the wetting front. Either of these situations could slow the wetting front advance as well as effect the saturation profile.

Experiments by Adrian and Franzini [2] for one-dimensional infiltration into a column with an impermeable lower boundary indicated that the pressure buildup in the air phase resulted in significantly decreased infiltration rates. The upward flow of air during infiltration was also observed. The results of Vachaud et al. [56] confirm that once the air phase is not allowed to escape freely, and compression and counter-flow take place, the one-phase approach is inadequate to describe the infiltration.

Vachaud et al. [56] found that, at low infiltration rates the saturation profiles are identical for more than an hour whether the air was allowed to escape freely or not.

Phuc and Morel-Seytoux [44] explain that infiltration into a porous medium with impermeable sides and bottom displaces the air downward and blocks its escape to the surface. As the amount of water infiltration increases the air is compressed more; when the pressure is high enough the air will be able to displace some of the water above the wetting front and form paths to the surface. The results of Phuc [43] indicate a lower water saturation near the surface as a result of the

escaping air from the counterflow. This lower saturation at the surface will tend to decrease the infiltration rate.

Wilson and Luthin [61] observed the same type of infiltration rate decrease when impermeable boundaries are considered. The conceptual explanation suggested was that behind the wetting front air saturation increases as the pressure in the air phase increases. Fingers of air are considered to be penetrating upwards from the front; with further wetting-front advancement some of the fingers are separated from the air phase ahead of the front. The existence of these fingers will increase the tortuosity of the downward flow of water thus slowing the infiltration. Wilson and Luthin [61] indicate that even for some semi-infinite porous media columns subject to one-dimensional infiltration the air pressure will exceed atmospheric conditions. Shorter columns with an air escape from the bottom are considered to be affected negligibly by air pressure effects.

During infiltration, the closer an impermeable boundary is to the surface a greater influence from the air phase is experienced, (Phuc and Morel-Seytoux [44])

If the viscous resistance to airflow and pressure build-up in the air phase can be neglected then the one-phase approach to infiltration is valid Vachaud et al. [56]. The results of Phuc and Morel-Seytoux [44], indicate some pressure buildup in the semi-infinite case (as suggested by Wilson and Luthin [61]) but the effect is not sufficient to warrant the two-phase approach. Where the air is allowed to escape freely, the one-phase approach will be adequate to describe the infiltration process.

Finally, Phuc [43], Burstkern and Morel-Seytoux [5], and

Noblanc and Morel-Seytoux [40], all estimated limiting infiltration rates below the saturated conductivity limit assumed in most one-phase approaches.

WATER FLOW THROUGH SNOW

The flow of water through snow is of particular interest to hydrologists predicting spring peak flows in temperate and Arctic watersheds. Treatment of the snowmelt waterflow is usually by an empirically based method. Physically based models are hard to test and verify as the physical properties of a snowpack are time and temperature dependant, and the properties are affected by the actual presence of liquid water. A description of physically based models employed to date, for flow of water through snow is given in this section.

Flow of Water Through Wet Isothermal Snow

Water movement through wet snow, as noted by de Quervain [15], was investigated as early as 1925. de Quervain [15] describes three physically based models of waterflow through a snow pack.

Film flow is associated with small saturations and low water flux. Conceptually this flow is considered as a thin film of water moving along vertical ice crystals; the thickness of the film is small compared to the size of the ice crystals and the flow is in response to gravitational forces.

The channel flow model recognizes that water percolation through a snowpack is not uniform. As the water movement from film flow increases, the film thickness becomes significant, capillary forces collect the water and drainage through preferred randomly spaced

channels takes place. The saturated flow through these channels is considered as Hagen-Poiseuille flow. de Quervain [15] presents an expression to relate the growth of pore diameter to time while experiencing gravitational water flow at 0°C,

$$d(t) = d_o / (1 - d_o^2 C_d t)^{1/2} \quad (24)$$

where:

$$C_d = \rho_w g^2 / 32L \nu \rho_i$$

d = pore diameter, cm

d_o = original pore diameter, cm

t = time, sec

g = gravitational acceleration, cm/sec²

ρ_w, ρ_i = density of water, and ice, g/cm³

L = latent heat of fusion, erg/g

ν = kinematic viscosity, cm²/sec .

de Quervain [15] notes conflicting observations of grain growth in the presence of melt water at isothermal 0°C conditions.

Fujino [20] notes that as the ratio of channel flow to film flow increases, the vertical velocity of water also increases.

The third physically based model of water flow in snow considered by de Quervain is that of saturated Darcian flow. Application of this type of model usually is for the case of water flow along the base of a snowpack over a sloped impermeable boundary.

Male and Norum [33] and Male, Norum and Besant [34] perform a thermodynamic analysis of the dynamic processes, including water flow, within a snowpack. The latter publication discusses the dimensionless

groups relevant to the analysis of snowpack processes. Unfortunately due to the delicate equilibrium balances in a snowpack, many of the parameters necessary for this type of approach are exceedingly difficult, if not impossible, to measure with available instruments.

Male, Norum and Besant [34] outline seven assumptions that must be satisfied before the unsaturated Darcy flow approach could be applied to water flow in snow. Firstly, the porous medium, snow, must be inelastic, crystal movement should be negligible compared to water flow. Secondly and thirdly, viscous and inertial effects should be insignificant. The fourth constraint and possibly most critical assumption to the present study is that liquid water movement is not affected by temperature gradients in the snowpack. Surface characteristics of the water, contact angle, surface tension as well as viscosity and intrinsic density are considered constant for the fifth restriction. Sixth, viscosity and density of air are considered to be negligible. The last assumption is that the air phase has a uniform pressure throughout and that gravitational effects on the air phase are insignificant.

Recent studies by Colbeck, [7], [8], [9],[10], [11],[12], and Colbeck and Davidson [13], represent the first concerted effort to develop physically based models to quantitatively predict the unsaturated flow of water through snow.

Colbeck [7] and [8], develops the equations for flow assuming a homogeneous snowpack, other than allowing a density gradient with depth. Darcy equations are written for both air and liquid water phases, and hysteresis is considered negligible. After numerous simplifications and approximations, the model for flow is reduced to a one-phase, one-

dimensional gravity flow where vertical velocity (positive downwards) is given by

$$\bar{u}_w = \frac{k_{rw} k_{ow}}{\mu_w} \left(\frac{\partial p_c}{\partial S_w} \frac{\partial S_w}{\partial z} + \frac{\partial p_c}{\partial \phi} \frac{\partial \phi}{\partial z} + \rho_w g \right) \quad (25)$$

The effects of capillarity and density gradient, other than relative permeability being a function of both, are considered negligible compared to gravity in the air-water-snow system dealt with by Colbeck. Thus

$$\bar{u}_w = \frac{\rho_w g}{\mu_w} k_{rw} k_{ow} \quad (26)$$

In particular, $\partial S_w / \partial z$ is assumed to be less than 0.01 cm^{-1} .

Although Colbeck [7] mentions the use of $n=3$ in the relationship

$$k_{rw} = S^{*n} \quad (27)$$

where:

$$S^* = \frac{S_w - S_{wi}}{1 - S_{wi}}, \quad (28)$$

in both publications [7] and [8], Colbeck uses $n=2$ for the relative permeability-effective saturation function. The wetting front advance is considered to be as a "shock-front", that is $\partial S_w / \partial z \rightarrow \infty$ in the region of the front.

Predicted results by Colbeck's [7] treatment compared with previous observations on Seward Glacier yield a wave propagation three to four times faster than actual rates. Colbeck attributes this to the inhomogeneities of ice lenses. This will lower the permeability and promote build up and horizontal flow above the lenses.

Colbeck [8] discusses his fundamental assumption that capillarity may be ignored and generalizes that the assumption holds in "mid-ranges" of saturation. Thus when saturations near the residual value or near fully saturated conditions are experienced, capillary effects will not be negligible. In these regions $\partial p_c / \partial S_w$ is not small; the so-called "shock-front" region where $\partial S_w / \partial z \rightarrow \infty$ will have large magnitudes of $\partial p_c / \partial S_w$ and capillarity effects will not be insignificant. Colbeck [8] indicates that observed front advancement is not as well defined as the assumed "shock-front" but assumes that the front region may be handled sufficiently by using continuity relationships.

Colbeck and Davidson [13], in response to the difficulties of laboratory measurement of relative permeability-saturation relationships, used an indirect method for estimating n in equation (27). The four values of n estimated from actual snowpack percolation were; 3.1, 2.8, 4.0 and 3.3. Although the average of these values is $n=3.3$, for mathematical ease Colbeck and Davidson [13] use $n=3$; the theoretical value for uniform spheres. The gravity-drainage "shock-front" model was compared with observed melting homogeneous snowpacks by Colbeck and Davidson [13] with considerable success. The snowpack columns used in these tests were uniformly mixed and packed before the tests were begun; no ice-layer effects were encountered as with the previous attempt of data matching, (Colbeck [7]).

A discussion of the effect of stratigraphic layers is presented by Colbeck [10]. Formation of ice layers in a snowpack is thought to be mainly a result of refreezing percolating water; surface phenomena (metamorphism) plays a minor role. As noted earlier, the ice layers are usually accompanied by developing channels of preferred drainage.

Colbeck [10] treats the problem as a perched-water-table-flow to drains, situation common to groundwater hydrology and irrigation problems (see Glover [22]). The analysis indicates that accumulation of water above an impermeable ice layer is significant during normal snowmelt percolation if the drain channels are spaced in the order of 1 meter or greater. Langman [32] noted that in naturally occurring snowmelt situations, the channels may be spaced as close as one centimeter.

Colbeck [12] takes a more detailed approach in analyzing capillarity effects but still concludes that during most naturally occurring snowmelt, the "shock-front" approximation is adequate. The fronts observed by Colbeck and Davidson, not distinctly defined, are attributed to fingering effects and not capillary forces at the wave front. At the surface when S^* decreases to 0.1 the capillary effects are 23 times as greater as gravity effects but Colbeck concludes that the magnitude of discrepancy introduced by assuming capillarity will be negligible due to the low flow associated with small values of saturation. Colbeck [12] does indicate that in nearly saturated zones, capillary forces will have an appreciable influence on the water flow. The unsaturated vertical percolation through snow is combined with saturated flow over an impermeable boundary to simulate the runoff process from a typical arctic watershed.

Flow of Water in Snow Below 0°C

A conceptual description of 0°C water percolating through sub-zero dry snow is proposed by de Quervain [15]. As the water moves through the snow, enough freezes to release the heat required to raise the temperature of the snow to 0°C. Another fraction of the water

remains as residual saturation with the rest available free for further percolation, freezing and residual saturation. This proceeds with no thawing of the ice crystals until the front is frozen, possibly where the temperature gradient of the snow steepens. Ice lenses are formed with the lateral expansion. de Quervain [15] notes that the location of these lenses will be partially controlled by stratified layers in the snowpack. Ensuing meltwaters break through the ice layer at discrete locations and drain through channels as in previously mentioned observations.

The U.S. Army Corps of Engineers [54] developed a simple expression for the penetration of water into a uniform snowpack,

$$D = \frac{t (i_r + m)}{\rho_s \left(\frac{T_s}{160} + \frac{f_{ll} p}{100} \right)} \quad (29)$$

where:

D = depth of penetration, in

i_r, m = rain, and melt intensities, in/hr

t = duration, hr

ρ_s = density of snow, g/cm³

T_s = snow temperature, - degrees below 0°C

$f_{ll} p$ = liquid water holding capacity .

This technique will be discussed in further detail in

Chapter IV.

SNOW AS A POROUS MEDIUM

If the flow of water through snow is conceptualized as immiscible flow through a porous medium, it will be necessary to estimate the parameters for porous media flow. Relationships between permeability and porosity, saturation and capillary pressure, and saturation and relative permeability are needed for a complete treatment.

Compared to usually encountered porous media systems, the air-water-snow system has very limited empirical data available for the desired relationships. Phase equilibrium and thermal complications prevent extensive experimental analysis of the parameters for this particular porous media system. Metamorphism of snow grains with time contributes to the non-ideality of the system.

Capillary Pressure - Saturation Relationships

Three capillary pressure-saturation investigations of snow during the drainage cycle have been carried out. Colbeck [12] used kerosene at -10°C , Friesen [19] used Soltrol-C with two densities of snow at -15°C . A snow-water system was studied under adiabatic conditions by Colbeck [9]. No capillary pressure-saturation tests have been performed for the imbibition cycle.

Snow grains for the Colbeck test with kerosine were approximately one mm in diameter, the snow used for the Friesen tests had grains less than one mm in diameter. There is no mention of grain size for the Colbeck snow-water tests.

All of the capillary pressure-saturation curves exhibit a relatively flat region in the middle saturation ranges, that is, there

exists a region where $\partial p_c / \partial S_w$ is small. This behaviour is characteristic of porous media having a more uniform pore-size distribution. Although a uniform pore-size distribution seems likely considering that the snow grains in a pack will normally be fairly constant in size, the existence of bonding between the grains and hence structure favours a wider range of pore sizes. Laliberte [31] indicates that porous media with a wide range of pore sizes have secondary porosity as a result of structure.

Residual wetting fluid saturations for the drainage cycles in Colbeck investigations [9] and [12] was approximately 0.07. Friesen [19] obtained residual saturations of 0.094 and 0.035 for snow with densities of 0.48 g/cm^3 and 0.40 g/cm^3 , respectively.

The most significant differences in the Colbeck and Friesen results is the entry pressure, the pressure at which the snow begins to desaturate. Friesen's [19] results indicate entry pressure heads of approximately four and two cm for the snow densities of 0.40 g/cm^3 and 0.48 g/cm^3 . All of the Colbeck curves indicate that the entry pressure approaches zero. The problems encountered by Friesen [19] in attempting a relative permeability-capillary pressure test indicate low entry pressures.

Pore-Size Distribution Index

A log-log plot of effective saturation, S^* , versus capillary pressure head, expressed as $p_c / \rho g$ will indicate the pore-size distribution index; λ , Laliberte [31]. The negative slope of the straight line portion of the curve represents the pore-size distribution index, the larger the index the more uniform is the pore-size distribution.

Friesen [19] obtained $\lambda = 9.9$ and $\lambda = 6.2$ for snow densities

of 0.48 g/cm^3 and 0.40 g/cm^3 , respectively. From Laliberte [31], the pore-size distribution index for glass beads is 7.3 while for fine sand it is 3.7 .

Plotting Colbeck's [9] and [12], capillary pressure-saturation curves in the same manner indicates a pore-size distribution index of 4.9 for the snow-water system of densities 0.55 and 0.59 g/cm^3 and an index of 2.4 for the snow-kerosene system with snow density 0.56 g/cm^3 .

Bubbling Pressure

The bubbling pressure head, $p_b/\rho g$, of a porous media-fluid system is defined as the intercept of the straight line in the log-log plot of S^* versus $p_c/\rho g$, Laliberte [31]. This head is normally very close to the minimum capillary pressure head where the non-wetting fluid permeability can be measured during drainage. The magnitude of this pressure head may give some indication as to the range of the residual non-wetting phase saturation during imbibition.

Bubbling pressure is a function of the largest continuous pores of the particular porous medium; a lower bubbling pressure indicates larger continuous pores.

The bubbling pressure head for the snow-kerosene system of Colbeck [12], is found to be five cm while for the snow-water system the head is 3.7 cm. Friesen [19] estimated a bubbling pressure head of eight cm for the snow density of 0.48 g/cm^3 and a head of nine cm for the snow density of 0.40 g/cm^3 .

Saturation - Relative Permeability Relationships

The relative permeability of the wetting phase, k_{rw} , at sat-

uration, S , can be approximated during the drainage cycle by

$$k_{rw} = \frac{(S-S_r)^2}{1-S_r} \frac{\int_0^S \frac{dS}{P_c^2}}{\int_0^1 \frac{dS}{P_c^2}} \quad (30)$$

Burdine's equation, from Laliberte [31].

Corey [14] showed that equation (30) could often be approximated by

$$k_{rw} = S^{*4} \quad (31)$$

Porous media of completely uniform pore-size distribution will have a relative permeability relationship

$$k_{rw} = S^{*n} \quad (32)$$

where $n=3$, Laliberte [31], while unconsolidated sands of one grain structure have an exponent $n=3.5$.

As previously cited, Colbeck and Davidson [13] indirectly measured the exponent in equation (32) to average $n=3.3$ although for simplicity in calculation, they used $n=3$.

At capillary pressures above the bubbling pressure Laliberte [29] shows that n may be approximated by

$$n = \frac{2 + 3\lambda}{\lambda} \quad (33)$$

Applying this to the Colbeck, [12], snow-kerosene system with $\lambda = 2.4$ results in $n=3.8$; the snow-water system investigated by Colbeck, [9], $\lambda = 4.9$, yields $n = 3.4$. Friesen [19] found that $n = 3.3$ and $n = 3.2$ for the snow densities of 0.40 g/cm^3 and

0.48 g/cm³ in the snow-Soltrol-C systems.

Permeability: Porosity Relationships

For a fully saturated porous medium with relatively uniform pore size distribution and low eccentricity the permeability may be approximated by the Kozeny-Carman equation (Laliberte [31]):

$$k_{ow} = \frac{\phi^3}{5s^2} \quad (34)$$

where:

k_{ow} = saturated permeability, cm²

ϕ = porosity, dimensionless

s = specific surface, ratio of surface area of solid pore boundaries to bulk volume of the medium, cm²/cm³.

Again this type of relationship breaks down for a porous medium containing secondary porosity. Although snow does exhibit structure, its pore size distribution is very uniform.

Several empirical studies of the saturated permeability of snow have been performed. Shimizu [50] defined a relationship for permeability as a function of both crystal size and density by:

$$k_{ow} = 7.7 \times 10^{-4} d^2 (\exp(-7.8 \times 10^{-3} \rho_s)) \quad (35)$$

where:

d = grain diameter, cm

ρ_s = snow density, g/cm³.

de Quervain [15] compares the saturated water conductivity of

snow with grain size:

<u>Grain Size</u>	<u>Conductivity (cm/sec)</u>
$d < 1 \text{ mm}$	0.57
$0.8\text{mm} < d < 1.5\text{mm}$	1.20
$d > 2 \text{ mm}$	2.24

Moskalev (noted by de Quervain [15]) proposes a conductivity based on structural parameters:

$$C_{OW} = 2.88 \phi d^{1.63} \text{ cm/sec} \quad (36)$$

Colbeck and Davidson [13] observed permeabilities during water percolation in snow:

Snow Density (gm/cm)	ϕ	$k_{OW} (\text{cm}^2)$
0.653	0.32	1.2×10^{-6}
0.623	0.36	3.2×10^{-6}

Colbeck [8] refers to Kuriowa's general relationship for the permeability of snow as a function of porosity:

$$k_{OW} = 1.17 \times 10^{-9} \exp(15.9\phi) \text{ cm}^2 \quad (37)$$

A complete study of saturated conductivity as a function of snow density and metamorphism stage (i.e. grain size) in a snow-kerosine system was performed by Kuriowa [30]. The proposed expression for saturated conductivity is:

$$C_{ow} = \frac{a \phi N}{N - \phi} \quad (38)$$

where:

C_{ow} = saturated conductivity, cm/sec

ϕ = porosity of snow, dimensionless

a, N = empirical constants dependent on snow structure.

The results include examples of fine grained snow in the field, or cold room, coarse grained snow, and artificially compressed snow.

Colbeck's [10] analysis of a snowpack with ice bands results in a permeability of $1.5 \times 10^{-6} \text{ cm}^2$, one half the value expected from that particular density using the general Kuriowa equation (37). With a porosity of 0.485 Colbeck [12] uses a permeability of $3.0 \times 10^{-6} \text{ cm}^2$.

HEAT TRANSFER

The general one dimensional, heat conduction equation without sources or sinks is

$$\frac{\partial}{\partial x} \left[\alpha \frac{\partial T}{\partial x} \right] = \frac{\partial T}{\partial t} \quad (39)$$

where:

T = temperature, °C

t = time, sec

x = spatial coordinate, cm

$\alpha = k/\rho C_p$: thermal diffusivity, cm^2/sec

ρ = density, g/cm^3

k = thermal conductivity, $\text{cal}/\text{cm}\text{-sec}\text{-}^\circ\text{C}$

C_p = specific heat, $\text{cal}/\text{g}\text{-}^\circ\text{C}$.

Equation (39) may be solved by a number of methods depending upon the characteristics of initial and boundary conditions and whether thermal diffusivity, α , varies. An explicit finite-difference solution for the conduction equation is presented in Appendix D.

The solution of the combined heat conduction and phase change situation (Stephan's problem) is solved in one dimension by Eckert and Drake [17] as

$$\bar{x} = K(t)^{1/2} \quad (40)$$

where:

\bar{x} = position of the interface between phases

t = time

K = an empirically derived constant.

Trupp [53] indicates that the movement of the phase interface in a soil-water-ice system is defined by

$$\frac{d\bar{x}}{dt} = \frac{1}{\rho L} \left[k_1 \frac{\partial T}{\partial x} \Big|_{x=\bar{x}} - k_2 \frac{\partial T}{\partial x} \Big|_{x=\bar{x}} \right] \quad (41)$$

where:

L = latent heat of fusion, cal/g

ρ = weight of water per unit volume, g/cm³

k_1 = thawed thermal conductivity, cal/cm-sec-°C

k_2 = frozen thermal conductivity, cal/cm-sec-°C.

Recent activity in northern Canada and Alaska has resulted in numerous investigations into heat conduction - phase change problems associated with freezing and thawing in soils. Wheeler [58] presents

a technique for modeling the movement of the freezing or thawing front by finite-element techniques. Trupp [53] utilized the "excess degree" method for solution of Stephan's problem by finite-difference techniques. The "excess degree" concept described in Appendix D is particularly well suited for simple geometries.

If the liquid phase is flowing, the heat exchange process is complicated by convection. Guyman and Luthin [25] and Harlan [27] use finite-element and finite-difference techniques respectively to solve

$$\frac{\partial}{\partial x} \left[k \frac{\partial T}{\partial x} \right] - C_w \frac{\partial (vT)}{\partial x} = \frac{\partial (C_a T)}{\partial t} \quad (42)$$

where:

k = thermal conductivity, cal/cm-sec-°C

v = fluid flux, cm/sec

C_w = volumetric heat capacity of water, cal/cm³-°C

C_a = "apparent" volumetric heat capacity of system, cal/cm³-°C
 $= C - L\rho_i \frac{\partial \theta_i}{\partial T}$

C = volumetric heat capacity, cal/cm³-°C

L = latent heat of fusion, cal/g

ρ_i = ice density, g/cm³

θ_i = volumetric ice content, cm³/cm³.

The heat balance equation (42) was coupled with unsaturated porous media flow relationships, such as equation (7), to study moisture redistribution in freezing and thawing soil systems by Harlan [27] and Guyman and Luthin [25]. Convective terms in these redistribution cases will be considerably less than in the ice-capping process.

THERMAL PROPERTIES OF SNOW

Pounder [45] indicates that the specific heat of pure ice at constant pressure, as a function of temperature, is

$$C_p = 0.5057 + 0.001863 T_s \quad (43)$$

where:

C_p = specific heat capacity, cal/g-°C

T_s = snow temperature °C .

The volumetric specific heat of snow is calculated by multiplying the specific heat of ice by the snow density.

Thermal conductivity of snow is usually discussed in terms of effective thermal conductivity that includes effects of all heat transfer mechanisms through the snow grain porous medium. This enables the net effect of these mechanisms to be approximated by the conduction equation (39). Yen [61] summarizes the empirical and theoretical investigations of heat transfer in snow.

Effective thermal conductivity will include effects of heat transfer by conduction between snow grains in contact, conduction through the pore space, radiative transfer across the pore space, and molecular diffusion. Yen [61] indicates that in most cases dealing with natural snow conditions, both radiation and conduction across air in the pore spaces is negligible.

More empirical results discussed by Yen [61] define the effective thermal conductivity as a quadratic function of snow density with reasonable accuracy over density ranges of 0.5 g/cm^3 . Over a smaller

density range, a linear function is adequate to fit empirical data

$$k_e = a + b\rho_s \quad (44)$$

where:

k_e = effective thermal conductivity, cal/cm-sec-°C

ρ_s = snow density, g/cm³

a,b = empirical constants.

In dense snow the conduction through snow grains and through the pore space are the most significant of the heat transfer mechanisms. The effective normal conductivity for dense snow may be approximated by

$$k_e = \frac{2k_i + k_a - 2\phi(k_i - k_a)k_i}{2k_i + k_a + \phi(k_i - k_a)} \quad (45)$$

where:

k_e = effective thermal conductivity, cal/cm-sec-°C

k_i = ice thermal conductivity, cal/cm-sec-°C

k_a = air thermal conductivity, cal/cm-sec-°C

ϕ = snow porosity, dimensionless.

For a liquid saturated porous medium Somerton [51] proposes

$$k_e = k_s \left(\frac{k_l}{k_s}\right)^m \quad (46)$$

where:

k_e = effective thermal conductivity, cal/cm-sec-°C

k_s = solid thermal conductivity, cal/cm-sec-°C

k_l = liquid thermal conductivity, cal/cm-sec-°C

$m = C\phi$

ϕ = solid porosity, dimensionless

C = empirically derived correction factor (≈ 1.0).

Pounder [45] suggests that for ice containing air bubbles, the conductivity is approximated by

$$k_e = 2k_i \left(\frac{1 - \phi}{2 + \phi} \right) \quad (47)$$

where

k_e = effective thermal conductivity, cal/cm-sec- $^{\circ}$ C

k_i = ice thermal conductivity, cal/cm-sec- $^{\circ}$ C

ϕ = ice porosity, dimensionless.

CHAPTER III

EXPERIMENTAL TECHNIQUES

The laboratory tests were performed with two primary objectives defined. Initially, relationships between dependent and independent variables, for the process of water infiltration into a packed snowbed, should be identified for predictive purposes. The preliminary tests would then provide direction for a more in-depth, physically based treatment of the process in an attempt to identify actual controlling mechanisms. Laboratory investigation was supplemented by numerical modeling in pursuit of this second objective.

Infiltration into Sand

Selkirk silica sand, because of its local availability and ease of handling, was chosen for a series of water infiltration tests into a porous medium below 0°C. Infiltration experiments, varying the sand sieve size, gr , the amount of water applied, W , the sand temperature, T_{sa} , the water temperature, T_w , and the type of flow, either one-phase or two-phase, were executed. The porosity of the sand used was approximately constant at $\phi = 0.37$. In all cases, the sand was oven dried before testing took place.

Cylindrical PVC containers 2.15 cm in height, inside-diameter of 10.0 cm, and wall thickness of 2.0 mm, were filled within approximately 5.0 cm from their top. Containers for two-phase, counterflow tests had airtight bottoms and sides. Air was allowed to escape freely through holes in the bottom of the containers for one-phase

flow conditions. The samples were placed in a Cold Stream environmental room and allowed to cool to the control temperature before water application. The containers were wrapped in glass wool insulation to minimize heat conduction and convection effects in the radial direction during infiltration.

Nominal water temperatures of 0°C were actually 0.1 to 0.5°C thus eliminating latent heat effects of sub-cooling the water before application. The water was poured by hand directly on the surface at an approximate rate of one $\text{cm}^3/\text{cm}^2/\text{sec}$. Infiltration time was recorded as the time from water contact on the sand surface until no water remained ponded. As infiltration was taking place, surface characteristics were observed.

After the samples had been allowed enough time to totally re-freeze, they were removed from their containers for further observation and photographing.

Infiltration into Compacted Snow

The initial tests of water infiltration into snow used sample containers identical to those used in the sand tests.

Natural snow from within Winnipeg during January and February 1975 was used for these experiments; ambient temperatures varied from approximately -30°C to -5°C during this time. The snow was collected so as to avoid the depth hoar or any crusted layers; in all cases, the snow grain diameter was between 0.25 and 1 mm. Snow was uniformly mixed, then tamped in the sample containers with a hand plunger to the desired density. Care was taken to minimize distinct layering.

During each series of tests, one sample was prepared solely for the purpose of estimating the temperature of the actual test samples. A thermometer was used to measure the snowpack temperatures, inserting it into one of the test samples would have destroyed the geometry of the one-dimensional flow. Glass wool was again used to insulate the sides of the containers.

To facilitate visual observations of the water penetration, a small amount of common food colouring was added to the application water. It was determined by tests beforehand that the small concentrations used neither induced an appreciable freezing point depression, nor a change in surface tension for the water.

Various sample tests were run altering the parameters; snow density, ρ_s , snow temperature, T_s , amount of water applied, W , temperature of water, T_w , the age-hardening time, t , and the type of flow, either one-phase or two-phase. The age hardening time was measured from the time of compaction to the time of water application. Infiltration time and surface observations were noted for each application.

When the samples were completely refrozen, they were removed from their containers for further observation and photographing.

Continuous Temperature Measurement Tests

This series of experiments was performed in the same manner as the previously described snow tests with the added feature of continuous temperature measurement.

A series of glass-sheathed thermocouples was inserted radially to the centre line of the snowpack through 4 mm diameter holes in the

side of the sample containers. The sheathed thermocouples and containers were sealed to prevent air or water escape radially. The copper-constantin "Type-T" thermocouples were placed at approximately 2 cm intervals from the surface downwards.

The difference in electrical potential between each thermocouple and a reference junction at 0°C was measured by a Hewlett Packard digital voltmeter, Data Acquisition System. The scanning was controlled by a Hewlett Packard HP 9830A mini-computer that enabled measurements between thermocouples over time intervals of less than 0.2 seconds. The data acquired were recorded, stored, and processed by the HP 9830A using a program prepared specifically for this series of tests.

All other observations were carried out in the same manner as the previous snow infiltration tests.

Scintillation Tests

Average densities of the ice capped zone for 22 of the snow infiltration tests were measured with a Nuclear-Chicago Model 8770 scaler. Cobalt 60 was used as a gamma-ray source which was directed as a beam through machined lead shielding bricks. Container and sample were placed between the radioactive source and detector tube, and least ten counts of one-minute duration were made for each sample. Standards for an empty container and one filled with water were measured for each series of tests to establish the linear density/count relationship.

Refreezing Test

The observation of temperatures within an ice-capped snowpack from time of water application until freeze-back was performed using a larger-diameter container to decrease the effects of radial heat transfer. A 20 cm inside-diameter PVC container with wall thickness 1.0 cm was packed with 30 cm of snow, simulating an actual snow road thickness. "Type-T" thermocouples were placed at the surface and 2, 4, and 8 cm below it. Glass wool insulation was wrapped about the container to minimize radial heat transfer effects. The temperatures were measured for 23 hours from the time of application with the Hewlett Packard Data Acquisition System.

Simulations

Three finite difference models were developed to compliment and expand upon the laboratory tests. The models were written in Fortran and run on the University of Manitoba IBM 370/158 system.

Both implicit and explicit models were developed for the solution of infiltration saturation profiles while only an explicit scheme was used for the heat transfer-phase change model. Details of the solution equations for each of the models are given in Appendix D.

CHAPTER IV

RESULTS AND DISCUSSION

The results of laboratory and simulation tests are given in Appendices A,B,C,E, and F. This chapter discusses the implications of these results.

INFILTRATION INTO SAND

The 38 tests of water infiltration into sand are tabulated in Tables A-1, A-2, and A-3. Selkirk silica sand of sieve size 35-50 and water at 0°C was used for all the tests of Table A-1; various water temperatures with the same size sand are summarized in Table A-2. Sand sieve sizes of 10-20 and 20-30 were tested with water at 0°C as indicated in Table A-3.

Front penetration indicates the depth to which the total cross-section of the sand sample has been wetted. Maximum penetration represents the furthest depth of water penetration; full penetration of the sample (approximately 16.5 cm) was usually accompanied by some build-up of water on the container bottom.

The most significant difference between the one-phase and two-phase experiments was the infiltration time. During infiltration, escaping air bubbles were observed in all two-phase tests. This counter-flow was neither homogeneous across the surface nor steady with time. Between one and three discrete locations would open on the sand surface to allow the air to escape; usually only one location of air escape would be evident at any time. In some instances no air bubbles would

be visible and the height of ponded water would remain constant until another location of air escape appeared. Infiltration for the two-phase test SA 20 stopped at 330 sec. and then started again at 440 sec.; Figure A-1 is a photograph showing the final air escape location. Some of the two-phase infiltration tests exhibited a build-up of air a few millimeters below the surface, and when the pressure was great enough the whole surface would heave to allow the air to escape. None of the one-phase tests exhibited any counterflow of air through the surface.

Average front penetration for sand temperatures above -10°C were slightly greater in the two-phase flow tests. Compare tests SA 9 and SA 10 with tests SA 11 and SA 12. The maximum penetration for these two-phase tests is significantly greater than the corresponding one-phase tests. When sand temperatures were as low as -20°C , the one-phase tests penetrated further than the two-phase; compare SA 21 and SA 22 with SA 23 and SA 24; or SA 25 and SA 26 with SA 27 and SA 28.

A photograph of SA 20 Figure A-1, shows a frequently encountered form of penetration. The average front penetration is 6.0 cm whereas what appears to be the beginning of fingering action is halted at 7.25 cm. Figure A-1 indicates more evident fingering development in tests SA 35 and SA 38. Test SA 35, grain sieve size of 20-30, shows multiple development of fingers from the wetting front and their joining before being frozen off from further development and penetration. The largest finger of SA 38 almost fully penetrated the sample container before it was frozen off. From the front penetration of 6.0 cm a number of fingers develop; the dominant finger developed along the side of the sample, in most cases of observed fingering the dominant finger would be offset from

the centerline of the sample,

Linear Regression Models for Sand Infiltration

Nine linear regression models, MSA 1 to MSA 9 were tested on the one-phase water infiltration into sand results. Table C-1 indicates which variables and tests were applied to each model, while Table C-2 summarizes the results of the models. Table C-2 indicates that for the sand tests:

$$FP \propto T_{sa}, T_w, gr, W$$

$$MP \propto T_{sa}, T_w, -gr, W$$

$$IT \propto -T_{sa}, T_w, gr, W$$

where:

FP = front penetration, cm

MP = maximum penetration, cm

IT = infiltration time, sec

T_{sa} = sand temperature, °C

T_w = water temperature, °C

gr = mean sieve size of sand

W = applied water, cm^3/cm^2 .

Regression models MSA 1, MSA 2, and MSA 3 tested front penetration, maximum penetration and infiltration time respectively as functions of sand temperature, T_{sa} , water temperature, T_w , median sieve size of sand, gr, and amount of water applied, W. The results of MSA 1 indicate that there is an extremely high correlation between water applied and the front penetration, also the grain size appears to be reasonably correlated with front penetration. Sand temperature and water temperature

are poorly correlated with front penetration in MSA 1 but the variable coefficients for each are large.

Grain size correlates with maximum penetration to a greater extent than water amount for model MSA 2; both sand and water temperatures are poorly correlated.

All four independent variables correlate with infiltration time in model MSA 3 with correlation coefficients between 0.3 and 0.7.

Models MSA 4, MSA 5 and MSA 6 use only the tests with sand of sieve size 35-50 and water temperature 0°C. Multiple correlation coefficients for the three dependent variables, front penetration, maximum penetration, and infiltration time, are all over 0.9. Infiltration time is the only dependent variable that correlates well with sand temperature.

Three tests from each of three different grain sizes were used for models MSA 7, MSA 8 and MSA 9. Front penetration, MSA 7, does not correlate well with grain size; as well the variable coefficient is negligible. Sand temperature does exhibit some correlation with front penetration but the amount of water applied is definitely the controlling variable. Grain size and water amount both correlate with infiltration time in MSA 8, with a coefficient of approximately 0.6. The correlation with sand temperature and infiltration time is not as significant.

Grain size is correlated much better with maximum penetration in MSA 8 than either sand temperature or amount of water applied.

Summary of Infiltration into Sand

As indicated before, the porosity of all three Selkirk silica sands is approximately 0.37, thus a change in grain size is accompanied

by changes in permeability, capillary pressure-saturation curves, etc., but not in porosity. It appears from model MSA 1 and MSA 7 that the unsaturated flow characteristics of the porous medium have little influence on the average uniform front penetration. Even though the correlation coefficient with grain size is not insignificant in MSA 1 the variable coefficient, 0.0039, for the defining equation is negligible. Both the correlation and variable coefficient are insignificant for grain size in model MSA 7.

From models MSA 2, MSA 8 and MSA 9, it is apparent that the flow properties of different media are significant for both infiltration time and maximum penetration.

Permeabilities for Selkirk Silica Sands 10-20, 20-30, and 35-50 are approximately $850 \times 10^{-6} \text{ cm}^2$, $320 \times 10^{-6} \text{ cm}^2$ and $60 \times 10^{-6} \text{ cm}^2$, respectively. Even though the smallest grain size sand, 35-50, has greater capillary suction the significantly higher permeabilities of the coarser sands tend to increase maximum penetration and decrease infiltration time.

Models MSA 3, MSA 5 and MSA 8 indicate that the sand temperature is also a significant variable for infiltration time. Although sand temperature does not correlate well with the maximum penetration models, its variable coefficient makes it a significant parameter.

INFILTRATION INTO SNOW

The 66 samples of water infiltration into compacted snow are summarized by tests SN 1 to SN 48 in Table A-4 and the continuous temperature scan tests TS 1 to TS 18 in Table A-5.

In all of the observed tests there occurred a reasonably well defined, within ± 0.25 cm, wetting-front penetration, where the total cross-section of the samples had been wetted. Beyond this front penetration, the water invariably continued to flow, developing in a fingering or channeling fashion. The extent of this further flow depended upon such variables as snow density, snow temperature, amount of water applied, temperature of water, age hardening time and whether the flow was one-phase or two-phase. The amount of flow past the penetration front in turn affected the saturation in the ice-capped upper zone. If fingers totally penetrated the sample containers, much of the water above the wetting front penetration level would be drained.

A set of representative photographs will serve to illustrate the different types of penetration encountered. Well controlled penetration with little fingering effect is exhibited by tests SN 16, TS 7 and TS 10 in Figures A-3 and A-6. Figure A-2 shows the cross-sectional view of the ice-capped zone in sample SN 7.

A finger developing but frozen off before complete penetration and desaturation could occur is illustrated by Figure A-5 from test TS6. A partial desaturation is visible near the surface of this sample (lower left of photograph). Figure A-2 of test SN 8 shows a substantial penetration of water past the wetting front with more desaturation evident near the surface of the sample.

Test SN 30 Figure A-3, exhibited an even desaturation near the surface; finger development here occurred along the side of the sample.

A cross-section of the ice-capped portion of test SN 24 in

Figure A-3 shows that, with 3 cm water being applied, the top 1.0 to 1.5 cm has desaturated even though there was only slight finger development past the wetting front.

Three cases of total penetration with partial desaturation are shown in Figure A-4 for test SN 33 and Figure A-5 for test TS 1. The finger for SN 34 is off to one side in the sample and has a diameter of approximately 2 cm; the 3 cm diameter channel of test TS 1 is down the center of the sample. Desaturation in the ice-capped zone for test SN 34, Figure A-4, is substantially more than in test TS 1, Figure A-5.

A photograph of test SN 12, Figure A-6, indicates complete penetration by fingering with a capillary build-up from the bottom of the container. Figure A-6, a cross-section of the ice-capped zone for SN 12 illustrates almost total desaturation with the exception of a thin layer at the surface and an ice lens type of formation 4 cm down. Test TS 5 is shown apparently desaturated in a cross-sectional view, Figure A-5.

A quite regularly appearing occurrence for highly saturated upper zones is indicated in Figure A-3, of test SN 18. This cross-section shows varying intensities of light across a horizontal layer. In all very saturated cases there were extremely small air bubbles visible, trapped in the nearly solid ice. The darker areas of Figure A-3, SN 18, were the zones of lower concentration of these entrapped air bubbles.

Figures A-4 and A-6 of samples SN 48 and TS 12 respectively, show some of the effects of varying water temperature. Test SN 48 with 3 cm of water at 5°C experienced total penetration of the container down one

side, but was not completely desaturated in the ice-capped zone. The upper surface of TS 1 was partially desaturated although complete penetration did not occur, Figure A-6. Tests SN 45, SN 47, SN 48, TS 11 and TS 15, all with applied water at 5°C had partially eroded surfaces with randomly spaced pores developed up to a diameter of 4 mm. The samples which had 10°C water applied to their surfaces, TS 12, TS 16 and TS 18, all developed pores at the surface as large as 7.5 mm in diameter that extended down at least 3 cm. These pores are desaturated in Figure A-6 of test TS12.

Linear Regression Models for Snow Infiltration

Twenty-six linear regression models were applied to the one-phase compacted snow infiltration tests. A summary of the model forms and tests used is given in Table C-1. Results of the model fitting are summarized in Table C-3 for cases MSN 1 to MSN 9; Table C-4 for MSN 10 to MSN 15, and Table C-5 for models MTS 1 to MTS 11.

Overall results for the series MSN 1 to MSN 9 indicate the following general results:

$$FP \propto T_s, T_w, \rho_s, W, -t$$

$$MP \propto T_s, T_s, -\rho_s, W, t$$

$$IT \propto T_s, -T_w, \rho_s, W, -t$$

where:

FP = front penetration, cm.

MP = maximum penetration, cm.

IT = infiltration time, sec

T_s = snow temperature, °C

ρ_s = snow density, g/cm³

W = applied water, cm^3/cm^2

t = age hardening time, hrs.

The summaries for models MSN 10, to MSN 15 reveal the relationships:

$$\text{FP} \propto -T_s, T_w, \rho_s, W, -t, -(\rho_s T_s)$$

$$\text{MP} \propto T_s, T_w, -\rho_s, W, t, -(\rho_s T_s)$$

Similarly the fitted models MTS 1 to MTS 11 result in:

$$\text{FP} \propto T_s, T_w, \rho_s, W$$

$$\text{MP} \propto T_s, T_w, -\rho_s, W$$

$$\text{IT} \propto T_s, -T_s, \rho_s, W$$

The amount of water applied, W , in all but two cases, MSN 9 and MTS 9 correlated better with the dependent variable than did any other independent variable.

Each of the series of linear regression models will be discussed in more detail.

Models MSN 1 to MSN 9

Front penetration, from models MSN 2, MSN 4, and MSN 7, correlates with applied water for a stronger than with any other independent variable, the lowest correlation coefficient being 0.91. In each of these models the fitted variable coefficient (constant) is large enough to make the amount of applied water the dominant factor in any of the linear equations for front penetration. Age hardening time does correlate with front penetration, MSN 2, but the fitted variable coefficient results in this variable becoming negligible. Snow density has a reasonably

strong correlation with water penetration and becomes a significant variable second to amount of water. Both water temperature and snow temperature become negligible variables in models MSN 2, MSN 4 and MSN 7

Models MSN1, MSN 6, and MSN 9 show that maximum penetration is primarily correlated and dependent upon the amount of water applied. Snow density, although not well correlated with maximum penetration does become a significant variable in these three models. Age hardening time and water temperature are correlated quite well with maximum penetration and are significant variables in the tested models. The correlation coefficient of maximum penetration with water temperature, 0.52, in model MSN 9 is actually greater than that with the applied water.

Infiltration time is correlated with snow density, with coefficients between 0.45 and 0.50 for models MSN 3, MSN 5 and MSN 8. Again, amount of applied water correlates strongly with the dependent variable; both snow density and applied water become significant variables in the tested linear equations for infiltration time. Both age hardening time and water temperature are significant to the model forms. Although snow temperature does correlate with infiltration time, the fitted variable coefficient makes the term insignificant.

Models MSN 10 to MSN 15

The multiple correlation coefficient front penetration in the three models, MSN 10, MSN 12 and MSN 14 is greater than 0.99. The correlation and significance of applied water in all three cases is strong. Snow density becomes an important variable and correlates quite well. Snow temperature, water temperature and $\rho_s T_s$ are of moderate importance. Age hardening

time correlates with front penetration. Model MSN 14 illustrates that for the tests used front penetration may be accurately represented as a function of applied water alone.

Models MSN 11, MSN 13 and MSN 15, all result in a correlation coefficient between maximum penetration and applied water of approximately 0.66. All other independent variables are moderately significant with ρ_s , T_s , and $\rho_s T_s$ being equally important although none of their correlations with maximum penetration are particularly strong. Snow density does have a greater correlation than either snow temperature or the combined independent variable.

Models MTS 1 to MTS 11

The models in this section were fitted to the data from the temperature-scanned tests; the snow densities varied over a small range from 0.46 to 0.50. All models in this series had multiple correlation coefficients greater than 0.92, Table C-5.

Applied water has a correlation coefficient of over 0.9 with front penetration for models MTS 1, MTS 3, MTS 7 and MTS 10. In these four models snow density and water temperature are the other significant variables.

Models MTS 6 and MTS 9 illustrate that the four dependent variables, snow temperature, water temperature, snow density, and applied water amount, are all fitted significantly to the independent variable, maximum penetration. Water temperature is particularly well correlated with the maximum penetration in these samples.

Infiltration time from models MTS 2, MTS 4 and MTS 11 is strongly related to the amount of applied water. Snow temperature, water tempera-

ture and snow density are all important variables in the model relationship for infiltration time. Snow temperature, in particular, exhibits its strongest correlation with any of the dependent variables, here in model MTS 11.

Penetration of Water

Incidents of partial infiltration and full penetration are indicated on the plots of Figure C-1. All of the one-phase, one water application, snow tests of both the SN and TS series, with water temperatures of 0°C are represented. For each of the three density ranges, the coordinates are snow temperature and amount of applied water. The region to the lower left of the dashed line indicates conditions free of total penetration of the 16.5 cm samples.

Two-Phase Infiltration into Snow

Five tests, SN 3, SN 4, TS 13, TS 17 and TS 18 were performed as two-phase flow examples; the air could only escape by counterflow back through the surface. In all cases, the front penetrations of the two-phase tests were the same as comparable one-phase tests.

Samples SN 3, SN 4, and TS 13 were not fully penetrated but the maximum penetration was significantly greater than in the associated one-phase cases. Tests TS 17 and TS 18 were both penetrated completely as were their similar one-phase samples.

All two-phase samples had infiltration times much greater than similar one-phase tests. With water temperatures of 0°C, the infiltration time for the two-phase tests are:

Applied Water (cm)	Two-Phase Infiltration Time (as a multiple of one-phase infiltration time)
1	2.3
2	3.4
3	5.8

Discrete locations of air bubble escape from the snow surface were observed for all the two-phase flow samples, similar in nature to those observed for the two-phase infiltration into sand. The air bubbles appeared after 25 seconds for test TS 13 but not until 70 seconds for test TS 17, 2 cm and 3 cm of water, respectively, were applied to the two samples. Air pressure build-up would need to be greater for escape from the higher pressure surface with 3 cm water applied. In test TS 18, the air counterflow was visible from the beginning of water application.

The multiple effects of the location and timing of the air escape routes is a possible catalyst for the greater maximum penetrations obtained in the two-phase tests. Instability of flow in porous media, near the wetting front tends to manifest itself as a fingering type of penetration. Air pressure build-up in pockets with corresponding lower pressure regions would tend to reinforce this fingering or channeling and would be consistent with the discrete locations of air counter-flow.

Delayed Water Application

Nine delayed application trials, SN 31, SN 32, SN 33, SN 35, SN 36, SN 39, SN 40, SN 42, and SN 43 were tested. Six of these resulted in total penetration of the compacted snow samples. In three of the four cases where the interval between the $1 \text{ cm}^3/\text{cm}^2$ applications was 30 seconds, the

front penetration was less than the front penetration when the time interval was 10 seconds. Tests SN 35 and SN 36, with delays of 10 seconds and 30 seconds, respectively, both had front penetrations of 40 cm. The front penetration also exhibits a direct relationship with snow density.

Single applications of 2 and 3 cm³/cm² respectively in tests SN 24 and SN 24 did not result in full penetration by the water. Delayed application tests SN 33, SN 35, and SN 36, with all other independent variables comparable, were all totally penetrated. Similarly, the dual application tests SN 39 and SN 40 both had full penetration while the single-application test SN 37 had only partial penetration.

Ice-Capped Densities

The twenty-two snow samples that were measured by the scintillation apparatus for final density in the ice-capped zones are summarized in Table B-1. Air and water saturations at the time of freezing are calculated from the initial snow porosities and final ice-capped densities.

Cases in which complete penetration, and hence severe desaturation did not occur are characterized by high ice-capped densities. All such samples have final densities above 0.87 g/cm³ from corresponding water saturations above 0.8. In Figure A-5, a photograph of test TS 5, with the highest measured ice-capped density, shows the solid ice-type appearance of these saturated samples. Pure ice has a density of 0.917 g/cm³, whereas that measured for sample TS 5 is 0.94 g/cm³. The high reading is probably a result of lateral expansion of the ice upon freezing with a corresponding expansion of the container diameter. This would result in a lower count from the scintillation scaler and thus a slightly high density measurement. In most cases, the compression of the

residual air would allow for the density change of water, upon phase change, without distortion of the sample container.

The samples which were fully penetrated by water exhibited much lower densities in the ice-capped region indicating substantial drainage. In all cases of full penetration, the final densities for the ice-capped region were below 0.81 g/cm^3 , with the majority of samples having densities of approximately 0.70 g/cm^3 . The water saturation for these cases were all below 0.70, with many falling in the range 0.4 to 0.65. Figure A-5 is a photograph of the sample TS 5 drained to a water saturation of 0.21 resulting in the final ice-capped density of 0.58 g/cm^3 .

The five tests with water temperatures significantly above 0°C have calculated water saturation that will probably be somewhat below those that actually existed in the upper portion of the ice-capped zone. This is a result of the formation of larger pores, as discussed earlier, by melting.

The residual air saturation is probably between 0.07 and 0.04 which were the lowest calculated air saturations, from tests SN 37 and TS 10, respectively.

Results with Implanted Thermocouples

Temperature-time profiles for the thermocouples of the eighteen tests TS 1 to TS 18 are plotted in Figures B-1 to B-18. Each set of symbols represents the equivalent temperature of the thermocouple reading, varying with time, at a particular depth. The one characteristic common to all of the tests is the abruptness of temperature change indicating progression of the wetting front during infiltration. The sharp rise in temperature at the surface is coincident with the application of water

to the snow pack.

For tests TS 4 and TS 5, the temperature at a depth of 2 cm appears to rise to 0°C immediately after water application. In both of these cases, fracturing of the upper snow pack occurred when the thermocouple at the 2 cm depth was inserted. Vertical fractures from the surface down to the thermocouple would result in an almost immediate penetration of water to the thermocouple.

The rapid changes from initial snow pack temperature to 0°C tend to suggest that the heat transfer associated with the infiltration is convection controlled. During the time scale of infiltration, temperature changes appear to be the result of water movement only. In many of the temperature profile figures the last thermocouple rising in temperature exhibits a slower rise than the other thermocouples for the same sample. This phenomenon will be discussed in further detail shortly.

In each case, except test TS 18, the deepest thermocouple plotted showed no change from its initial temperature over the time considered. Test TS 18 was fully penetrated with a channel running off-centre; thus from Figure B-18 the channel has probably developed by 75 sec. and there is radial heat transfer taking place from the warmer channel to the cooler surrounding snowpack.

Table B-2 presents some of the previously summarized data along with two new variables for the tests TS 1 to TS 18. The column headed "Water / (0.95 x Porosity)" indicates the depth of snow required to absorb the water applied if the residual air saturation was considered to be 0.05 and the snow was saturated to that point. It has been discussed earlier in this study that the residual air saturation may be as low as

0.05.

Apparent front penetration at infiltration time, in Table B-2 represents the depth to which thermocouple measurements indicate water penetration, from water application to the observed infiltration time.

For all cases where the water temperature is 0°C the observed front penetration is always greater than, but within 0.5 cm of the calculated saturated penetration value. The fracturing in tests TS 4 and TS 5 does not seem to have effected front penetration in this respect. When the water temperature is greater than 0°C the front penetration is more than 1 cm greater than the calculated saturated penetration. Test TS 11 is the only exception with the difference being 0.6 cm.

In all cases, the apparent front penetration at infiltration time is very close to the observed front penetration. When the water temperature is 0°C this is also close to the saturated penetration depth.

Tests TS 2, TS 4, and TS 9, (Figures B-2, B-4, and B-9) illustrate the slower approach to 0°C for the deepest thermocouple indicating a temperature rise over the time interval. In each of these cases, the thermocouple in question is near the penetration front and hence did not experience the magnitude of flow past it that less deeply placed thermocouples did. The slower change to 0°C is indicative of this lower flow that is also coupled with the freezing at the front which will partially determine how great the maximum penetration will be. In cases where the thermocouple reading indicates a rapid change to zero, the water at that depth is able to give up enough latent heat to bring the snowpack into thermal equilibrium with the water of 0°C . For the deepest thermocouples showing temperature rise, the amount of latent heat required for thermal equilibrium between the snow and water is not available from the water

present. This situation could be a combination of two effects. Firstly, as the water has been flowing through the snow pack more and more heat has been taken out of it, specifically in the front region; at a certain level the leading water may be without sufficient latent heat due to the previous cooling. Secondly, the first water penetrating any level during infiltration will be at considerably less than full saturation quantities; if this fringe is not rapidly followed by higher saturations the amount of water at the level of penetration may limit the latent heat available to raise the snow pack temperature.

From the five figures B-11, B-12, B-15, B-16, and B-18 of tests TS 11, TS 12, TS 15, TS 16 and TS 18, it is clear that even when water of temperatures as high as 10°C is flooded onto these snowpacks, the temperatures at the 2-cm depth do not go above 0°C.

SIMULATION OF INFILTRATION

The numerical simulation examples of infiltration into snow cited in this study are summarized in Tables E-1 and E-2 and Figures E-1 to E-7. All results presented are from the explicit model, Appendix D, as the steep saturation gradients resulted in instability of the implicit finite-difference scheme.

For all cases, one-phase flow assumptions are in effect; the air phase is stationary and has a pressure of one atmosphere. Only the initial infiltration is modeled; hysteresis is not considered. A 10-cm-long model of 20 finite-difference intervals, each being 0.5 cm, is used. Water density and viscosity taken at 0°C are 1 g/cm³ and 0.0170 poise, respectively; the gravitational constant is 980 cm/sec². Initial

saturation throughout the snowpack is assigned a value of 0.002; the residual air saturation is assumed to be 0.05 on the imbibition cycle. Permeability of snow is either $3.0 \times 10^{-6} \text{ cm}^2$ or calculated from Kuriowa [28].

$$k_{ow} = 1.17 \times 10^{-9} \exp(15.9 \phi) \quad (48)$$

as indicated in Tables E-1 and E-2. Relative permeability is assumed to be defined by the relationship

$$k_{rw} = S^{*n} \quad (49)$$

where n is defined as either 2.5, 3.0 or 4.0.

Infiltration Without Phase Change

The first simulations discussed, Table E-2, assume no physical changes to either the snow or water during infiltration.

Figure E-1 illustrates the response of the finite difference model to different capillary pressure-water saturation curves. The drainage curve in Figure E-1 is similar to that found by Colbeck [12] but is shifted to the left to fit a residual air saturation of 0.05 and a residual water saturation of 0.0. The imbibition curve is constructed by arbitrarily lowering the flat portion of the curve by approximately 1500 dyne/cm^2 . This relative difference in capillary pressure-water saturation relationship would also be anticipated with variations in porosity (which consequently represent variations of average pore size). Lower-porosity snow, with smaller pore sizes, would have relatively higher flat portions in the capillary pressure-water saturation curve than would higher-porosity snow. From Figure E-1 it is clear that these different curves do

effect the rate of advancement of the wetting front but the relative shape remains the same.

There is not enough information in either the work by Colbeck [9] [12] or Friesen [19] to define a set of capillary pressure-water saturation curves for various snow porosities. For the remaining simulations only one curve is used. This curve is illustrated in Figure E-2; it is the same as the imbibition like curve of Figure E-1, except at higher water saturations. The gradient of this capillary pressure water saturation curve is flatter, at greater water saturations, then approaches a capillary pressure of zero, slower. The data from Friesen [19] indicate that the capillary pressure relationship will exhibit this type of behaviour; the Colbeck [9], [12] data does not define the desaturation curve in detail near complete saturation.

The top boundary of the numerical model had a narrow interval of 0.25 cm to enable finer treatment of upper boundary conditions. Simulations CB 1 to CB 4 illustrate the model response to two types of conditions. First CB 1 and CB 3 consider the upper boundary to be under a pressure head of the calculated ponded water while the second type of boundary condition used in simulations CB 2 and CB 4 considers the top interval to be saturated, with no ponding effect. In Table E-1 these conditions are referred to as ponded and saturated, respectively.

Figure E-3 shows the infiltration profiles of these four cases. A faster front advancement for a porosity of 0.49, is indicated, when the top surface is considered to be under ponded conditions. Final infiltration time for CB 1 and CB 2 are 2.68 and 2.95 seconds respectively; the relative shapes of the profiles are the same for both upper boundary conditions.

For a porosity of 0.56, Figure E-3, the rate of advancement for the two boundary conditions is nearly the same; final infiltration times for CB 3 and CB 4 are 1.1 and 1.15 seconds, respectively. Both of these are more than twice as fast as the infiltration in the 0.49 porosity simulations. Permeability for the higher-porosity cases is approximately three times greater than for the lower-porosity examples. The similar rates of advancement for CB 3 and CB 4 are a result of very limited ponding predicted by the model.

Figure E-4 gives a more complete illustration of the model response to porosity and permeability differences under saturated surface conditions. The simulation with a porosity of 0.49, CP 4, indicated an infiltration time of approximately 8.6 seconds for 2 cm of water. With a porosity of 0.56, CP 5, it took only 3.1 seconds for the 2 cm of water to infiltrate.

Figure E-5 represents the infiltration profiles of simulations CP 1, CP 2 and CP 3, under ponded conditions, one second from the start of infiltration, for porosities of 0.56, 0.50 and 0.45. The relative shape of each wetting front profile is very similar.

The model response to varying the exponent in the relationship

$$k_{rw} = S^{*n} \quad (50)$$

is shown in Figure E-5. Assigning values of n over the range 2.5 to 4.0 slightly changes the shape of the wetting front. As the exponent n increases the wetting front does tend to become more abrupt. The infiltration time increases with increasing magnitude of n ; for CN 1, CN 2, and CN 3 the calculated infiltration times are 3.1, 2.85, and 2.7 seconds, respectively.

Pseudo Freezing

A series of simulations was designed to investigate the time scale of the freezing process upon infiltration of water into a snowpack. The tests for this section CF 1 to CF 7, are summarized in Table E-2. In all cases 1 cm of water was applied over one second; the ponding upper boundary condition was used.

For each simulation, the initial snowpack temperature was assumed to be uniform at -20°C . Once any interval has reached a predetermined "saturation at freezing", an amount of water that will release sufficient heat, through phase transition, to raise the snowpack temperature of the interval to 0°C , is assumed to freeze. The newly frozen water becomes part of the pore matrix; the porosity, saturation, and permeabilities are accordingly adjusted as shown in Table E-2. As indicated before, not enough information is available to make adjustments to the capillary pressure-water saturation relationship, for different porosities. The larger the assigned value of "saturation at freezing", the longer each interval will stay at the initial porosity.

Although this is a crude method of observing the dynamics of the phase change process, it does offer some instructive information.

Most conceptual models of simultaneous fluid flow and heat transfer in porous media consider that the intimate contact of the fluid and the solid pore matrix is sufficient to justify the assumption of complete thermal equilibrium, with the flow rates encountered. de Quervain [15] assumes that enough water, percolating in snow below 0°C will freeze to bring the snow temperature to 0°C . Alexeev et al. [3], in their discussion of snowmelt water infiltration into frozen soil, makes the same assumption. If this assumption were followed, the "saturation at

freezing" would be less than 0.1.

Figure E-6 indicates the effect of an imposed phase change with a "saturation at freezing" of 0.9. With initial porosities of 0.49, simulations CF 1, without phase change, and CF 2 with phase change, indicate that there is a noticeable change in the rate of front advancement. The infiltration times are 4.25 and 2.85 seconds for the simulations with and without phase change, respectively. The wetting profile is not as abrupt for the case with phase change.

Initial porosities of 0.56 are used for simulations CF 3 and CF 4. Phase change occurs at a saturation of 0.9 for CF 4, the infiltration time is 1.5 seconds, slightly more than the 1.1 second infiltration time for CF 3. Again the wetting profile for the simulation with phase change is not as well defined, Figure E-6.

Figure E-7, of simulations CF 2, CF 5, CF 6, and CF 7, shows the effect of varying the "saturation at freezing" for an initial porosity of 0.49. The infiltration times are 4.25, 4.75, 5.85 and 6.1 seconds for freezing saturations of 0.9, 0.75, 0.5, and 0.1, respectively. The lower values for "saturation at freezing" result in greater infiltration times, as well as more abrupt wetting fronts.

Snow tests TS 6 and TS 9 with temperatures of approximately -12°C and -17.5°C , both with porosities of 0.49, had infiltration times of 3.6 and 3.4 seconds, respectively, for one cm of water. From the results of simulations CF 1, CF 2, CF 5, CF 6 and CF 7, it is tempting to postulate a "saturation at freezing" between 0.90 and 0.95. It would be dangerous at this time to fit one of many parameters to match a limited quantity experimental data. The effects of porosity change on the capillary

pressure-water saturation curve are not anticipated to be extreme on the infiltration over the porosity ranges encountered with freezing. At least a small moderation in the time delay could be expected, with the greatest decrease of infiltration time for the smallest "saturation at freezing" value.

Summary of Infiltration Simulation

A more detailed and quantitative approach to the infiltration simulation could be used if the capillary pressure-water saturation relationship was defined over a range of snow porosities. Although the results of this portion of the study cannot be directly applied and compared with the experimental results certain qualitative statements are of importance.

Firstly, it is evident that the hydraulic properties of snow do effect the rate of infiltration, but at the same porosity these changes will not affect the shape of the wetting front significantly.

Similarly, upper boundary conditions do have an effect on the infiltration time, but whether the water is ponded, or just supplied at a rate sufficient to keep the surface saturated without ponding, the infiltration profile has the same shape. Even changing the exponent he relative permeability relationship, $k_{rw} = S^{*n}$, only changes the shape of the profile a small amount.

Finally, the simulations modeling phase change suggest that contrary to similar studies, the first water infiltrating into a frozen porous medium does not necessarily freeze.

OVERVIEW OF INFILTRATION INTO SNOW

Validity of One-Phase Approach

The infiltration of water into a packed snowbed is a process where one-phase flow assumptions should normally be valid. In the first place, water application on a snow road surface will not be uniform over the entire surface at any particular time. This would allow air to escape upwards through the surface where no water has as yet been applied. Secondly, lateral flow of air would take place through the side of the road bed. In any case, the experimental tests discussed earlier indicate front penetration will not be significantly different whether counter-flow of air is experienced or not.

If the pressure build-up in the air phase is significant in localized areas, counter-flow of air in discrete locations could occur. This in turn may result in a greater maximum penetration by the water with possible desaturation of the ice-capped zone.

At this point, the simulation of two-phase flow is not warranted as the occurrence of the fluctuating counterflow with combined effects of freezing passageways is not predictable.

Channeling/Fingering

When full penetration of a snow test sample occurred, a distinct channel formed from a zone of random-like penetration below the well defined front penetration. As noted earlier, there was no preference for location of the channels over the cross-section of the sample.

The channeling or fingering activity is probably the result of interrelated phenomena. The most obvious explanations for the discrete

location of these channels are; firstly, that the channels are developed along paths of higher permeability, and secondly, that the channels form in areas where the water is not frozen as readily across the rest of the cross-section. Relating to both of these, inhomogeneities of a snow-pack in the horizontal plane may result in distinct locations of lower density. The lower density in these areas would result in higher permeabilities. As well, these low density areas would not be capable of absorbing as much heat, as the higher density areas, by a rise in temperature to the equilibrium 0°C . Thus, these low density areas would be locations of less freezing as well as higher permeability.

In a study by Gupta et al [24], the characteristics of fingering formation in Hele-Shaw models are discussed. It is noted that irregularities in a porous medium may cause perturbations that will result in fingering phenomena along a drainage or imbibition front. Numerous fingers would begin to form at the front in the Hele-Shaw models but would normally merge into one; some of the shorter fingers would be damped out without merging.

From a wave length perturbation analysis discussed by Gupta et al. [24], a higher fluid velocity requires less significant irregularities in the medium to result in fingering. Once fingering has started, viscous forces and pressure gradients within the porous medium will tend to favour the development of one of the fingers.

For the snow infiltration tests where water only penetrated the snow sample partially, freezing controlled the development of all fingering or channeling. When snow samples were fully penetrated, freezing across the sample, other than where the channeling was occurring, would reinforce the fingering phenomena of development of one major finger.

freezing across the sample, other than where the channeling was occurring, would reinforce the fingering phenomena of development of one major finger.

Laminar Flow

The Reynolds number for saturated flow in porous media is defined

$$Re = \frac{\bar{u}\bar{d}}{\nu} \quad (51)$$

where:

Re = Reynolds number, dimensionless

\bar{u} = Darcy or bulk velocity, $\text{cm}^3/\text{cm}^2/\text{sec}$

\bar{d} = average grain diameter, cm

ν = kinematic viscosity, cm^2/sec .

It is normally considered that below a Reynolds number of approximately 1.0, the flow is in the linear laminar range and Darcy's law holds. The transition range from Reynolds numbers 1.0 to 10.0 indicate the beginning of departure from Darcian flow.

From Laliberte [31]

$$\bar{u} = \bar{v} \phi S_w \quad (52)$$

where

\bar{u} = Darcy or bulk velocity, $\text{cm}^3/\text{cm}^2/\text{sec}$

\bar{v} = average velocity in porous medium, cm/sec

ϕ = porosity, dimensionless

S_w = water saturation, dimensionless.

\bar{v} is approximated from Figures B-7, B-9, and B-16 of tests TS 7, TS 9 and TS 16 by the apparent front penetration at infiltration time.

As indicated below, the calculated value of \bar{u} , using $S_w = 0.95$, is very close to the amount of water applied divided by the infiltration time.

Test	\bar{v} (cm/sec)	\bar{u} (cm/sec)	W/LT (cm/sec)	Re
TS 7	0.435	0.20	0.22	0.84
TS 9	0.59	0.28	0.30	1.19
TS 16	0.67	0.30	0.26	1.26

The calculated Reynolds numbers above are based on the indicated values of \bar{u} , water kinematic viscosity at 0°C, 0.0179 cm²/sec, and average snow grain diameter of 0.75 mm. If an average grain diameter of 0.50 mm is used, the Reynolds numbers for tests TS 7, TS 9 and TS 16 are 0.50, 0.80, and 0.84, respectively.

From the Reynolds number calculations, it seems that the flow for the infiltration tests into snow are in the laminar range but may experience slight non-linearity. This non-linearity could cause a slight departure from Darcian flow. However, the effects should not be great, particularly because the infiltration is actually unsaturated flow, and the above calculations of Reynolds number will over-estimate the actual relationship of inertial to viscous forces.

Significance of Snow Permeability

From the experimental tests and the simulation of infiltration, it appears that the permeability of the snow is critical in determining

the final character of the ice-capped zone. Whether the upper zone desaturates or not, probably depends to a large extent on the rate of front advancement. Although the capillary suction of lower permeability media is greater, the greater permeability controls the penetration. This is also substantiated by the results of tests with Selkirk silica sand of different grain sizes.

The work of Friesen [19] indicates that for higher density snow, the capillary pressure curve tends to be flatter for the more dense snow, especially at lower saturations. The average capillary pressures across the flat portion of Friesen's curves [19] for densities of 0.48 g/cm^3 and 0.40 g/cm^3 are approximately 10% higher for the denser snow. The permeability for the less dense snow, from Kuriowa's equation (37), would be approximately 400% greater than the high density snow.

Effect of Age Hardening of Snow

A processed, compacted, snowroad will undergo metamorphism, called sintering, as the snow grains bond together at their points of contact. This process will result in a reduced surface area of the grains within the snowpack. The joining of the snow grains is what gives a normal snowroad its strength. For the ice-capping process, this metamorphosis has further implications.

The decrease in surface area of the snow grains results in a decrease of specific surface, s , in the Kozeny-Carman equation (34), $k_{ow} = \phi^3 / 5s^2$. Thus, the longer the interval between preparation of a snowbed and the application of water, the greater the permeability.

The results of linear regression models MSN 1, MSN 2, MSN 10 and MSN 11, all substantiate a reduction of specific surface. Increased

permeability will have a significant effect on the maximum penetration. In cases where total penetration is a strong possibility, the age hardening time may be critical.

THERMAL EFFECTS

Freezing of Water

The latent heat lost by water freezing at 0°C is 79.7 cal/g . Snow with a density of 0.5 g/cm^3 and a specific heat of $0.5 \text{ cal/g } ^{\circ}\text{C}$ requires 0.25 cal/cm^3 for each 1°C its temperature is raised. Thus, over a rise of 20°C , 1 cm^3 of this snow would absorb 5.0 calories, the equivalent of only 0.063 g of water freezing.

Pore Changes

From de Quervain [15], equation (24), when initial pore diameters are as small as 1 mm the diameter changes are insignificant even after month of gravitational water flow at 0°C . The thermal gradients associated with snow grain growth in these cases are small, Colbeck [9]. The increased pore sizes observed in tests SN 45 to SN 48, TS 11, TS 12, TS 15, TS 16, and TS 18 are probably a result of rapid melting due to the high water temperatures.

Evaporation

An analysis of energy requirements due to the evaporation within the snowpack shows that the effects would be negligible in contributing to the freezing of the penetrating water. As an extreme case consider the air to be saturated at -20°C ; when infiltration occurs, assume enough water evaporates to saturate the air at 0°C . Using the saturated vapour

pressures and ideal gas law, approximately 2.25×10^{-6} g-moles, or 4.05×10^{-6} g of water per cm^3 of air need to evaporate in order to saturate the air at the higher temperature. The latent heat of vaporization at 0°C is 597 cal/g, thus the amount of heat lost by the water would be only 2.42×10^{-3} calories per cm^3 of air undergoing this temperature rise.

Heat Loss in the Radial Direction

A simple analysis of natural convection heat transfer from the side of a uninsulated sample indicates that during the infiltration process, heat loss in the radial direction for the tests performed is not significant.

For this analysis the area of interest considered is the top 6 cm of the sample where infiltration has occurred and the wall temperatures are 0°C . Ambient air temperature is assumed to be -20°C .

The Prandtl number

$$\text{Pr} = \frac{\mu C_p}{k} \quad (53)$$

where

Pr = Prandtl number, dimensionless

μ = viscosity, g/cm-sec

C_p = specific heat capacity, cal/ $^\circ\text{C}$

k = thermal conductivity, cal/sec-cm- $^\circ\text{C}$.

The Grashof number

$$\text{Gr}_L = \frac{\beta g \rho^2 L^3 \Delta T}{\mu} \quad (54)$$

where

Gr_L = Grashof number, dimensionless

β = coefficient of thermal expansion for air, $^{\circ}C^{-1}$

g = acceleration of gravity, cm/sec^2

L = characteristic length for heat exchange, cm

ΔT = temperature difference between side of sample and bulk
air temperature, $^{\circ}C$

μ = air viscosity, g/cm-sec .

When $L = 6$ cm, and $\Delta T = 20^{\circ}C$, $Gr_L = 1.1 \times 10^6$. Thus for $Gr_L Pr \approx 7.9 \times 10^5$, the convective heat transfer coefficient from Welty, Wicks, and Wilson [57] is $h \approx 5.25 \times 10^{-5}$ cal/sec-cm²- $^{\circ}C$. The rate of heat exchange is defined as

$$q = hA(\Delta T) \quad (55)$$

where

q = heat flux, cal/sec

h = convective heat transfer coefficient, cal/cm-sec- $^{\circ}C$

A = surface area of exchange, cm²

ΔT = temperature difference, $^{\circ}C$.

The top 6 cm of a 10-cm diameter sample has an area of 188 cm². The heat flux without insulation would be approximately 1.98×10^{-1} cal/sec. Even without the insulation the heat loss from the sides of the test samples, over the time period of infiltration, is small.

Freezing at the Front

The extent of freezing at the wetting front determines whether

the ice-capped zone will remain saturated, or will experience drainage through channeling. Simulation of infiltration into snow predicts a sharp, well defined wetting front, but not as well defined as the experimental results indicate. Cross-sections of the snow infiltration tests showed a definite boundary between totally unsaturated snow below and almost totally saturated snow above.

As the last water from the surface has infiltrated into the snow and desaturation at the top begins, the wetting front is moving much more slowly than during initial stages of infiltration. At the front, the advancing low saturation portion will begin to freeze, decreasing the permeability of the snow and slowing the rate of wetting front penetration even more. This will result in more water freezing and continually slower front advancement. Finally, the front is completely frozen off, and saturated above. This slowing of advance rate is consistent with the thermocouple observations noted earlier. Of course, fingering or channeling may subsequently take place, past the frozen front.

If the capillary pressure relationships, permeabilities and other medium properties associated with the infiltration simulation, model actual snow characteristics well, it appears that little freezing of water takes place until the front is close to its final penetration depth. Relatively high velocities above the final front penetration may result in latent heat effects being distributed over a volume of water significantly greater than the low saturation zone of the front. Sub-cooling of the water with little freezing could result. If any turbulence were present at the front, the cooling of the water would definitely be over a greater volume.

The validity of the capillary pressure and permeability relationships for snow of different age-hardening times will have to be investigated further before this type of description can be completely accepted.

RE-FREEZING TEST AND SIMULATION

Compacted snow, with a density of 0.42 g/cm^3 , at approximately -18°C was ice-capped with 2 cm of 0°C water. The cooling of the ice-cap is indicated in Figure F-1. It takes approximately one day for the snow in the sample container to return to its initial temperature. The front penetration for this sample was approximately 4.5 cm with significant penetration to 6 cm. The upper ice-capped zone was observed to be partially desaturated.

A simulation of the re-freezing, using the one-dimensional finite-difference "excess-degree" technique of Appendix D, is compared with the experimental test in Figure F-1. The model has a 0.5-cm interval at the top with thirty 1.0-cm intervals below; thus nodes are at the surface, -1 cm, -2 cm, etc. with a total model depth of 30.5 cm. Water saturation is approximated as being 0.60 over the top 5.5 cm. The top boundary temperature is fitted to the observed results while the bottom boundary is held constant at -18°C . Initial temperatures are 0°C where water has penetrated and -18°C where it has not.

The effective thermal conductivity of dry snow is approximated as $k_e = (5.35 - 6.6 \rho_s) \times 0.001 \text{ cal/cm-}^\circ\text{C-sec}$. When liquid water and snow co-exist the expression from equation (45) is used.

From Figure F-1 it is evident that the freezing of the one-dimensional simulation model is somewhat slower than for the actual test. Several conditions are responsible for this. Firstly, over the time period

considered, radial heat transfer will not be negligible. The heat transfer will be accelerated due to the heat requirements necessary to raise the temperature of the 1-cm thick PVC container. On a more localized scale, the glass sheathing of the thermocouples will result in a higher conductivity away from the area directly around the thermocouples. Consequently, the freezing times predicted by the simulation model are probably reasonable even if they are somewhat conservative.

Five simulations were carried out with snow densities of 0.50 g/cm^3 and water temperatures of 0°C . For snow and ambient temperatures both at -18°C or -10°C , water applications of $2 \text{ cm}^3/\text{cm}^2$ and $3 \text{ cm}^3/\text{cm}^2$ are simulated. The penetration for these cases is assumed to be uniform to depths of 4.5 cm and 6.5 cm; equivalent to final densities of approximately 0.9 g/cm^3 . The upper boundary is temperature controlled from observed surface temperatures. Predicted times for re-freezing are given in Table F-1.

The bottom boundary temperature used is not critical. Simulations RF 1 and RF 5 are identical except the bottom boundary temperature for RF 5 is 8°C higher than RF 1; the re-freezing time for RF 5 is only 0.3 hours greater.

The use of a temperature controlled top boundary condition has been shown to be effective over longer periods of time, (Wilson [60]). More accurate results would be obtained for this short-time -freezing situation with a complete energy balance at the surface. This would include radiative, convective and evaporative considerations that would be unique for any given location and time. The top boundary temperatures used were from experimental observations in a controlled cold room. Convective heat transfer from the surface with limited air circulation

would be small, and although the surface of an ice-capped snow road is relatively smooth, the convective surface heat exchange in natural conditions would be greater.

The predicted times for re-freezing should be assumed to be an upper boundary.

PRACTICAL IMPLICATIONS

One of the major objectives of this study was to develop guidelines for practical use in ice-capped snow road construction.

The U.S. Army Corps of Engineers equation (29), for penetration of water into cold snow is unsuitable for this ice-capping process where application rates are high, and where freezing at the wetting front can retain high saturations near the surface.

From an efficiency and conservation point of view, the less water wasted, in arctic and sub-arctic regions, the better. It will be more desirable to achieve a high saturation in the ice-capped zone on the first application of water. It would be undesirable to have the ice-capped zone desaturate significantly. Figure C-1 defined relatively safe conditions for the application of water to a compacted snowbed without significant desaturation. In all cases, the water temperature is 0°C . The guidelines of Figure C-1 should be used for field operation; the snow temperature is the average temperature in the upper 2 to 7 cm depending on what front penetration is expected. Water temperatures significantly greater than 0°C result in greater drainage of the ice-capped zone with slightly increased front penetration.

If more detail is required, in the response of infiltration to variations in independent variables, any of the linear regression models of Appendix C, for the particular range of variables should yield

further information. In all cases, the front penetration will be well defined. For most situations the models MSN 4, MTS 7 and MTS 8 should be suitable.

$$\text{MSN 4: } FP = -0.68 + 0.013 T_s + 1.18 \rho_s + 2.36 W$$

$$\text{MTS 7: } FP = -0.11 + 2.30 W$$

$$\text{MTS 8: } FP = -3.90 + 8.27 \rho_s + 2.24 W$$

Model MSN 4 was fitted over a density range of 0.35 to 0.50 g/cm³, both MTS 7 and MTS 8 were fitted over a range of snow densities 0.45 to 0.50 g/cm³.

The problem of estimating maximum penetration is not as well defined due to its randomness. Different models will have different critical values, for various water application amounts, indicating when significant desaturation could occur. Tests SN 30 and SN 38 had maximum penetrations of 11.5 cm and "full penetration", respectively. Using the data for these two tests, model MTS 6 predicts maximum penetrations of 8.6 cm and 9.8 cm, respectively. Model MSN 6 on the other hand predicts maximum penetrations of 14.6 cm and 15.9 cm for tests SN 30 and SN 38. In both cases a critical range of predicted maximum water penetration is defined for 3 cm³/cm² of water application. If model MTS 6 were being used, a predicted maximum penetration of approximately 9.0 to 9.5 cm would indicate a strong possibility of significant desaturation in the ice-capped zone. Similarly when using model MSN 6, the critical depth of predicted maximum penetration would be approximately 15.0 cm.

The application of water to a packed snowbed should be a one-

step process. To ensure small losses from run-off the water application rate should be estimated from one of the linear regression models for infiltration time. This will ensure that only limited ponding at the snow surface will occur. Slower infiltration rates will be experienced when only limited ponding is allowed; this could tend to reduce the occurrence of channel formation. Uneven flooding should be avoided as it could result in localized pressure build-up in the air phase; again contributing to channel formation and desaturation of the ice-capped zone. A snowpack with few heterogeneities will be less prone to desaturation than one that has significant permeability differences. The processing of the road surface should be reasonably uniform. Re-freezing of the ice-capped zone will take place within approximately one half day from the time of water application.

CHAPTER V

CONCLUSIONS AND RECOMMENDATIONS

The laboratory and numerical simulation results of this study have identified the controlling parameters, and some general relationships, of water infiltration into a packed snowbed. Consequently, guidelines for practical use are recommended, and phenomena important to further investigations of water flow in snow are cited.

The infiltration of water into a packed snowbed results in two distinct zones of penetration. To a depth, referred to here as the front penetration depth, the penetration is uniform; this is the ice-capped zone. Below this level, penetration may occur to significant depths by developing discrete channels or fingers. Well defined relationships for the depth of front penetration have been established by this study. In all cases when the water temperature was 0°C the front penetration was slightly greater than the depth required to hold the applied water at a saturation 0.95. For an initial snow density of 0.50 g/cm³ the front penetration will be approximately 2.2 cm per cm³/cm² of water applied.

Formation and penetration of channels past the front penetration is not as well defined. The further these channels or fingers penetrated past the front penetration, the more desaturation occurred in the ice-capped zone. Higher values of water temperature, amount of water applied, snow temperature and lower values of snow density favour the formation of channels and hence desaturation. The linear regression models of Appendix C provide details of the response of maximum penetration to the various independent variables.

Figure C-1 indicates operating conditions that should be followed in order to minimize the effects of desaturation. If 3 cm of water is applied the snow temperature will need to be lower than -20°C to ensure limited desaturation.

In order to obtain highly saturated ice-capped zones of greater than 7 cm, more than 3 cm of water will need to be applied to a snowpack of density significantly greater than 0.50 g/cm^3 at a temperature significantly less than -20°C .

Final density determinations indicate that the residual air saturation for the imbibition of water into snow is approximately 0.05. When desaturation of the ice-capped zone occurs, the final water saturation above the front penetration may be as low as 0.30. The saturation in the ice-capped zone may be high enough to result in a density approaching that of pure ice.

From high speed thermocouple measurements it appears that heat transfer during the infiltration process is convection controlled.

If the hydraulic properties of snow used in the infiltration model are reliable, the actual freezing of significant amounts of water does not take place near the surface, although sub-cooling certainly occurs.

Analysis of experimental data indicates that metamorphism during the age-hardening time has a significant effect on increasing the permeability of the snow. This, in turn, increases the possibility of channeling and associated desaturation.

The infiltration simulation indicates that changes in properties of snow do not significantly affect the shape of the wetting front although the infiltration time can be greatly affected. Permeability

controls the rate of infiltration more than any other porous medium characteristic of snow.

Several studies that could further the work of this, and other investigations of water infiltration into a packed snowbed are desirable. These include:

i) Further laboratory work using snow of high densities at low temperatures to investigate the possibilities of saturated ice-capping to a depth greater than 7 cm.

ii) Full scale field tests are needed to substantiate and, if necessary, modify the results of this study.

iii) A detailed investigation into the occurrence and formation of channels during the infiltration process.

iv) More information about the physical properties of snow as a porous medium are needed. Capillary pressure relationships, during imbibition, and for a range of densities.

v) The effect of change of physical properties during age hardening metamorphism needs to be investigated in greater detail.

vi) Tests should be performed with continuous monitoring of single thermocouples during the infiltration process in order to more thoroughly understand the coupling of fluid flow and heat transfer.

vii) Further lab testing with non-linear data analysis, and dimensional analysis should be pursued placing emphasis on identification of desaturation situations.

viii) Re-freezing simulation should be dealt with in more detail using a complete surface energy balance.

BIBLIOGRAPHY

- [1] Adam, K.M., Normal Wells Winter Road Research Study, to Canadian Arctic Gas Study Limited, Inter-Disciplinary Systems Limited, Winnipeg, Manitoba, 1973.
- [2] Adrian, D.D. and Franzini, Impedance to infiltration by pressure build-up ahead of the melting front, *J. Geophys. Res.*, Vol. 71, No. 24, 5857-5862, 1966.
- [3] Alexeev, G.A., Kaljuzhny, I.L., Kulik, V. Ya., Pavlova, K.K., and Romanov, V.V., Infiltration of snowmelt water into frozen soil, *The Role of Snow and Ice in Hydrology Symposium*, IAHS-AISH Publication No. 107, Vol. 1, 313-324, IAHS-UNESCO-WMO, 1973.
- [4] Bruch, J.C., and Zyvoloski, G., Solution of equation for vertical unsaturated flow of soil water; *Soil Sc.*, Vol. 116, No. 6, 417-422, 1973.
- [5] Brustkern, R.L., and Morel-Seytous, H.J., Analytical treatment of two-phase infiltration, *J. Hydraul. Div., Proc. Amer. Soc. Civil Eng.*, Vol. 96, No. Hy 12, 2535-2548, 1970.
- [6] Brustaert, W., A solution for vertical infiltration into a dry porous medium, *Water Resour. Res.*, Vol. 4, No. 5, 1031-1038, 1968.
- [7] Colbeck, S.C., One-dimensional water flow through snow, U.S. Army Cold Regions Research and Engineering Laboratory, Research Report 296, Hanover, New Hampshire, 1971.
- [8] Colbeck, S.C., A theory of water percolation in snow, *Journal of Glaciology*, Vol. 11, No. 63, 369-385, 1972.
- [9] Colbeck, S.C., Theory of metamorphism of wet snow, U.S. Army Cold Regions Research and Engineering Laboratory, Research Report, Hanover, New Hampshire, 1973.

- [10] Colbeck, S.C., Effects of stratigraphic layers on water flow through snow, U.S. Army Cold Regions Research and Engineering Laboratory, Research Report, Namover, New Hampshire, 1973.
- [11] Colbeck, S.C., Water flow through snow overlying an impermeable boundary, Water Resour. Res., Vol. 10, No. 1, 119-123, 1974.
- [12] Colbeck, S.C., The capillary effects on water percolation in homogeneous snow, Journal of Glaciology, Vol. 13, No. 67, 85-97, 1974.
- [13] Colbeck, S.C. and Davidson, G., Water percolation through homogeneous snow, The Role of Snow and Ice in Hydrology Symposium, IAHS-AISH Publication No. 107, 242-256, IAHS-UNESCO-WMO, 1973.
- [14] Corey, A.T., The interrelation between gas and oil relative permeabilities, Producer's Monthly, Vol. XIX, No. 1, November 1954.
- [15] de Quervain, M.R., Snow structure, heat, and mass flux through snow, The Role of Snow and Ice in Hydrology Symposium, IAHS-AISH Publication No. 107, 203-223, IAHS-UNESCO-WMO, 1973.
- [16] De Wiest, R.J.M., Ed., Flow Through Porous Media, Academic Press, New York, 1969.
- [17] Eckert, E.R.G., and Drake, R.M., Heat and Mass Transfer, McGraw-Hill Book Co. Inc., New York, 1959.
- [18] Freeze, A.R., The mechanism of natural ground-water recharge and discharge
1. One dimensional, vertical, unsteady, unsaturated flow above a recharging or discharging groundwater flow system, Water Resour. Res., Vol. 5, No. 1, 153-171, 1969.
- [19] Friesen, D., A Study of Snow as a Porous Medium, Unpublished Undergraduate Civil Engineering Thesis, University of Manitoba, April 1974.
- [20] Fujino, K., Measurement of flow down speed of melt water in snow cover.
II - Flow of meltwater in snow cover on slope, Low Temp. Sci., Ser. A, Vol. 29, 151-158, 1971.

- [21] Fiesel, W., Renger, M., and Strebel, O., Numerical treatment of the unsaturated flow equations: comparison of experimental and computed results, *Water Resour. Res.*, Vol. 9, No. 1, 174-177, 1973.
- [22] Glover, R.E., *Ground Water Movement*, Engineering Monograph No. 31, U.S. Department of the Interior, Bureau of Reclamation, United States Government Printing Office, Washington, 1966.
- [23] Green, D.W., Dabiri, H., Prill, R., and Weinancy, C.F., Numerical modeling of unsaturated groundwater flow and comparison of the model to a field experiment, *Water Resour. Res.*, Vol. 6, No. 3, 862-874, 1970.
- [24] Gupta, S.P., Varnon, J.E., and Greenkorn, R.A., Viscous finger wavelength degeneration in Hele Shaw Models, *Water Resour. Res.*, Vol. 9, No. 4, 1039-1046, 1973.
- [25] Guyman, G.L., and Luthin, J.N., A coupled heat and moisture transport model for arctic soils, *Water Resour. Res.*, Vol. 10, No. 5, 995-1001, 1974.
- [26] Hanks, R.J., and Bowers, S.A., Numerical solution of the moisture flow equation for infiltration into layered soils, *Soil Sci. Soc. Amer., Proc.*, Vol. 26, 530-534, 1962.
- [27] Harlan, R.L., Ground conditioning and the groundwater response to surface freezing, *The Role of Snow and Ice in Hydrology Symposium*, IAHS-AISH, Publication No. 107, 326-240, IAHS-UNESCO, WMO, 1973.
- [28] Hillel, D., *Soil and Water, Physical Principles and Processes*, Academic Press, New York, 1971.
- [29] Ibrahim, H.A., and Brutsaert, W., Intermittent infiltration into soils with hysteresis, *J. Hydraul. Div., Proc. Amer. Soc. Civil Eng.*, Vol. 94, No. Hy 1, 113-137, 1968.
- [30] Kuriowa, D., Liquid permeability of snow, *Low Temp. Sci., Ser. A*, Vol. 26, 29-52, 1968.

- [31] Laliberte, G.E., Fluid Mechanics of Unsaturated Porous Solids, Course Outline for 34:704, Dept. of Agricultural Engineering, University of Manitoba, Winnipeg, Manitoba, 1970.
- [32] Langman, E.J., A new method of using dye to study meltwater movement within a snowpack, Runoff from Snow and Ice, Hydrology Symposium No. 8, Vol. 2, 74-81, Inland Waters Branch, Department of Energy, Mines and Resources, Ottawa, 1971.
- [33] Male, D.H., and Norum, D.I., Movement of water through snow and ice: a thermodynamic analysis, Runoff from Snow and Ice, Hydrology Symposium No. 8, Vol. 1, 83-107, Inland Waters Branch, Department of Energy, Mines and Resources, Ottawa, 1971.
- [34] Male, D.H., Norum, D.I., and Besant, R.W., A dimensional analysis of heat and mass transfer in a snowpack, The Role of Ice and Snow in Hydrology Symposium, IAHS-AISH Publication No. 107, 258-289, IAHS-UNESCO-WMO, 1973.
- [35] McWhorter, D.B., Infiltration affected by flow of air, Hydrology Papers, Colorado State University, No. 49, Fort Collins, Colorado, 1971.
- [36] Mein, R.G., and Larson, C.L., Modeling infiltration during a steady rain, Water Resour, Res., Vol. 9, No. 2, 384-394, 1973.
- [37] Morel-Seytoux, H.J., Introduction to flow of immiscible liquids in porous media, Flow Through Porous Media (R. De Wiest, ed.), 455-516, Academic Press, New York, 1969.
- [38] Morel-Seytoux, H.J., Two-phase flows in porous media, Advances in Hydro-science (V.T. Chow, ed.), Academic Press, New York, Vol. 9, 199-202, 1973.
- [39] Morel-Seytoux, H.J., and Khanji, J., Derivation of an equation of infiltration, Water Resour, Res. Vol. 10, No. 4, 795-800, 1974.

- [40] Noblanc, A., and Morel-Seytoux, H.J., Perturbation analysis of two-phase infiltration, J. Hydraul. Div., Proc. Amer. Soc. Civil Eng., Vol. 98, No. Hy 9, 1526-1541, 1972.
- [41] Philip, J.R., Theory of infiltration, Advances in Hydroscience (V.T. Chow, ed.), Academic Press, New York, Vol. 5, 215-305, 1969.
- [42] Pikul, M.R., Street, R.L., and Remson, I., A numerical model based on coupled one-dimensional Richards and Boussinesq equations, Water Resour. Res., Vol. 10, No. 2, 295-302, 1974.
- [43] Phuc, Le Van, General One-Dimensional Model for Infiltration, 83 pp. M.S. Thesis, Dept. of Divil Eng., Colorado State University, Fort Collins, Colorado, 1969.
- [44] Phuc, Le Van, and Morel-Seytoux, H.J., Effect of soil air movement and compressibility on infiltration rates, Soil Sci. Soc. Amer., Proc., Vol. 36, 237-241, 1972.
- [45] Pounder, E.R., The Physics of Ice, Pergamon Press Ltd., London, 1965.
- [46] Rubin, J., Theory of rainfall uptake by soils initially drier than their field capacity and its applications, Water Resour. Res., Vol. 2, No. 4, 739-749, 1966.
- [47] Rubin, J., Numerical method for analyzing hysteresis-affected post-infiltration redistribution of soil moisture, Soil Sci. Soc. Amer., Proc., Vol. 31, 13-20, 1967.
- [48] Rubin, J., and Steinhardt, R., Soil water relations during rain infiltration: I. Theory, Soil Sci. Soc. Amer., Proc Vol. 28, 246-251, 1963.
- [49] Rumer, R.R., and Drinker, P.A., Resistance to laminar flow through porous media, J. Hydraul, Div., Proc. Amer. Soc. Civil Eng., Vol. 92, No. Hy 5, 155-163, 1966.

- [50] Shimizu, J., Air permeability of deposited snow, *Low Temp. Sci., Ser. A*, Vol. 22, 1-32, 1970.
- [51] Somerton, W.H., Some thermal characteristics of porous rocks, *Petroleum Transactions, AIME*, Vol. 213, 375-378, 1958.
- [52] Swartzendruber, D., The flow of water in unsaturated soils, *Flow Through Porous Media* (R. De Wiest, ed.), 201-292, Academic Press, New York, 1969.
- [53] Trupp, A.C., The numerical finite-difference approach to heat and mass diffusion problems, *Western Canadian Heat Transfer Conference*, Saskatoon, Saskatchewan, Sept. 6, 1966.
- [54] U.S. Army Corps of Engineers, Snow Hydrology, Report P.D. 20 - 25/52, Office of Divisional Engineer, North Pacific Division, Portland, Oregon, 1956.
- [55] Vachaud, G., and Thony, J.L., Hysteresis during infiltration and re-distribution in a soil column at different initial water contents, *Water Resour. Res.*, Vol. 7, No. 1, 111-127, 1971.
- [56] Vachaud, G., Vauclin, M., Khanji, D., and Wakil, M., Effects of air pressure on water flow in an unsaturated stratified vertical column of sand, *Water Resour. Res.*, Vol. 9, No. 1, 161-173, 1973.
- [57] Welty, J.R., Wicks, C.E., Wilson, R.E., *Fundamentals of Momentum, Heat and Mass Transfer*, John Wiley and Sons, Inc., New York, 1969.
- [58] Wheeler, J.A., Simulation of heat transfer from a warm pipeline buried in permafrost, 74th National Meeting, American Institute of Chemical Engineers, New Orleans, Louisiana, March 1973.
- [59] Whisler, F.D., and Klute, A. The numerical analysis of infiltration, considering hysteresis, into a vertical soil column at equilibrium under gravity, *Soil Sci. Soc. Amer., Proc.*, Vol. 29, No. 5, 489-494, 1965.

- [60] Wilson, T.M., Thermal Simulation-Artificial Islands, Unpublished Report.
Frontier Planning, Imperial Oil Ltd., 1974.
- [61] Wilson, L.G., and Luthin, J.N., Effect of airflow ahead of the melting
front on infiltration, Soil Sci., Vol. 96, 136-143, 1963
- [62] Yen, Y.C., Recent studies on snow properties, Advances in Hydrosience
(V.T. Chow, ed.) Academic Press, New York, Vol. 5, 173-214, 1969.

APPENDIX A

EXPERIMENTAL DATA AND PHOTOGRAPHS OF
INFILTRATION TESTS

Table A-1
 Selkirk Silica Sand (35-50) Tests: Water Temperature 0°C

Test No.	Sand Temperature (°C)	Flow Type	Water (cm ³ /cm ²)	Infiltration Time (sec)	Front Penetration (cm)	Maximum Penetration (cm)
SA 1	- 5	2 Phase	2	118	6	7.5
SA 2	- 5	2 Phase	1	11	3.25	4
SA 3	- 5	1 Phase	2	41	6	7.5
SA 4	- 5	1 Phase	1	15	3	4
SA 5	-20	1 Phase	1	30	2.75	3
SA 6	-20	1 Phase	2	174	5.25	6
SA 7	-20	2 Phase	1	78	2.5	3
SA 8a	-20	2 Phase	2	196	5.5	7
SA 8b	-20	2 Phase	2	222	5.5	8
SA 9	- 5	1 Phase	1	9	3.75	4.5
SA 10	- 5	1 Phase	2	21	8	9.5
SA 11	- 5	2 Phase	1	11	4.5	6
SA 12	- 5	2 Phase	2	45	9.25	full penetration

Table A-1
(continued)

Test No.	Sand Temperature (°C)	Flow Type	Water (cm ³ /cm ²)	Infiltration Time (sec)	Front Penetration (cm)	Maximum Penetration (cm)
SA 13	- 8.5	1 Phase	1	18	3.75	4.75
SA 14	- 8.5	1 Phase	2	46	6.5	8
SA 15	- 8.5	2 Phase	1	29	3.75	4.5
SA 16	- 8.5	2 Phase	2	94	6.5	7.5
SA 17	- 9.5	1 Phase	2	43	5.75	6.5
SA 18	- 9.5	1 Phase	3	112	9.75	11
SA 19	- 9.5	2 Phase	2	137	7	8
SA 20	- 9.5	2 Phase	3	800	10.25	11.5
SA 21	-20	1 Phase	2	188	6.25	7.5
SA 22	-20	1 Phase	3	281	9.5	11.5
SA 23	-20	2 Phase	2	960	6.5	7
SA 24	-20	2 Phase	3	>20 min	8.25	10.5

Table A-2
Selkirk Silica Sand (35-50) Tests

Test No.	Sand Temperature (°C)	Water Temperature (°C)	Flow Type	Water (cm ³ /cm ²)	Infiltration Time (sec)	Front Penetration (cm)	Maximum Penetration (cm)
SA 25	-20	15	1 Phase	2	205	6.5	8
SA 26	-20	0	1 Phase	2	150	6.0	7.25
SA 27	-20	15	2 Phase	2	15 min.	4.75	5
SA 28	-20	0	2 Phase	2	7 min.	5.25	6
SA 29	-10	5	1 Phase	2	42	6.5	8.5
SA 30	-10	0	1 Phase	2	49	6.5	8
SA 31	-10	5	2 Phase	2	>15 min.	7.5	8.5
SA 32	-10	0	2 Phase	2	130	6.5	7

Table A-3

Selkirk Silica Sand Tests: Water Temperature 0°C, 1 Phase Flow

Test No.	Sand	Sand Temperature (°C)	Water (cm ³ /cm ²)	Infiltration Time (sec)	Front Penetration (cm)	Maximum Penetration (cm)
SA 33	20-30	-10	1	3.5	3.0	6.5
SA 34	10-20	-10	1	2.5	2.75	full penetration
SA 35	20-30	-20	1	7.5	2.75	6.5
SA 36	10-20	-20	1	4.5	3.0	6.75
SA 37	20-30	-20	2	40.	5.75	10.25
SA 38	10-20	-20	2	11.	6.0	15.75

Table A-4

Snow Tests

Test No.	Snow Density (g/cm ³)	Snow Temperature (°C)	Aging (hrs)	Water (cm ³ /cm ²)	Water Temperature (°C)	Infiltration Time (sec)	Front Penetration (cm)	Maximum Penetration (cm)
SN 1	0.38	- 8.0	1	1	0	4.5	2.	8.0
SN 2	0.37	- 8.0	1	1	0	5.0	2.	8.5
SN 3 ^{1*}	0.37	- 8.0	1	1	0	11.0	2.	12.0
SN 4 ^{1*}	0.38	- 8.0	1	1	0	11.5	2.	9.0
SN 5	0.44	- 9.0	1	1	0	4.	2.24	5.0
SN 6	0.44	- 9.0	1	2	0	13.	4.5	full penetration
SN 7	0.35	- 9.0	1	1	0	3.	2.0	5.5
SN 8	0.35	- 9.0	1	2	0	12.	4.0	8.5
SN 9	0.43	-10.0	24	1	0	4.	2.25	4.5
SN 10	0.43	-10.0	24	2	0	13.5	4.5	9.5
SN 11	0.35	-10.0	24	1	0	2.5	2.0	9.5
SN 12	0.35	-10.0	24	2	0	7.	4.0	full penetration
SN 13	0.44	-18.0	1	1	0	4.3	2.0	4.0
SN 14	0.44	-18.0	1	2	0	13.2	4.5	6.5

Table A-4
(continued)

Test No.	Snow Density (g/cm ³)	Snow Temperature (°C)	Aging (hrs)	Water (cm ³ /cm ²)	Water Temperature (°C)	Infiltration Time (sec)	Front Penetration (cm)	Maximum Penetration (cm)
SN 15	0.35	-18.0	1	1	0	4.0	2.0	4.0
SN 16	0.35	-18.0	1	2	0	10.2	4.25	6.5
SN 17	0.43	-20.0	24	1	0	5.4	2.0	4.0
SN 18	0.43	-20.0	24	2	0	12.7	4.0	6.0
SN 19	0.35	-20.0	24	1	0	2.9	2.0	6.0
SN 20	0.35	-20.0	24	2	0	8.3	4.25	7.0
SN 21	0.44	-19.0	24	2	0	11.7	4.0	7.0
SN 22	0.44	-19.0	24	3	0	26.1	7.0	10.0
SN 23	0.43	-19.0	24	2	0	14.0	4.75	6.0
SN 24	0.43	-19.0	24	3	0	24.6	7.0	10.0
SN 25	0.35	-19.0	24	2	0	7.4	4.25	10.0
SN 26	0.35	-19.0	24	2	0	8.8	4.0	7.0
SN 27	0.35	-19.0	24	3	0	11.0	7.0	full penetration
SN 28	0.35	-19.0	24	3	0	10.3	7.0	full penetration

Table A-4
(continued)

Test No.	Snow Density (g/cm ³)	Snow Temperature (°C)	Aging (hrs)	Water (cm ³ /cm ²)	Water Temperature (°C)	Infiltration Time (sec)	Front Penetration (cm)	Maximum Penetration (cm)
SN 29	0.49	-19.0	24	2	0	10.9	4.5	9.5
SN 30	0.49	-19.0	24	3	0	23.4	6.5	11.5
SN 31 ⁺	0.49	-19.0	24	1+1	0	5.0(10)10.2	4.5	11.0
SN 32 ⁺	0.49	-19.0	24	1+1	0	3.4(30)10.6	4.25	8.0
SN 33 ⁺	0.43	-19.0	24	1+1	0	2.5(10)3.7	3.75	full penetration
SN 34	0.43	-19.0	24	2.5	0	9.9	3.5	full penetration
SN 35 ⁺	0.41	-19.0	24	1+1	0	2.2(10)3.6	4.0	full penetration
SN 36 ⁺	0.41	-19.0	24	1+1	0	1.9(30)2.4	4.0	full penetration
SN 37	0.50	-16.0	24	2	0	9.0	4.5	10.0
SN 38	0.49	-16.0	24	3	0	15.6	7.25	full penetration
SN 39 ⁺	0.49	-16.0	24	1+1	0	2.7(10)5.9	4.5	16.0
SN 40 ⁺	0.51	-16.0	24	1+1	0	3.3(30)7.0	4.25	full penetration
SN 41	0.40	-16.0	24	2	0	4.0	4.25	full penetration
SN 42 ⁺	0.42	-16.0	24	1+1	0	2.2(30)3.0	4.0	full penetration

Table A-4
(continued)

Test No.	Snow Density (g/cm ³)	Snow Temperature (°C)	Aging (hrs)	Water (cm ³ /cm ²)	Water Temperature (°C)	Infiltration Time (sec)	Front Penetration (cm)	Maximum Penetration (cm)
SN 43 ⁺	0.42	-16.0	24	1+1	0	1.8(10)2.6	4.5	full penetration
SN 44	0.41	-16.0	24	3	0	7.6	6.25	full penetration
SN 45	0.41	-19.0	24	2	5	4.2	4.0	full penetration
SN 46	0.41	-19.0	24	3	5	6.3	6.0	full penetration
SN 47	0.49	-19.0	24	2	5	13.4	5.0	9.0
SN 48	0.50	-19.0	24	3	5	18.1	8.0	full penetration

* Two-Phase Flow

+ Delayed Application: two $1 \text{ cm}^3/\text{cm}^2$ applications of water, infiltration time for the first application is followed by the time delay in brackets, then infiltration time for the second application

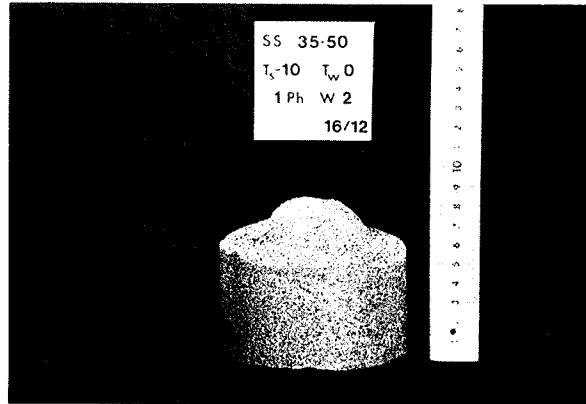
Table A-5
Snow Test with Temperature Measurement

Test No.	Snow Density (g/cm ³)	Snow Temperature (°C)	Water (cm ³ /cm ²)	Water Temperature (°C)	Infiltration Time (sec)	Front Penetration (cm)	Maximum Penetration (cm)
TS 1	0.46	-17	2	0	7.0	4.5	full penetration
TS 2	0.46	-18	2	0	7.2	4.5	full penetration
TS 3	0.48	-16.5	3	0	12.8	7.0	full penetration
TS 4	0.47	-11	2	0	5.8	4.5	full penetration
TS 5	0.48	-11.5	2	0	5.8	4.5	full penetration
TS 6	0.47	-12	1	0	3.6	2.25	7.5
TS 7	0.47	-20	2	0	9.2	4.25	8.0
TS 8	0.47	-19.5	3	0	15.0	6.5	full penetration
TS 9	0.47	-17.5	1	0	3.4	2.25	5.25
TS 10	0.48	-19	2	0	9.4	4.5	7.0
TS 11	0.48	-18.5	2	5	9.8	5.0	8.0
TS 12	0.48	-18	2	10	7.8	5.75	12.0
TS 13*	0.48	-17.5	2	0	31.8	4.5	8.5

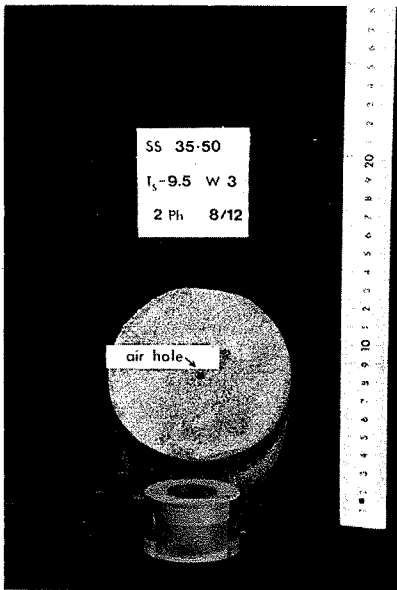
Table A-5
(continued)

Test No.	Snow Density (g/cm ³)	Snow Temperature (°C)	Water (cm ³ /cm ²)	Water Temperature (°C)	Infiltration Time (sec)	Front Penetration (cm)	Maximum Penetration (cm)
TS 14	0.50	-16	3	0	14.2	7.0	full penetration
TS 15	0.49	-16	3	5	15.0	7.75	full penetration
TS 16	0.49	-16.5	3	10	11.6	8.5	full penetration
TS 17*	0.48	-17.5	3	0	82.2	7.0	full penetration
TS 18*	0.49	-18	3	10	36.0	7.75	full penetration

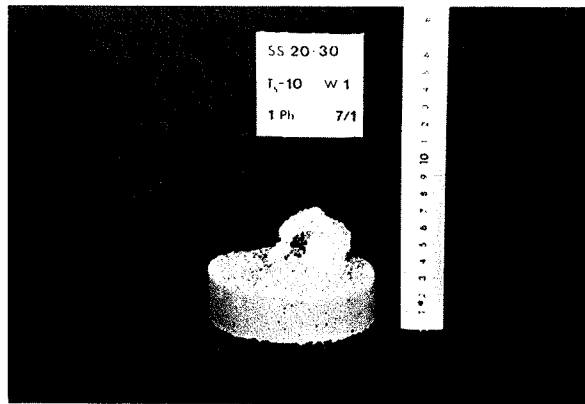
* Two Phase Flow



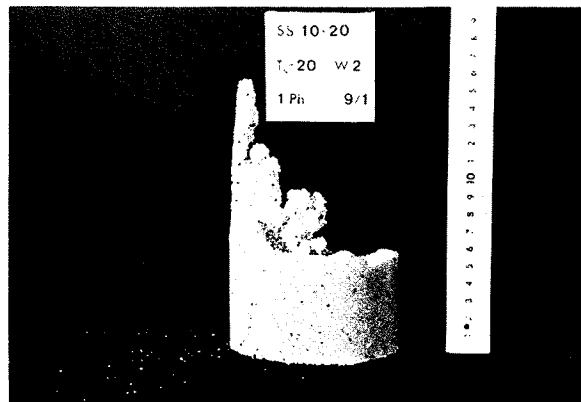
Test SA26



Test SA20

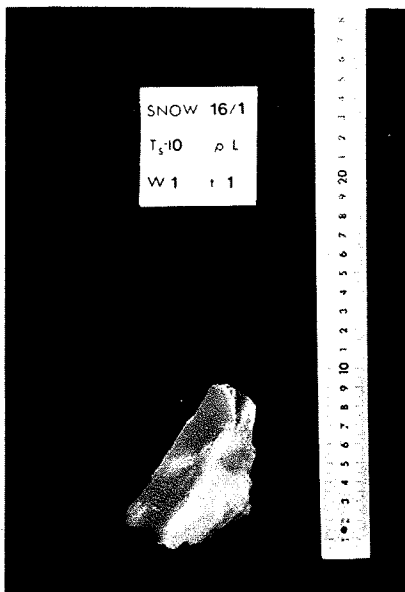


Test SA35

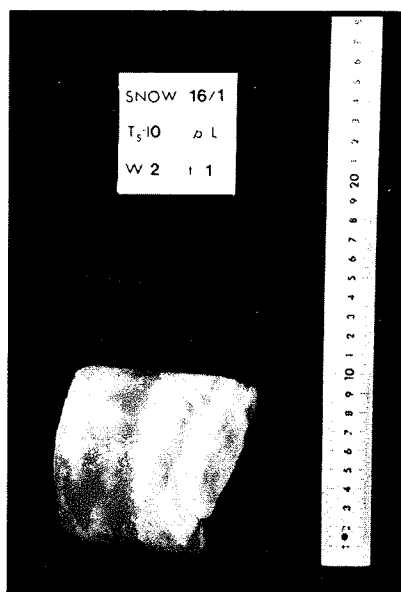


Test SA38

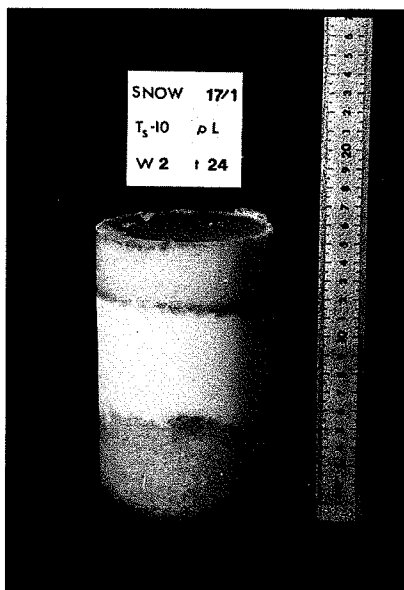
Figure A-1: Photographs of sand infiltration tests



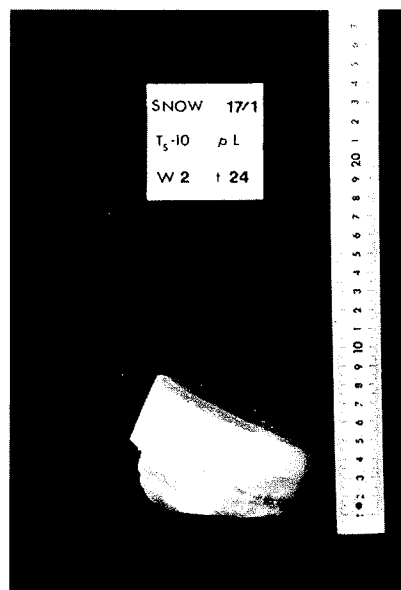
Test SN7



Test SN8

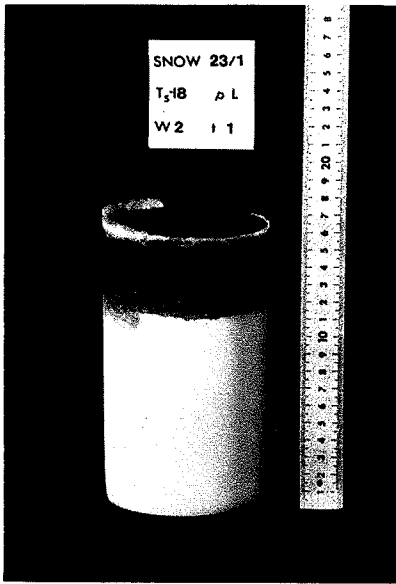


Test SN12

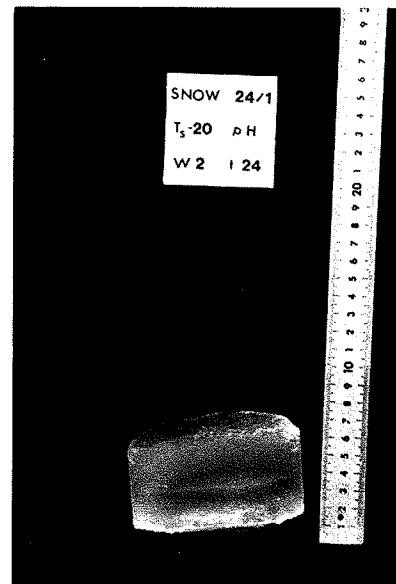


Test SN12

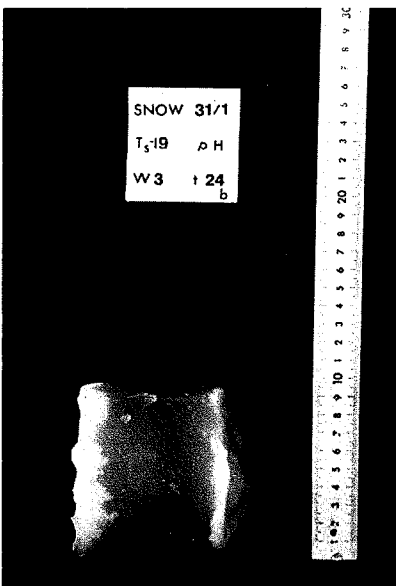
Figure A-2: Photographs of snow infiltration tests



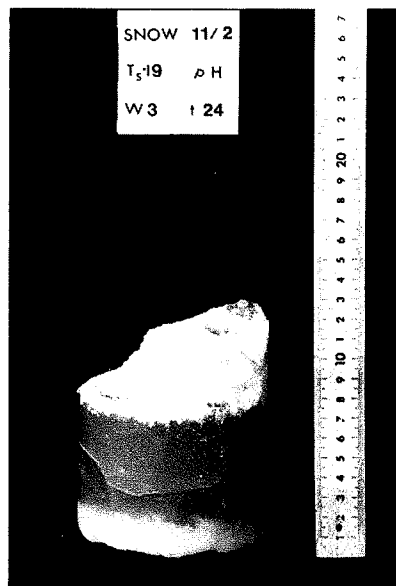
Test SN16



Test SN18

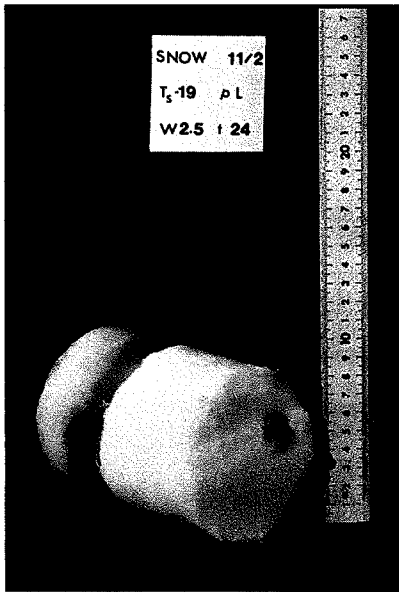


Test SN24

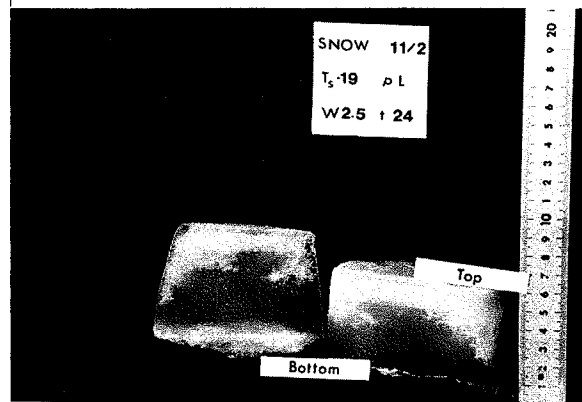


Test SN30

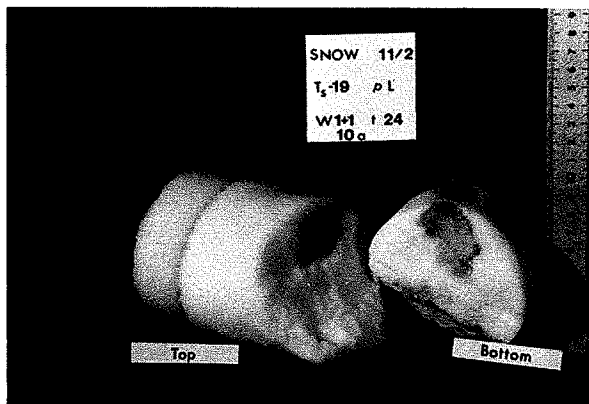
Figure A-3: Photographs of snow infiltration tests



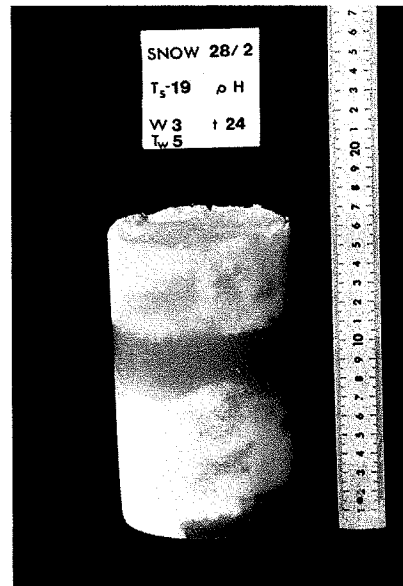
Test SN34



Test SN34

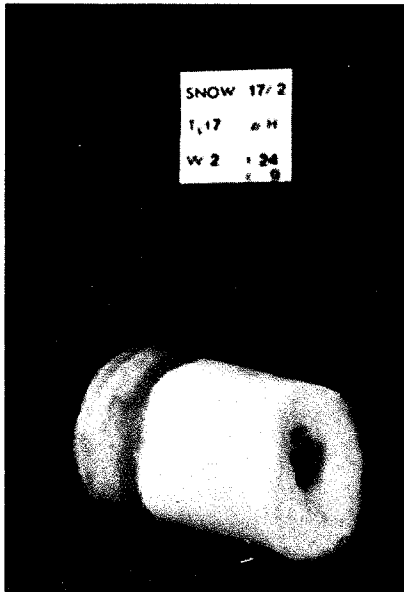


Test SN33

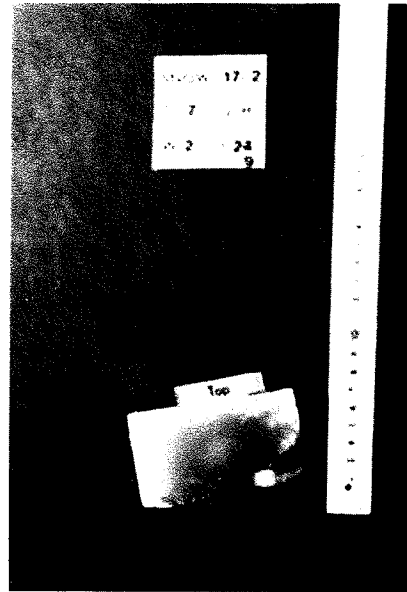


Test SN48

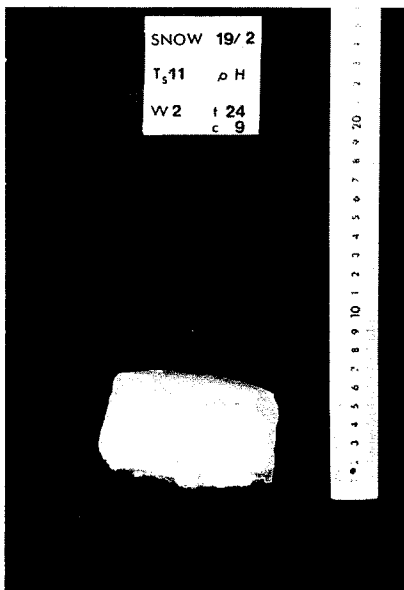
Figure A-4: Photographs of snow infiltration tests



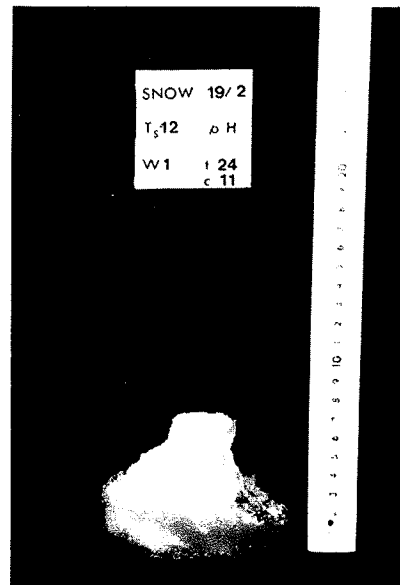
Test TS1



Test TS1

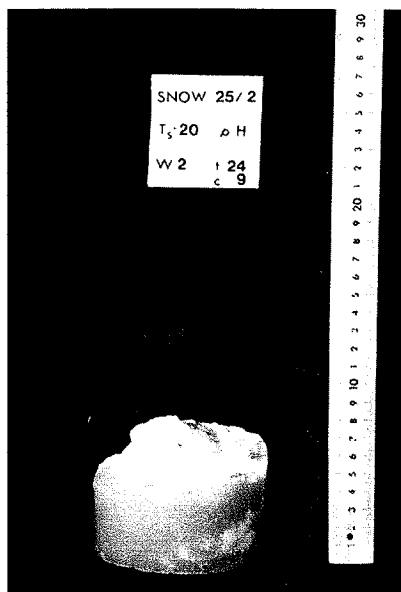


Test TS5

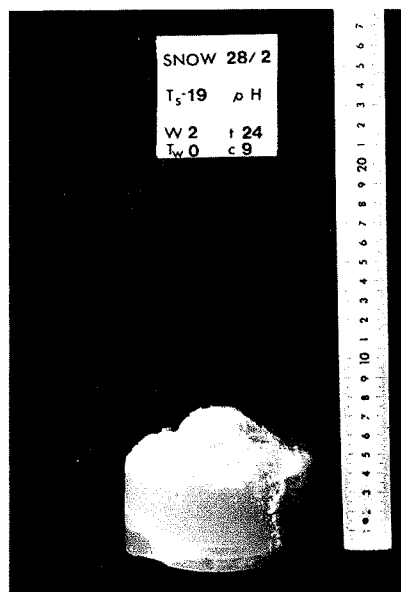


Test TS6

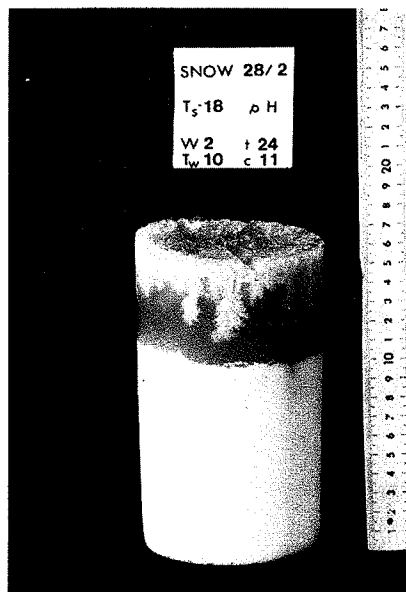
Figure A-5: Photographs of snow infiltration tests



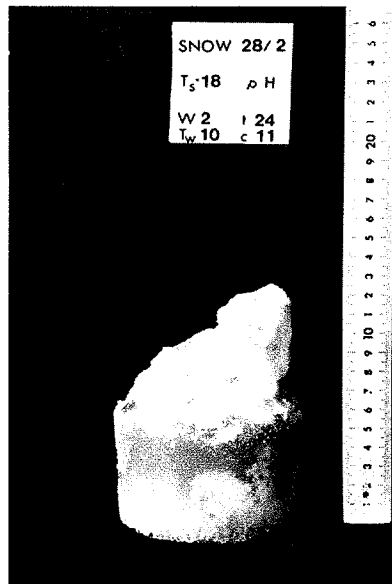
Test TS7



Test TS10



Test TS12



Test TS12

Figure A-6: Photographs of snow infiltration tests

APPENDIX B

EXPERIMENTAL RESULTS FROM SCINTILLATION AND
THERMOCOUPLE MEASUREMENTS

Table B-1
Scintillation Results

Test No.	Snow Density (g/cm ³)	Porosity	Capped Density (g/cm ³)	Water Saturation	Air Saturation
SN 37	0.50	0.45	0.92	0.93	0.07
SN 39	0.49	0.47	0.91	0.90	0.10
SN 41	0.40	0.56	0.56	0.29	0.71
SN 44	0.41	0.55	0.63	0.40	0.60
TS 1*	0.46	0.50	0.81	0.70	0.30
TS 2*	0.46	0.50	0.80	0.68	0.32
TS 3*	0.48	0.48	0.62	0.29	0.71
TS 4*	0.47	0.49	0.69	0.46	0.54
TS 5*	0.48	0.48	0.58	0.21	0.79
TS 6	0.47	0.49	0.88	0.84	0.16
TS 7	0.47	0.49	0.90	0.88	0.12
TS 8*	0.47	0.49	0.72	0.51	0.49
TS 9	0.47	0.49	0.92	0.90	0.10
TS 10	0.48	0.48	0.94	0.96	0.04
TS 11	0.48	0.48	0.88	0.83	0.17
TS 12	0.48	0.48	0.87	0.81	0.19
TS 13 ⁺	0.48	0.48	0.88	0.83	0.17
TS 14*	0.50	0.45	0.70	0.44	0.56
TS 15*	0.49	0.47	0.68	0.40	0.60
TS 16*	0.49	0.47	0.71	0.47	0.53

Table B-1
(continued)

Test No.	Snow Density (g/cm ³)	Porosity	Capped Density (g/cm ³)	Water Saturation	Air Saturation
TS 17* [†]	0.48	0.48	0.78	0.63	0.37
TS 18* [†]	0.49	0.47	0.78	0.62	0.38

* full penetration

[†] two phase flow

Table B-2

Front Penetration Summary

Test No.	Snow Porosity	Water (cm ³ /cm ²)	Infiltration Time (sec)	Front Penetration (cm)	Water ÷ (0.95xPorosity) (cm)	Apparent Front Penetration at Infiltration Time (cm)
TS 1	0.50	2	7.0	4.5	4.2	4
TS 2	0.50	2	7.2	4.5	4.2	>4
TS 3	0.48	3	12.8	7.0	6.6	>6
TS 4	0.49	2	5.8	4.5	4.3	<4
TS 5	0.48	2	5.8	4.5	4.4	>4
TS 6	0.49	1	3.6	2.25	2.1	>2
TS 7	0.49	2	9.2	4.25	4.3	4
TS 8	0.49	3	15.0	6.5	6.4	>6
TS 9	0.49	1	3.4	2.25	2.1	2
TS 10	0.48	2	9.4	4.5	4.4	>4
TS 11 ⁺	0.48	2	9.8	5.0	4.4	<6
TS 12 ⁺	0.48	2	7.8	5.75	4.4	>4
TS 13 [*]	0.48	2	31.8	4.5	4.4	>4
TS 14	0.45	3	1.42	7.0	7.0	>6

Table B-2
(continued)

Test No.	Snow Porosity	Water (cm ³ /cm ²)	Infiltration Time (sec.)	Front Penetration (cm)	Water † (0.95xPorosity) (cm)	Apparent Front Penetration at Infiltration Time (cm)
TS 15 ⁺	0.47	3	15.0	7.75	6.7	<8
TS 16 ⁺	0.47	3	11.6	8.5	6.7	<8
TS 17 [*]	0.48	3	82.2	7.0	6.6	8
TS 18 ^{**+}	0.47	3	36.0	7.75	6.7	>8

* two phase flow

+ water temperature above 0°C

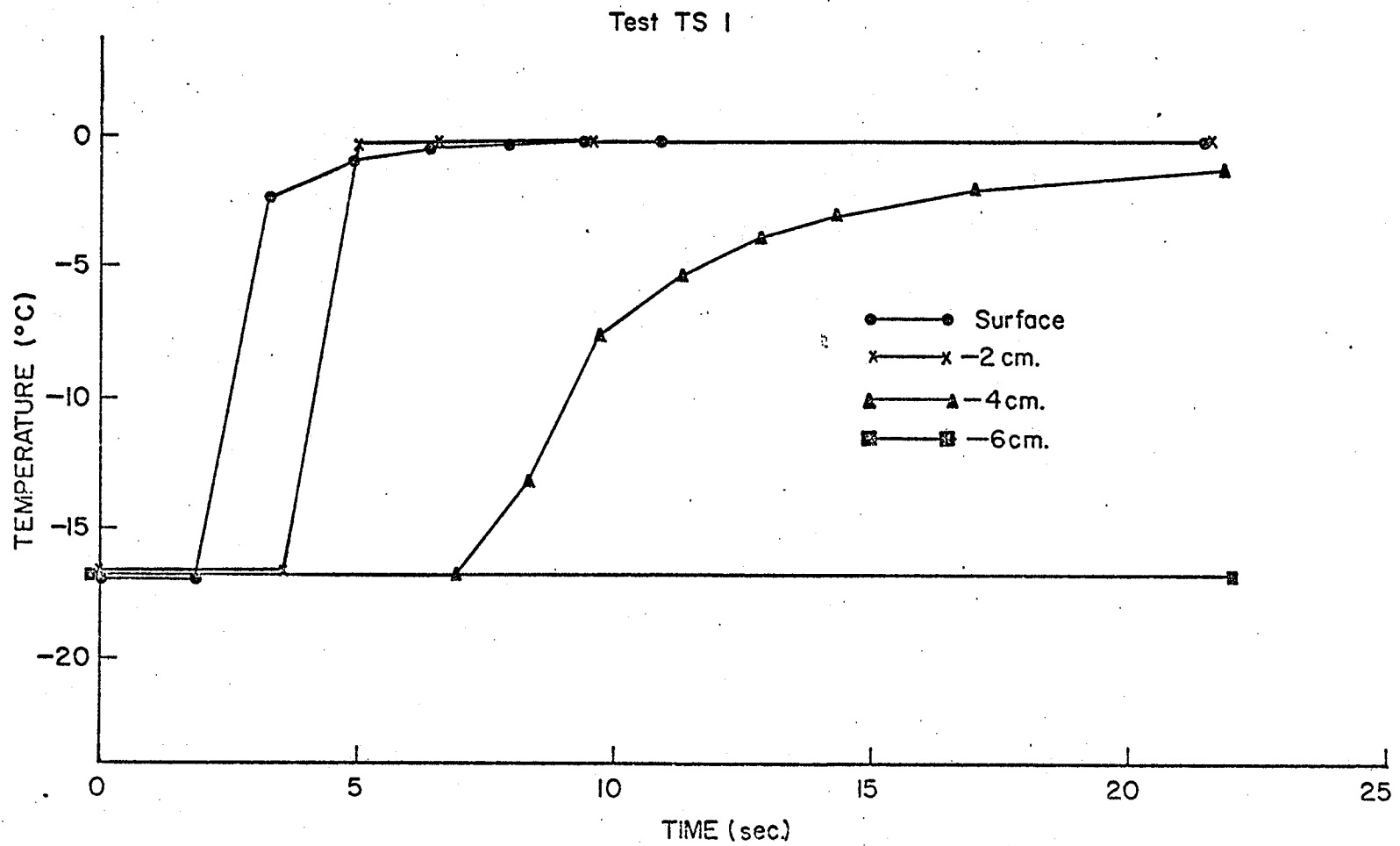


Figure B-1: Temperature Measurements During Water Infiltration into Snow

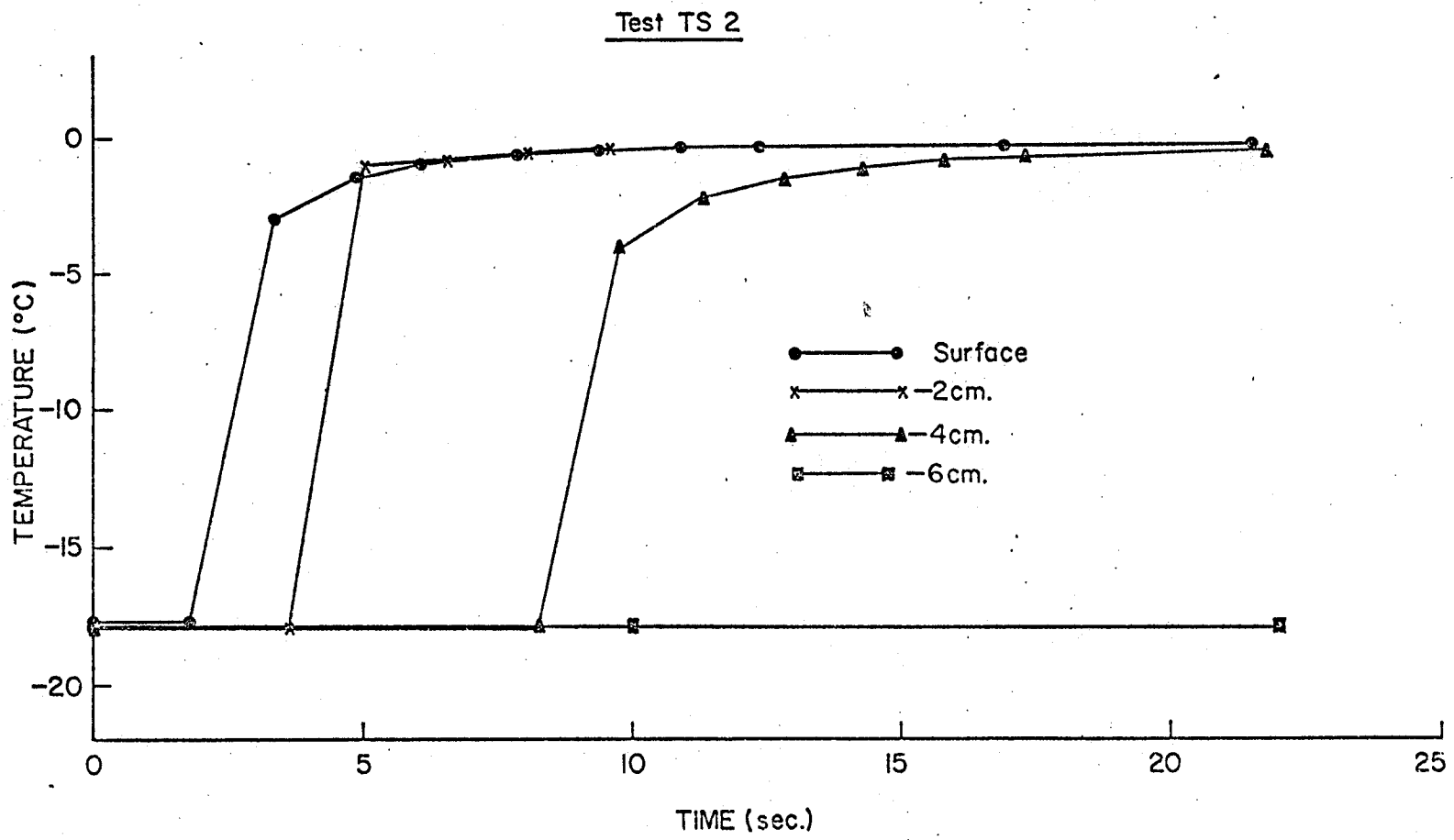


Figure B-2: Temperature Measurements During Water Infiltration into Snow

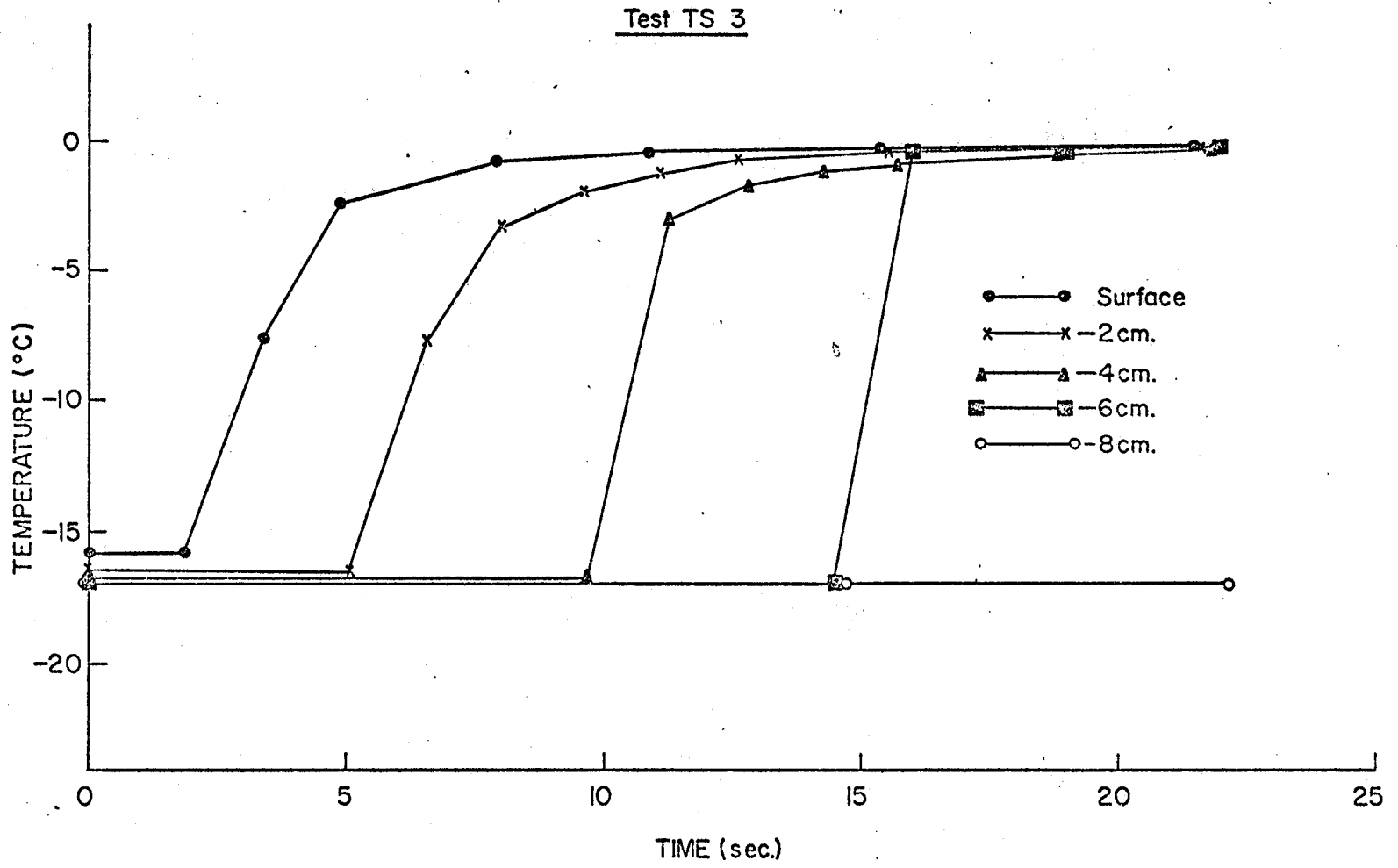


Figure B-3: Temperature Measurements During Water Infiltration into Snow

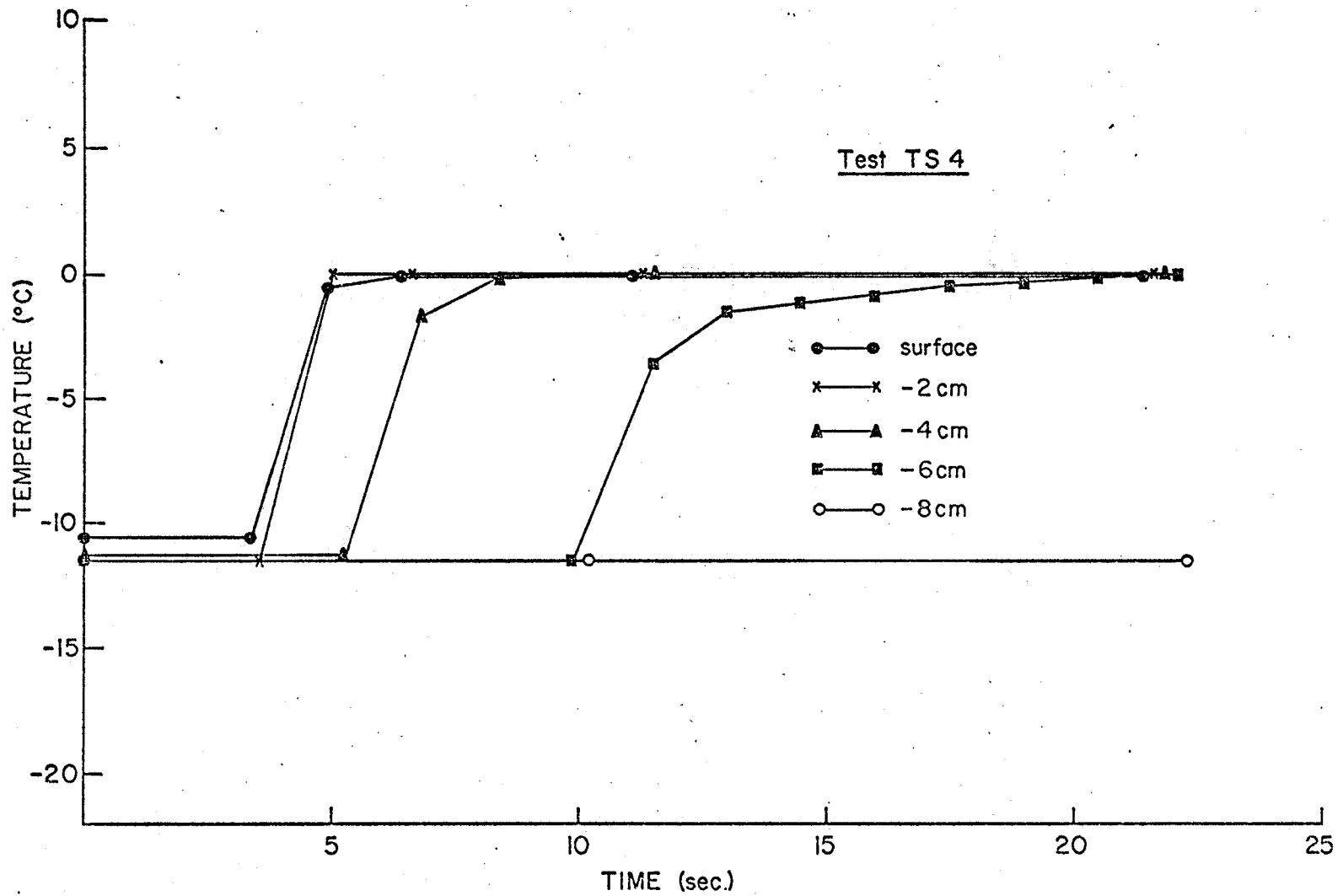


Figure B-4: Temperature Measurements During Water Infiltration into Snow

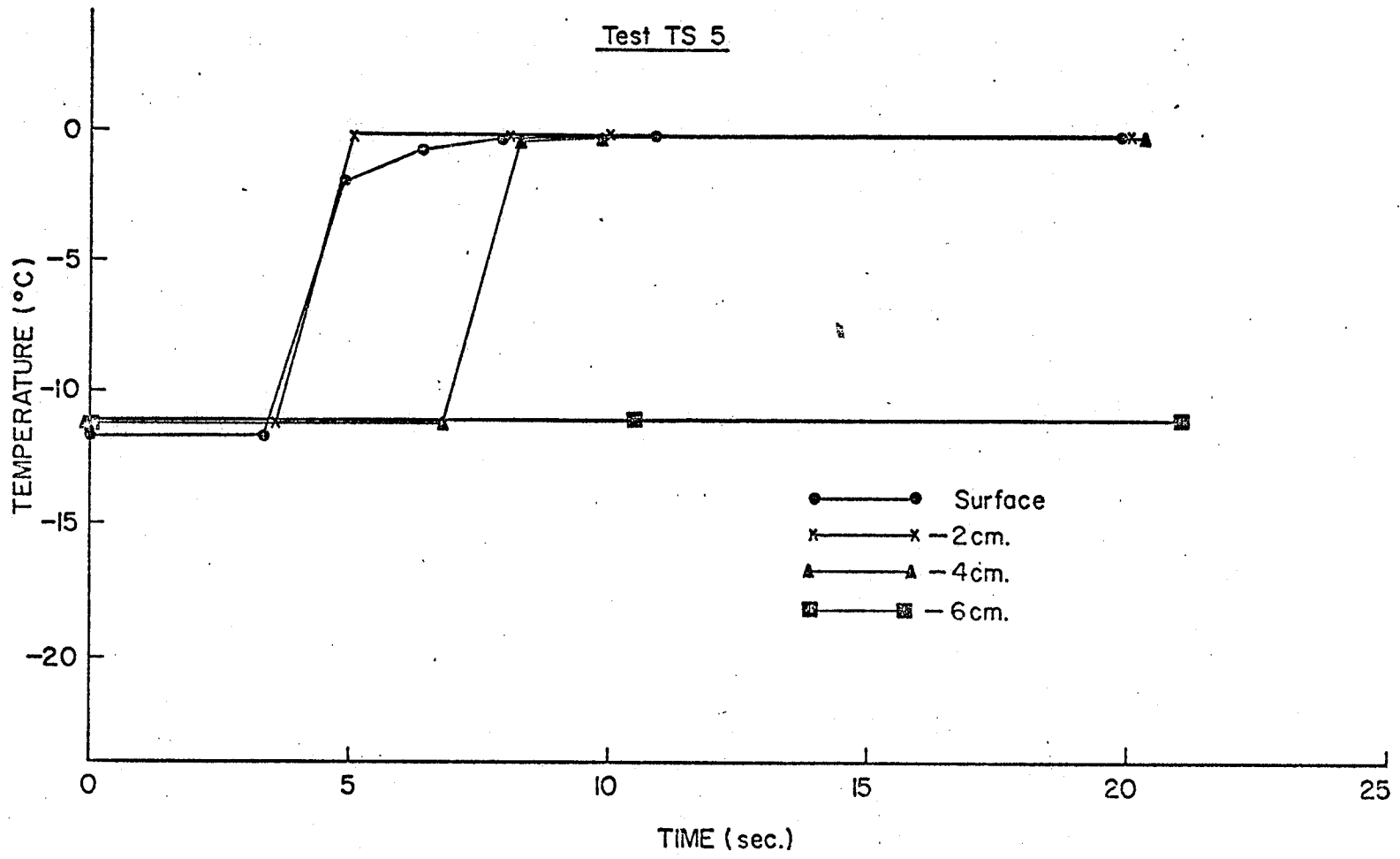


Figure B-5: Temperature Measurements During Water Infiltration into Snow

Test TS 6

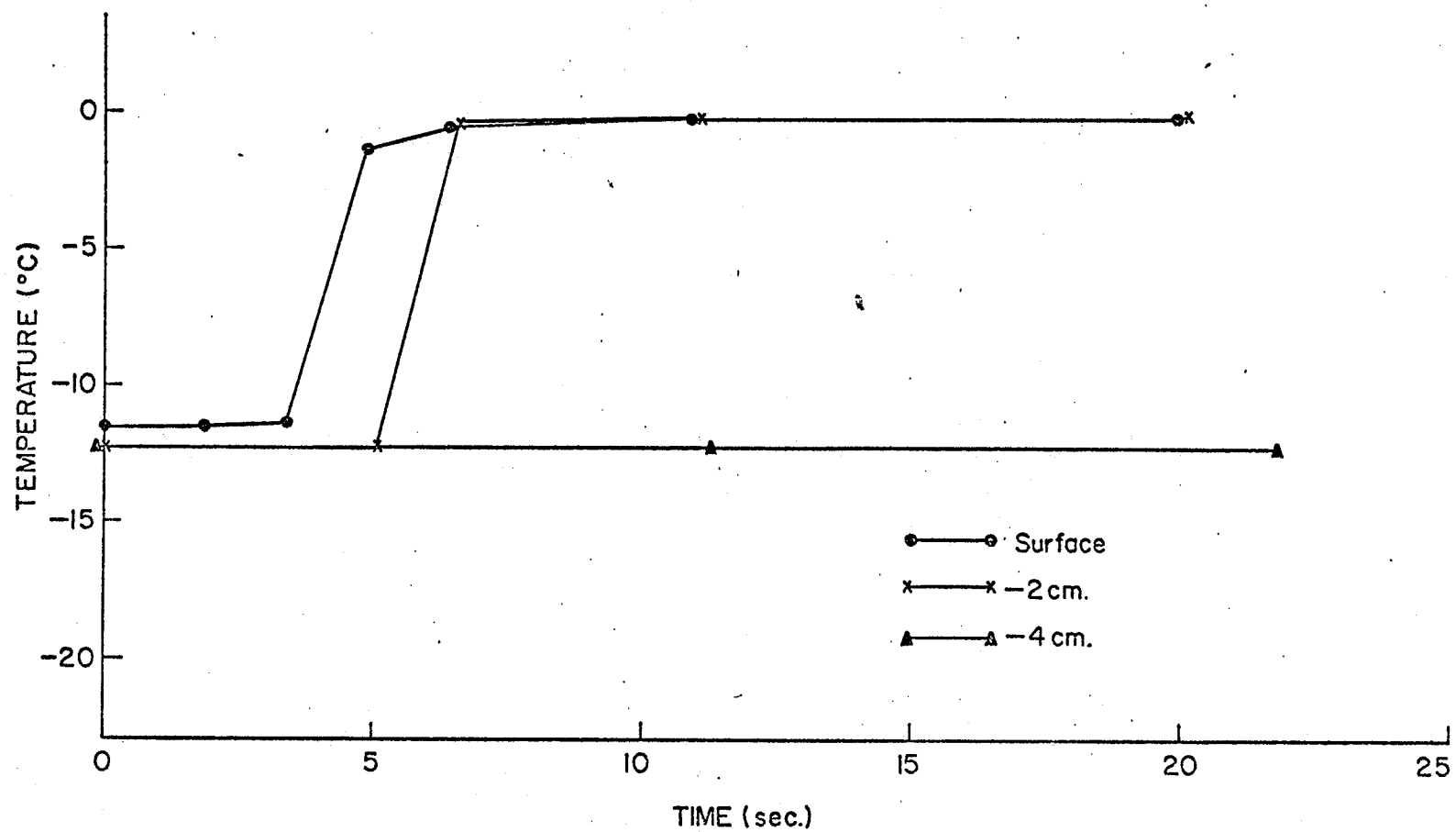


Figure B-6: Temperature Measurements During Water Infiltration into Snow

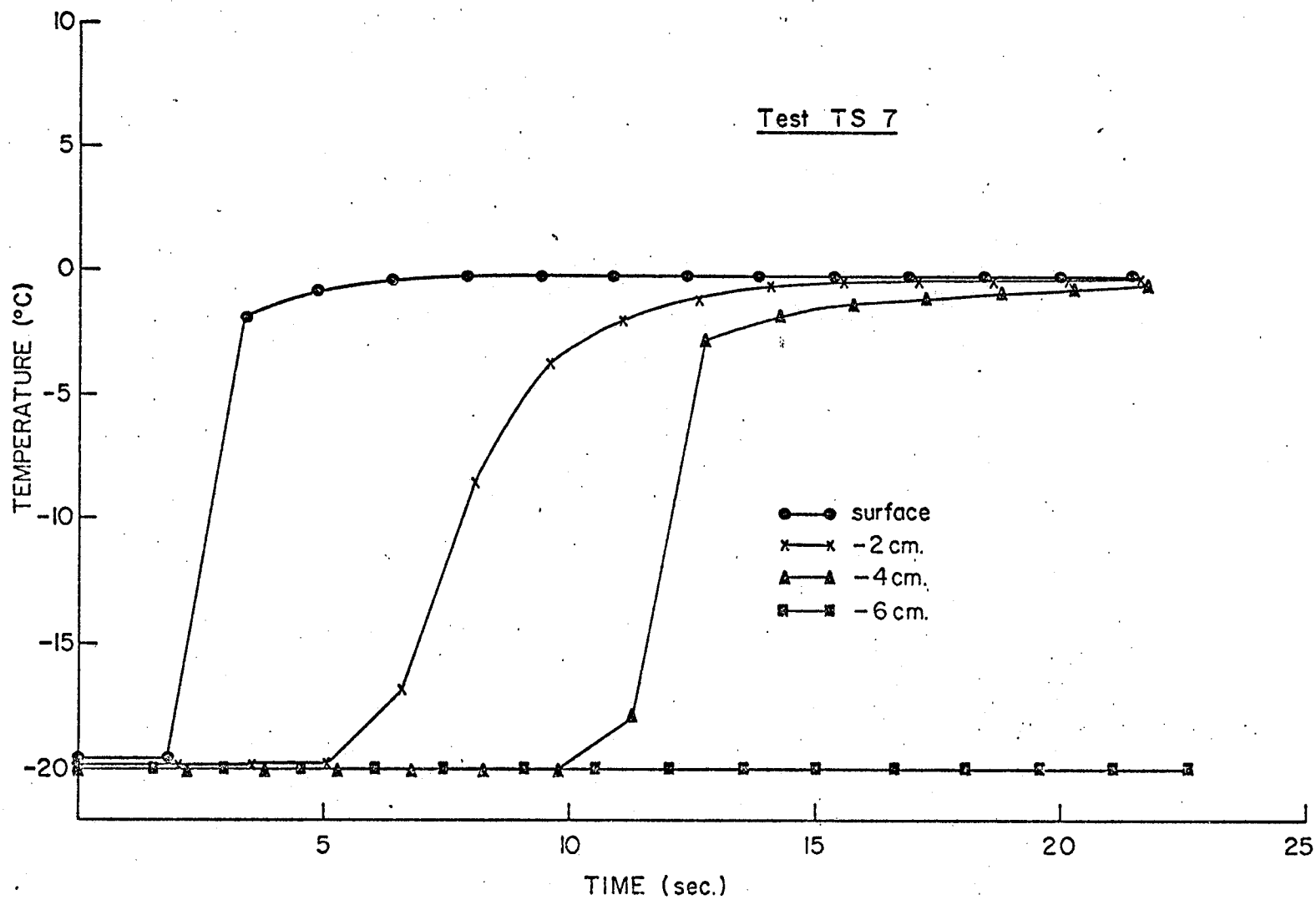


Figure B-7: Temperature Measurements During Water Infiltration into Snow

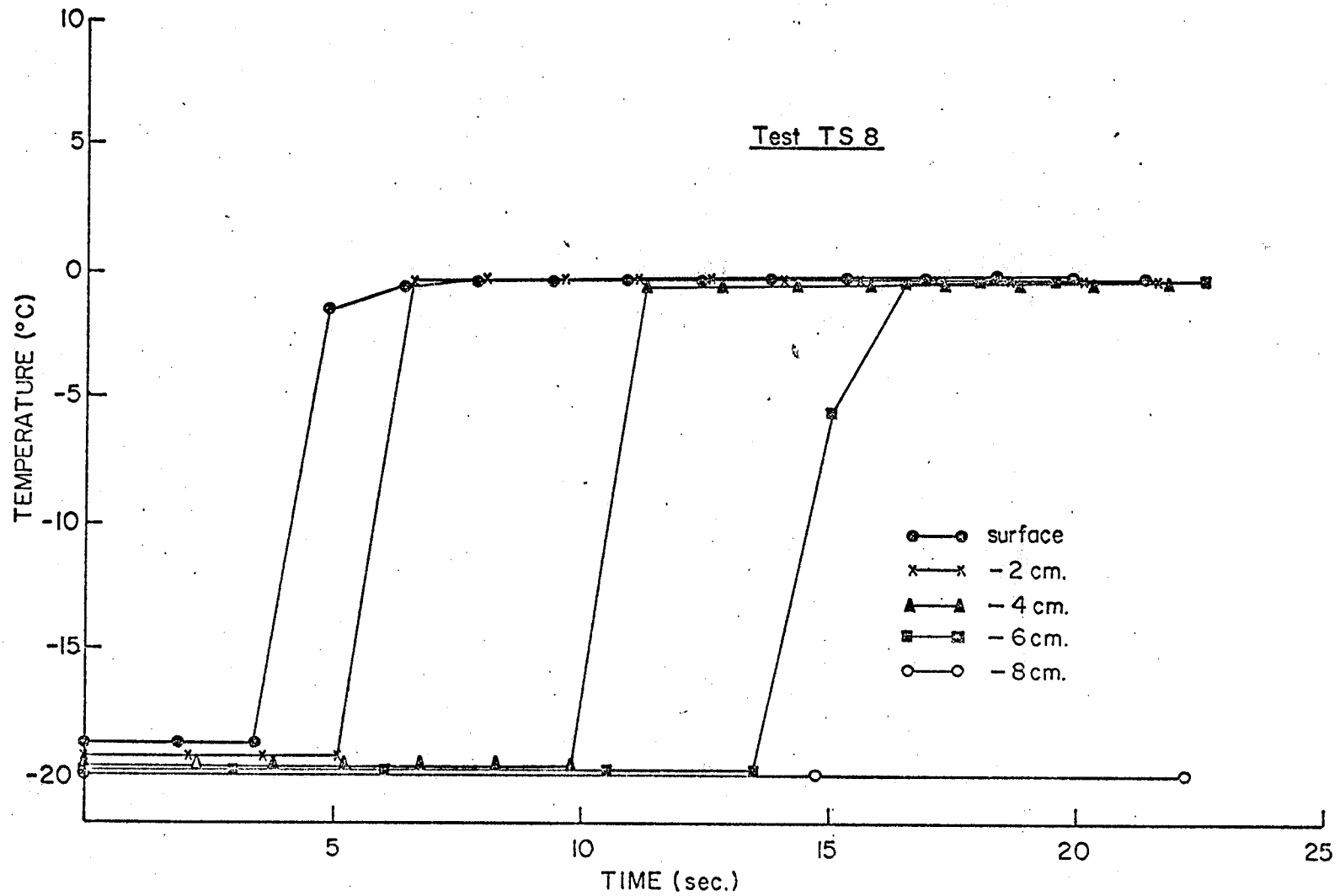


Figure B-8: Temperature Measurements During Water Infiltration into Snow

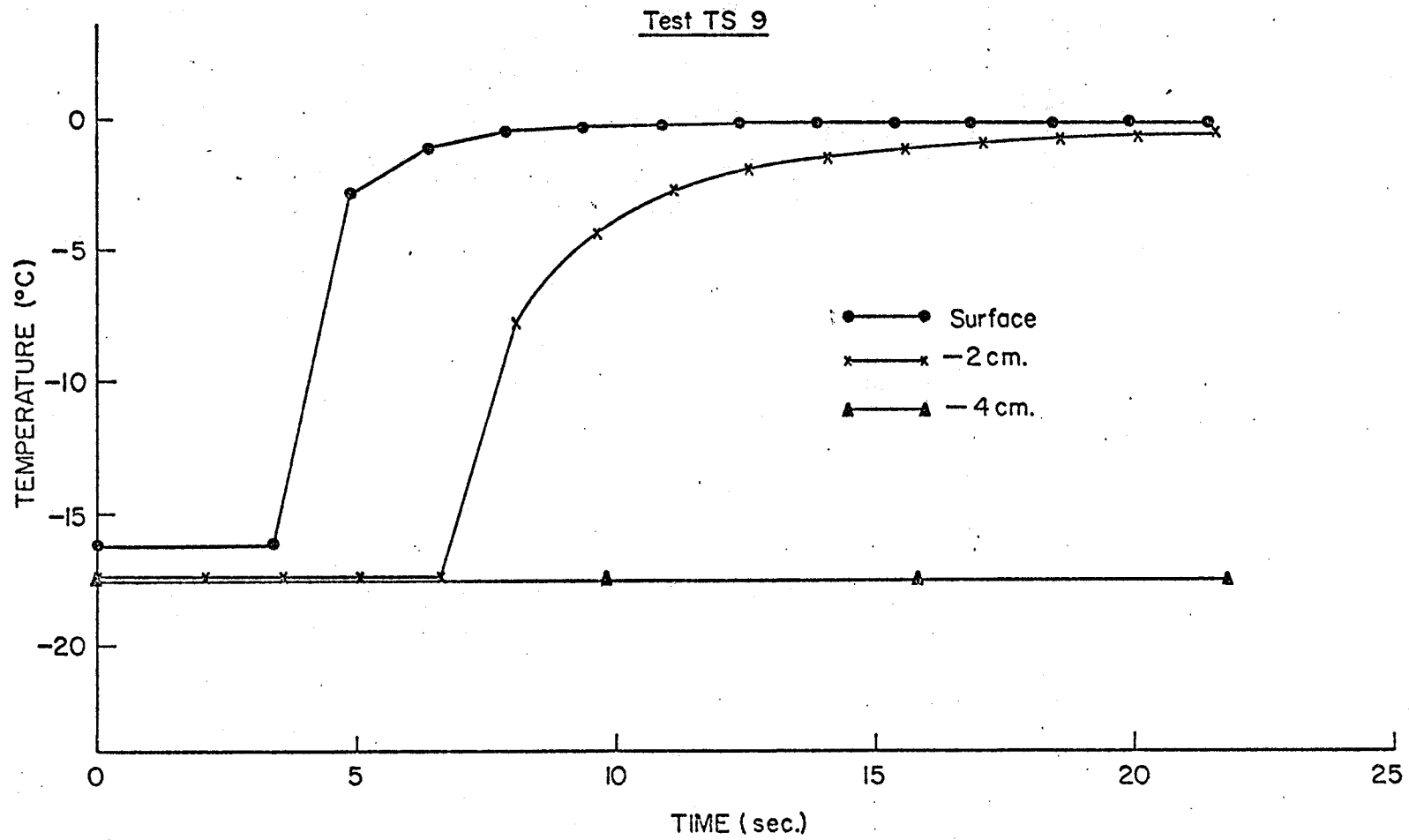


Figure B-9: Temperature Measurements During Water Infiltration into Snow

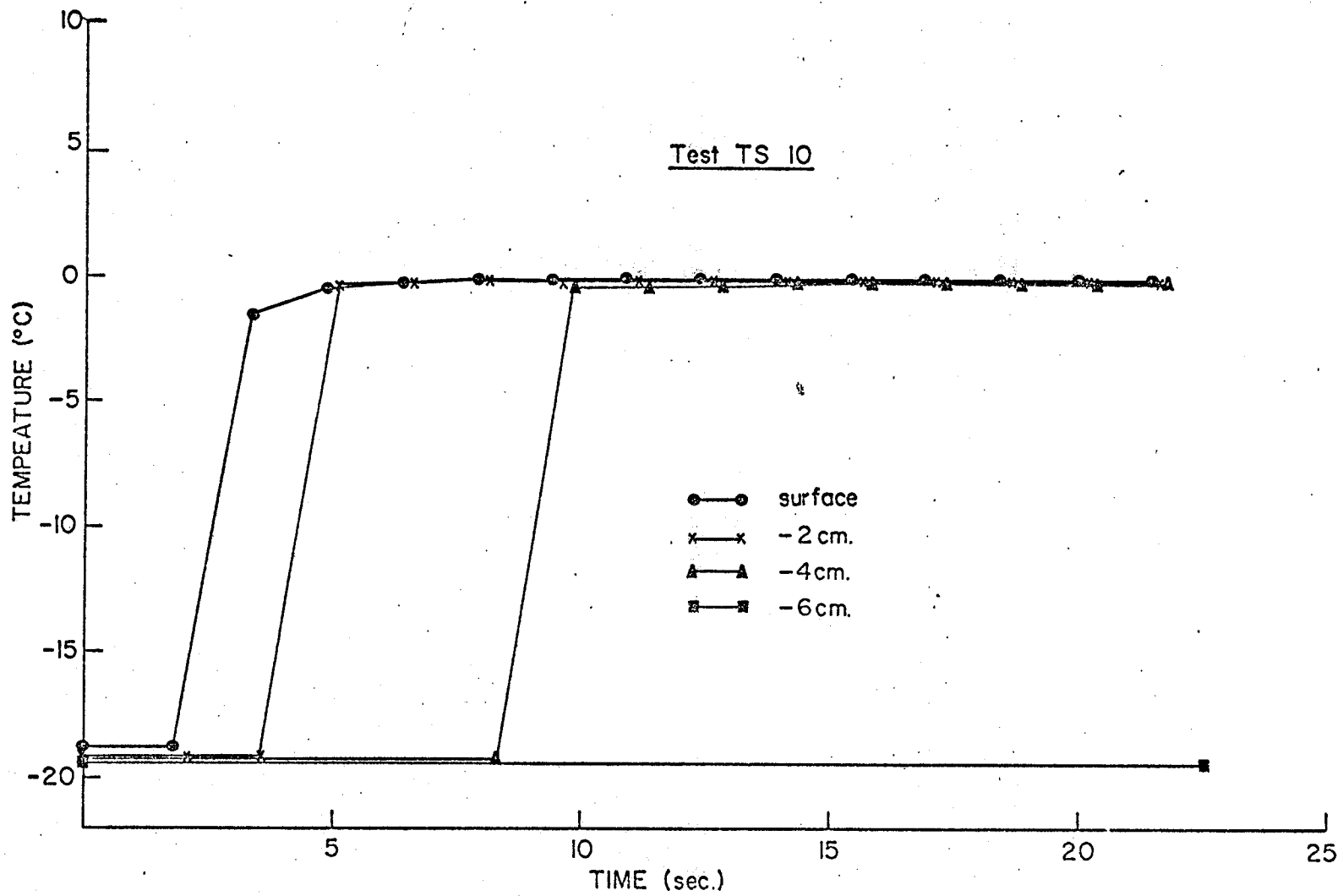


Figure B-10: Temperature Measurements During Water Infiltration into Snow

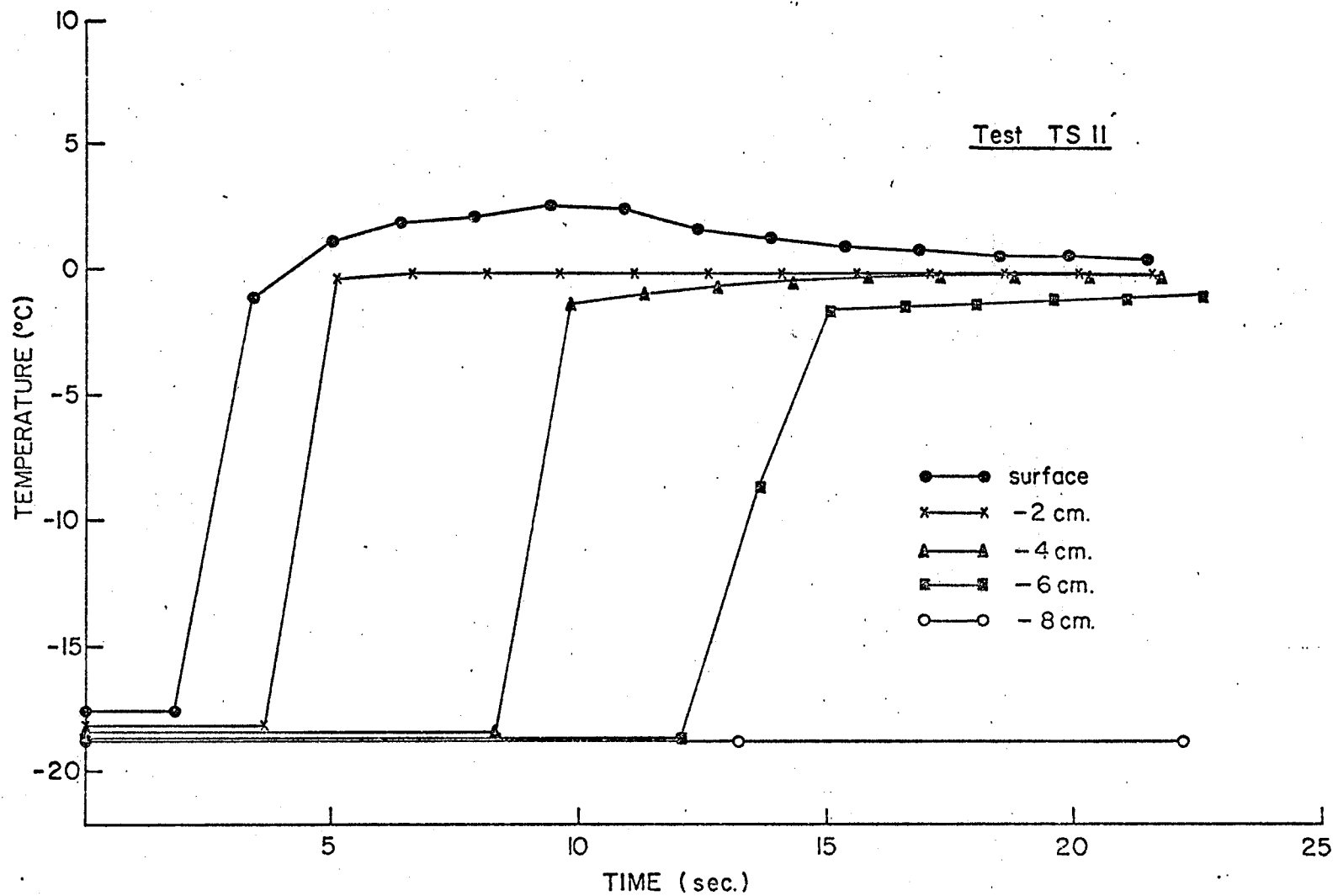


Figure B-11: Temperature Measurements During Water Infiltration into Snow

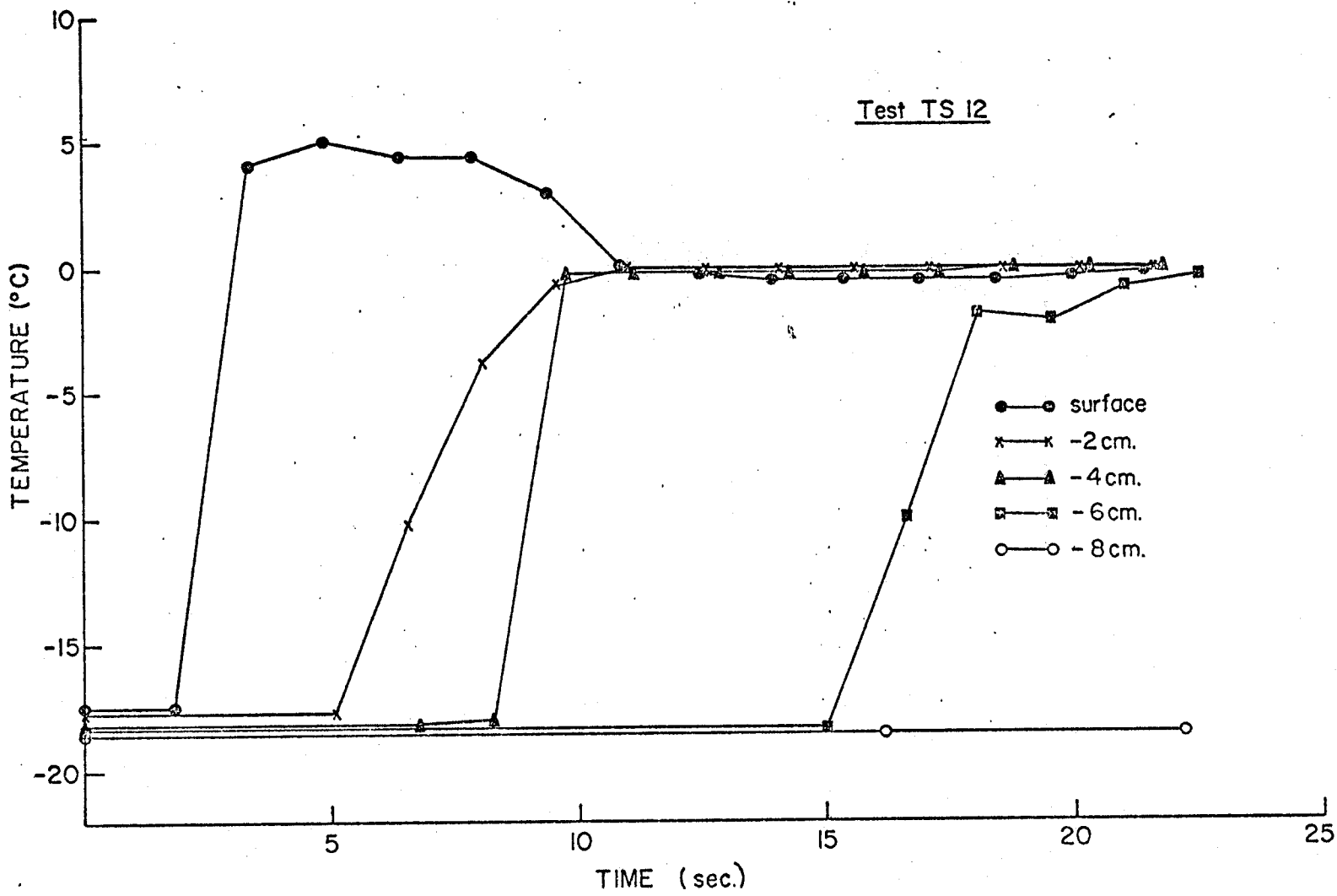


Figure B-12: Temperature Measurements During Water Infiltration into Snow

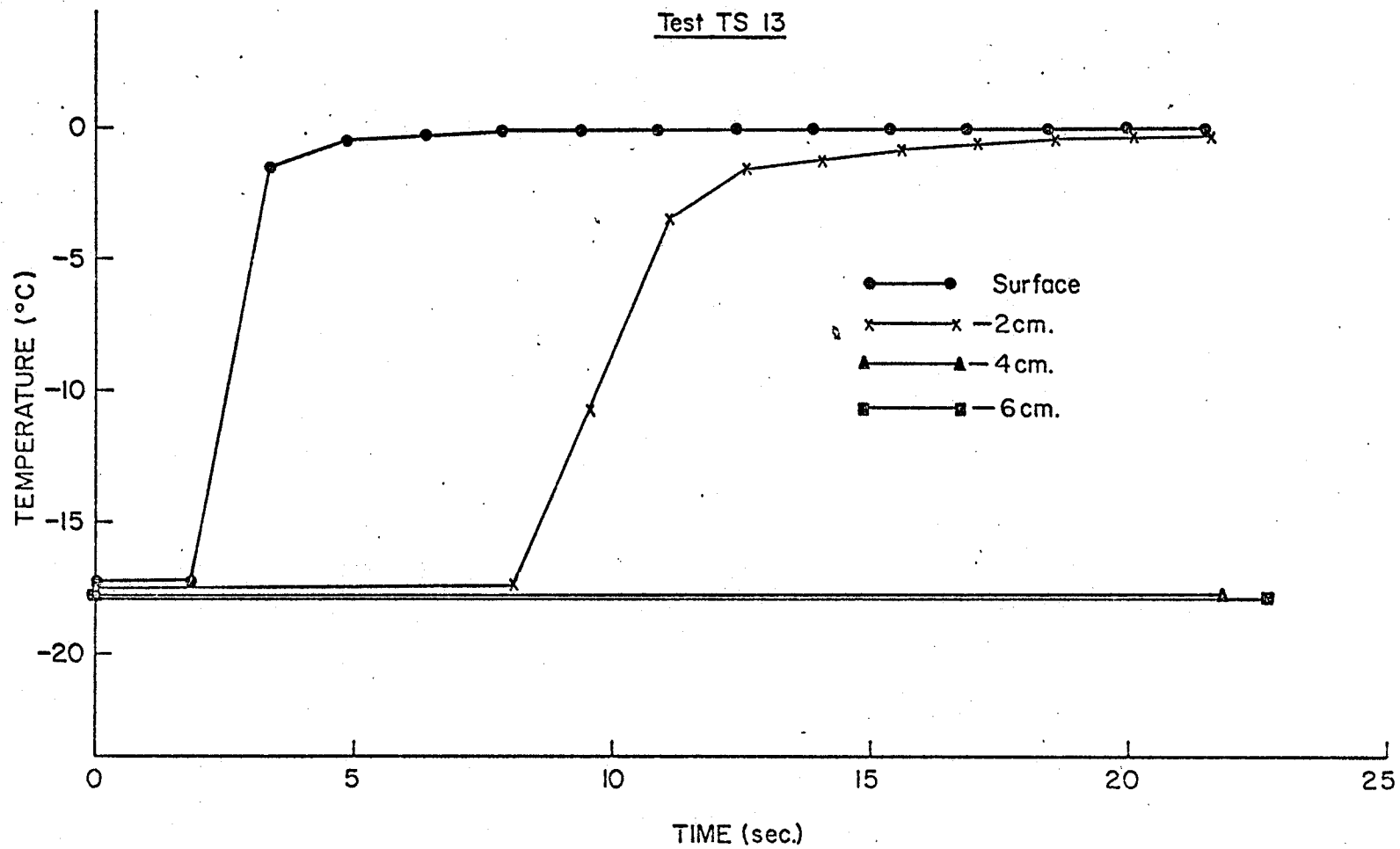


Figure B-13: Temperature Measurements During Water Infiltration into Snow

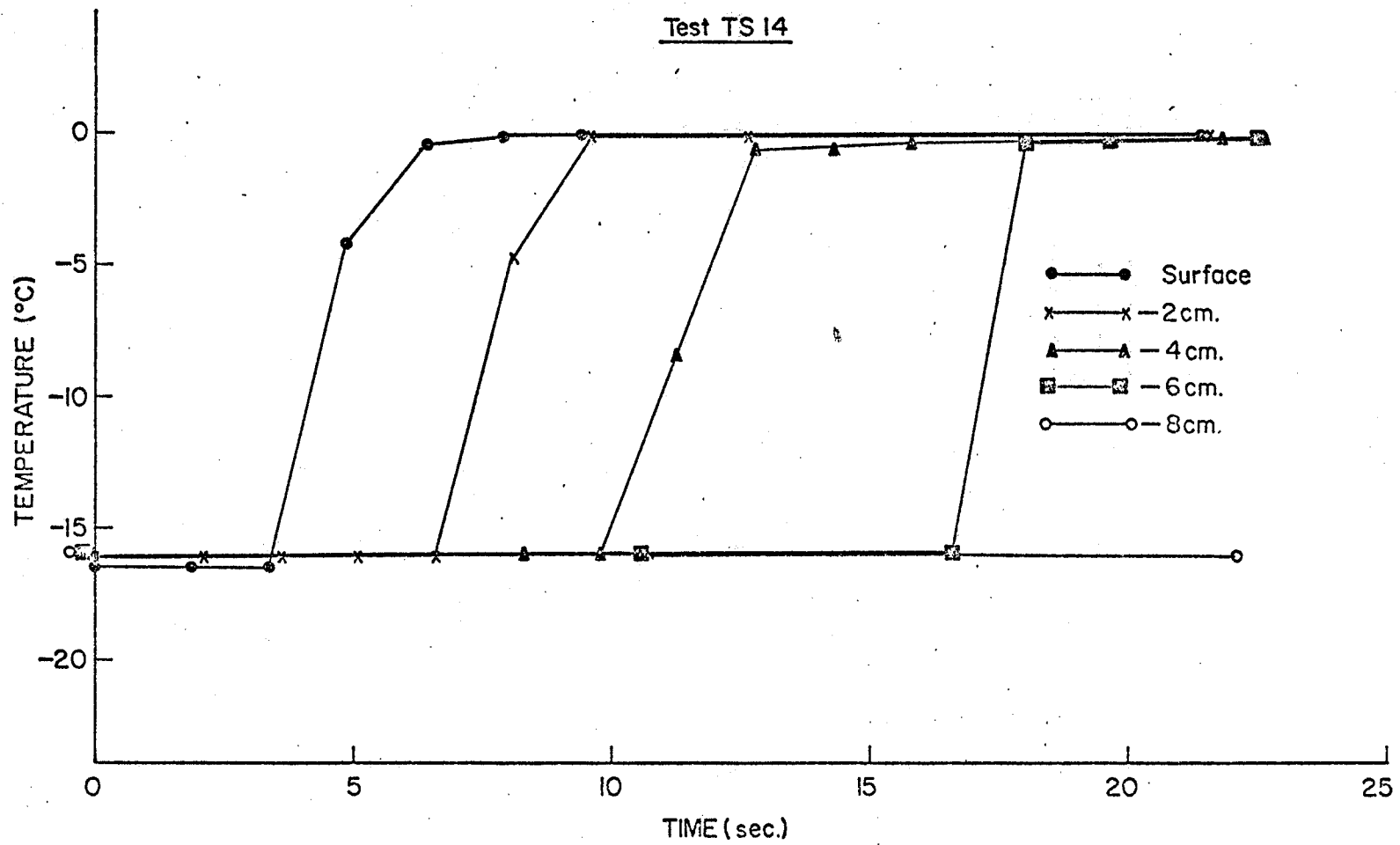


Figure B-14: Temperature Measurements During Water Infiltration into Snow

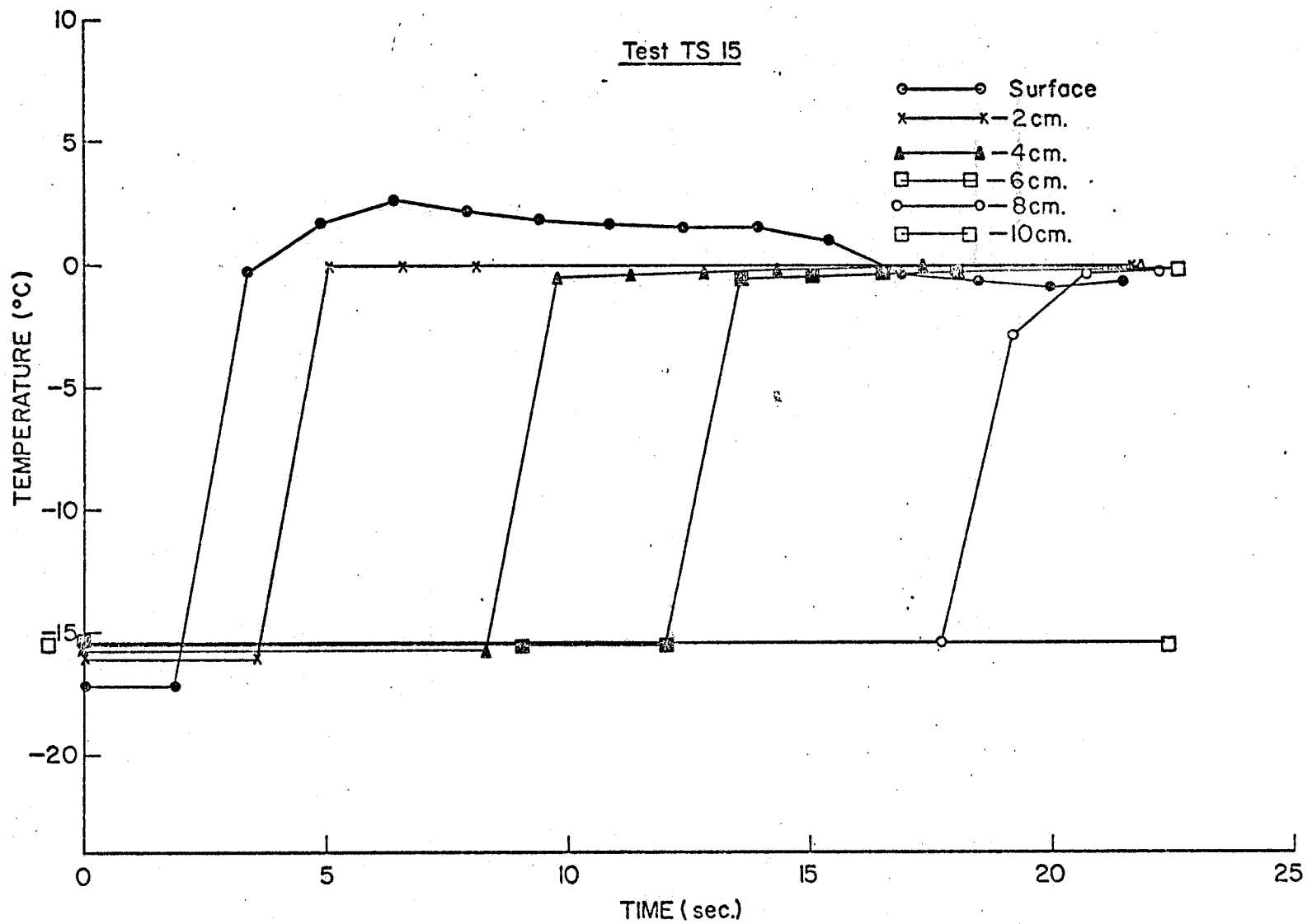


Figure B-15: Temperature Measurements During Water Infiltration into Snow

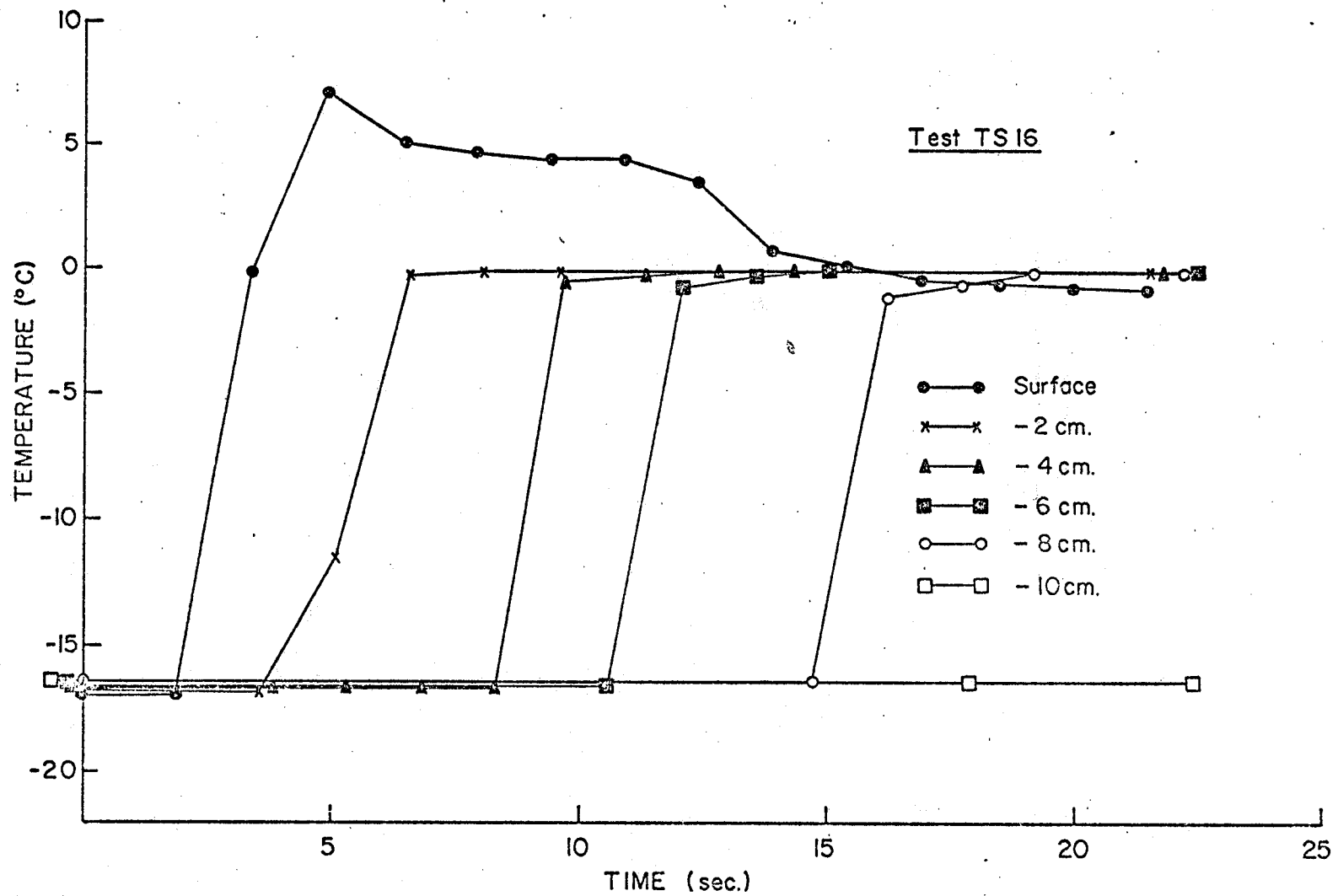


Figure B-16: Temperature Measurements During Water Infiltration into Snow

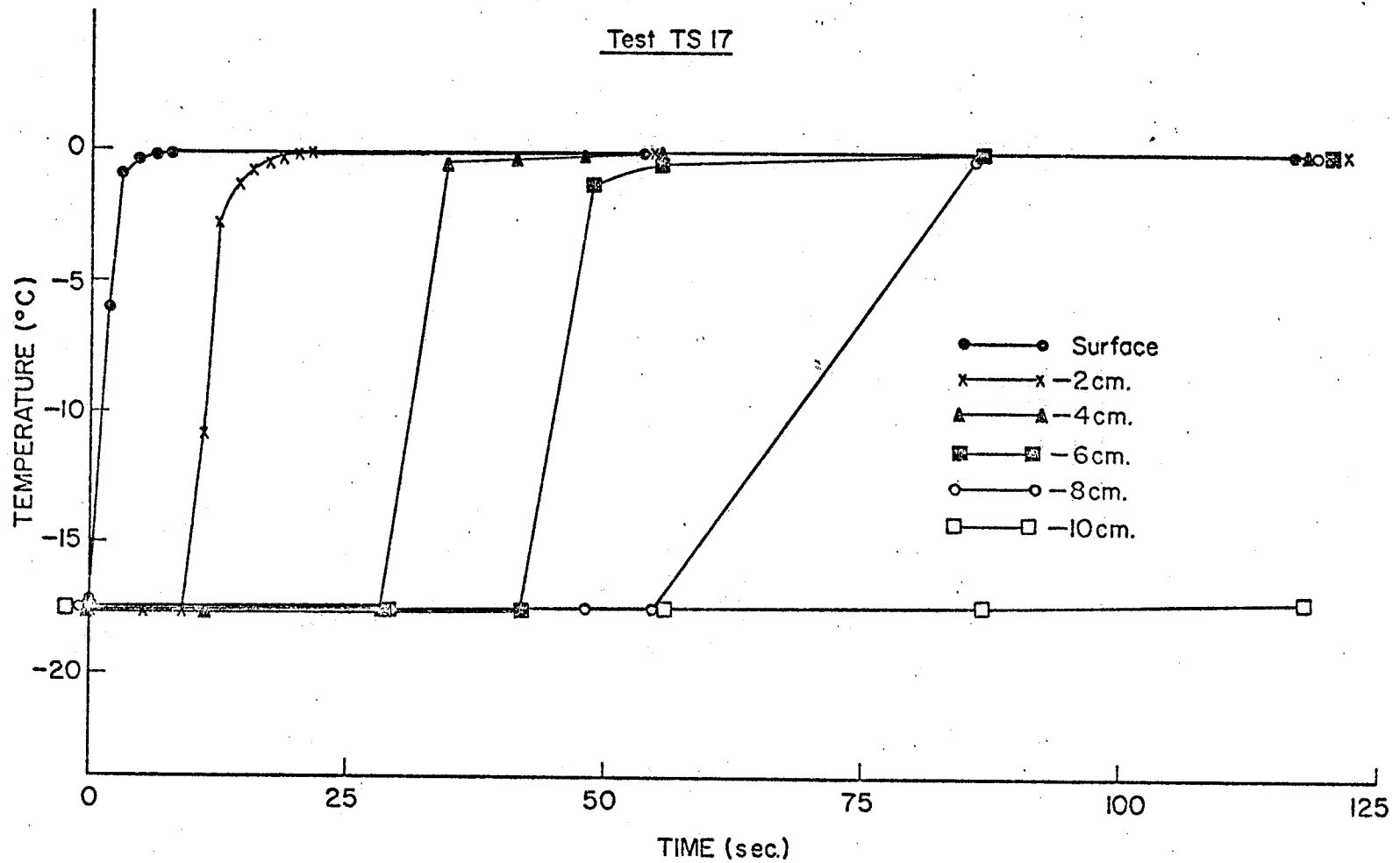


Figure B-17: Temperature Measurements During Water Infiltration into Snow

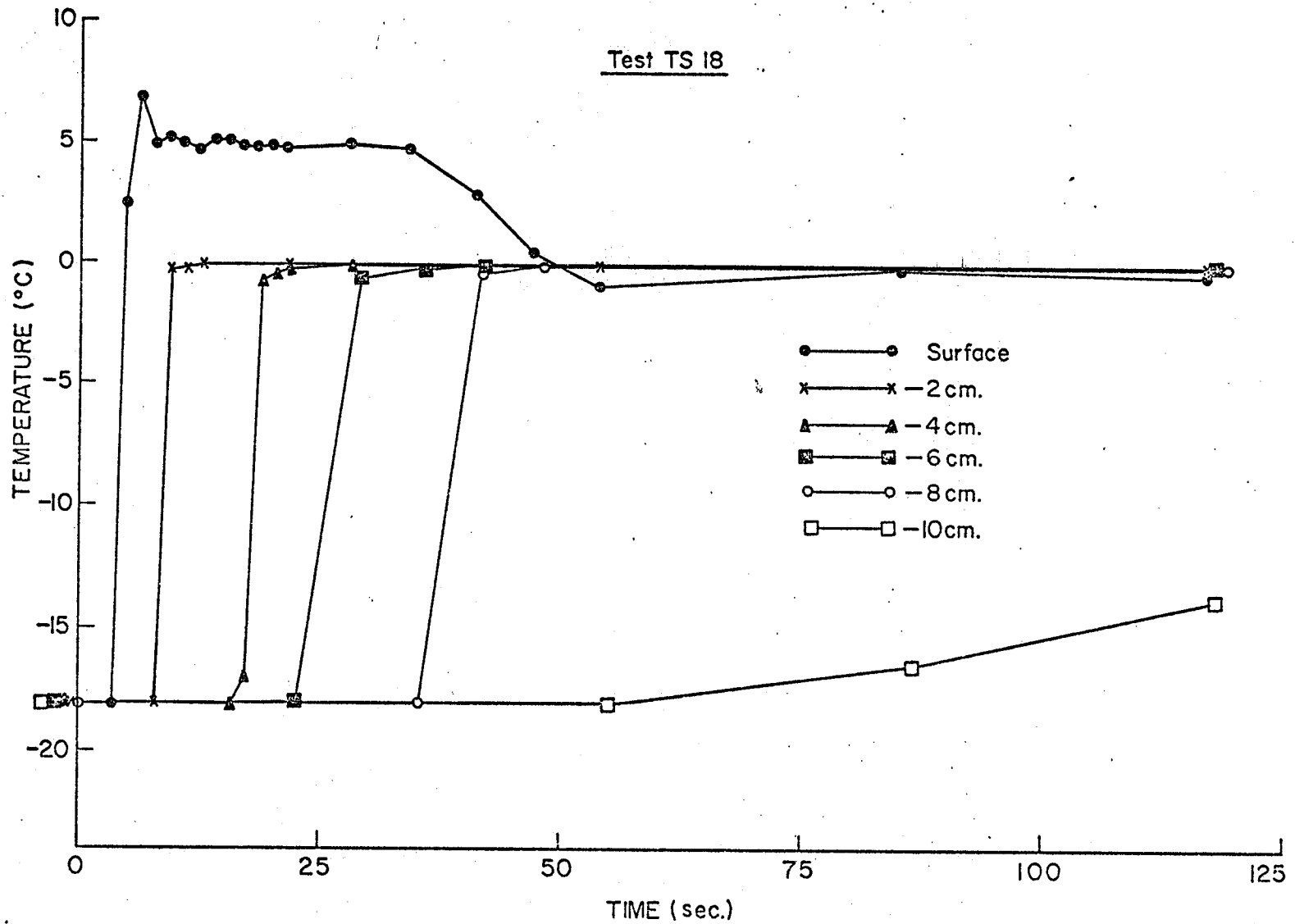


Figure B-18: Temperature Measurements During Water Infiltration into Snow

APPENDIX C

ANALYSIS OF INFILTRATION DATA

Table C-1
Empirically Fitted Linear Models

Model	Dependant Variable	Independent Variables	Tests
MSA 1	FP	T_{sa}, T_w, g_r, W	SA3-SA6, SA9, SA10, SA13, SA14, SA17, SA18, SA21, SA22, SA25, SA26, SA29, SA30, SA33-SA38.
MSA 2	MP	T_{sa}, T_w, g_r, W	same as MSA 1
MSA 3	IT	T_{sa}, T_w, g_r, W	same as MSA 1
MSA 4	FP	T_{sa}, W	SA3-SA6, SA9, SA10, SA13, SA14, SA17, SA18, SA21, SA22, SA 26, SA30.
MSA 5	IT	T_{sa}, W	same as MSA 4
MSA 6	MP	T_{sa}, W	same as MSA 4
MSA 7	FP	T_{sa}, g_r, W	SA5, SA6, SA13, SA33-SA38.
MSA 8	IT	T_{sa}, g_r, W	same as MSA 7
MSA 9	MP	T_{sa}, g_r, W	same as MSA 7
MSN 1	MP	$T_{sn}, T_w, \rho_s, W, t$	SN1, SN2, SN5-SN30, SN34, SN37, SN38, SN41, SN44-SN48.
MSN 2	FP	$T_{sn}, T_w, \rho_s, W, t$	same as MSN 1
MSN 3	IT	T_s, T_w, ρ_s, W, t	same as MSN 1
MSN 4	FP	T_{sn}, ρ_s, W	SN1, SN2, SN5-SN30.
MSN 5	IT	T_{sn}, ρ_s, W	same as MSN 4
MSN 6	MP	T_{sn}, ρ_s, W	same as MSN 4
MSN 7	FP	T_w, ρ_s, W	SN24, SN26, SN27, SN29, SN30, SN45-SN48.
MSN 8	IT	T_w, ρ_s, W	same as MSN 7
MSN 9	MP	T_w, ρ_s, W	same as MSN 7

Table C-1
(continued)

Model	Dependant Variable	Independent Variables	Tests
MSN 10	FP	$T_S, T_W, \rho_S, W, t,$ $(\rho_S T_S)$	SN1, SN2, SN5, SN7-SN11, SN13-SN26, SN29, SN30, SN37, SN47.
MSN 11	MP	$T_S, T_n, \rho_S, W, t,$ $(\rho_S T_S)$	same as MSN 10
MSN 12	FP	$T_S, \rho_S, W, (\rho_S T_S)$	SN1, SN2, SN5, SN7-SN11, SN13-SN26, SN29, SN30, SN37.
MSN 13	MP	$T_S, \rho_S, W, (\rho_S T_S)$	same as MSN 12
MSN 14	FP	$W, (\rho_S T_S)$	same as MSN 12
MSN 15	MP	$W, (\rho_S T_S)$	same as MSN 12
MTS 1	FP	T_S, ρ_S, W	TS1-TS10, TS14
MTS 2	IT	T_S, ρ_S, W	same as MTS 1
MTS 3	FP	T_S, T_W, ρ_S, W	TS1-TS12, TS14-TS16.
MTS 4	IT	T_S, T_W, ρ_S, W	same as MTS 3
MTS 5	FP	T_S, T_W, ρ_S, W, IT	same as MTS 3
MTS 6	MP	T_S, T_W, ρ_S, W	TS6, TS7, TS9-TS12.
MTS 7	FP	W	same as MTS 1
MTS 8	FP	ρ_S, W	same as MTS 1
MTS 9	MP	T_S, T_W, W	same as MTS 6
MTS 10	FP	T_S, T_W, W	same as MTS 6
MTS 11	IT	T_S, T_W, W	same as MTS 6

Table C-1

LEGEND

Dependant Variables:

FP = front penetration, cm

IT = infiltration time, sec

MP = maximum penetration, cm

Independent Variables:

T_{sa} = sand temperature, °C

T_s = snow temperature, °C

T_n = water temperature, °C

ρ_s = snow density, g/cm³

gr = sand grain size parameter

W = applied water, cm³/cm²

t = snow age hardening, hrs

Linear Regression Models

All linear regression equations tested are of the form:

$$y = b + \sum_{i=1}^n c_i x_i \quad (C-1)$$

where

y = the dependant variable

b = the intercept

x_i, c_i = independant variables and their coefficients

n = number of independant variables

The linear regression program was part of the University of Manitoba's Statistical Package.

Table C-2

Model Fitting Results for Sand

Model	Dependant Variable	Multiple Correlation Coefficient	Intercept	Coefficient for Independant Variables and Correlation with Dependant Variables			
				T _{sa}	T _w	g _r	W
MSA 1	FP	0.9769	0.2667	0.0468 (0.0017)	0.0321 (0.1484)	0.0039 (0.4390)	3.2427 (0.9654)
MSA 2	MP	0.8303	15.5535	0.1915 (-0.0853)	0.1346 (-0.0084)	-0.3335 (-0.5429)	4.2059 (0.3134)
MSA 3	IT	0.8767	-232.4821	-6.7059 (-0.4847)	3.0427 (0.3560)	3.1661 (0.4374)	53.3938 (0.6710)
MSA 4	FP	0.9677	0.513	0.0559 (-0.0919)	--	--	3.2624 (0.9540)
MSA 5	IT	0.9128	-131.9158	-8.0588 (-0.7657)	--	--	64.8486 (0.6795)
MSA 6	MP	0.9579	0.9789	0.0756 (0.0619)	--	--	3.7635 (0.9389)
MSA 7	FP	0.9729	0.6870	0.0367 (-0.3758)	--	-0.0002 (0.0047)	2.8595 (0.9653)
MSA 8	IT	0.8163	-131.7007	-0.8239 (-0.3262)	--	2.5772 (0.5648)	59.6746 (0.5854)
MSA 9	MP	0.8455	18.9111	0.4666 (0.1762)	--	-0.3386 (-0.7128)	5.1998 (0.2467)

* bracketed values are the correlation coefficients

Table C-3

Model Fitting Results for Snow Tests

Model	Dependant Variable	Multiple Correlation Coefficient	Intercept	Coefficient for Independant Variables and Correlation with Dependant Variables*				
				T_s	T_w	ρ_s	W	t
MSN 1	MP	0.7902	13.5362	0.5697 (0.0593)	1.0647 (0.3515)	-19.8370 (0.0909)	6.3098 (0.6716)	0.1007 (0.3544)
MSN 2	FP	0.9657	-1.2557	0.0099 (0.4263)	0.0412 (0.2844)	2.7382 (0.3598)	2.3291 (0.9614)	-0.0031 (0.4656)
MSN 3	IT	0.8151	-19.0267	-0.0862 (-0.3271)	-0.8778 (0.0359)	43.8984 (0.4950)	5.8623 (0.7146)	-0.0934 (0.2629)
MSN 4	FP	0.9692	-0.6784	0.0129 (-0.4083)	--	1.1831 (0.2826)	2.3605 (0.9682)	--
MSN 5	IT	0.8538	-15.0647	0.0454 (-0.3468)	--	32.9266 (0.4639)	6.5118 (0.8121)	--
MSN 6	MP	0.7230	11.0237	0.4798 (0.0345)	--	-14.2122 (0.0284)	6.5445 (0.6202)	--
MSN 7	FP	0.9347	-2.8292	--	0.0107 (-0.0180)	4.8885 (0.2148)	2.5255 (0.9114)	--
MSN 8	IT	0.8609	-32.1143	--	-1.3595 (-0.3831)	72.7202 (0.4792)	6.6025 (0.5377)	--
MSN 9	MP	0.8046	10.9113	--	1.4472 (0.5220)	-33.3755 (-0.1694)	5.6820 (0.4550)	--

* bracketed values are the correlation coefficients

Table C-4

Model Fitting Results for Snow Tests with ($\rho_s T_s$) as a Variable

Model	Dependant Variable	Multiple Correlation Coefficient	Intercept	Coefficient for Independant Variables and Correlation with Dependant Variables*					
				T_s	T_w	ρ_s	W	t	$\rho_s T_s$
MSN 10	FP	0.9934	-2.9092	-0.1120 (-0.4751)	0.1173 (0.1600)	6.9381 (0.4488)	2.3378 (0.9881)	-0.0001 (0.4526)	0.3092 (-0.5773)
MSN 11	MP	0.8322	21.6845	1.1399 (0.0089)	0.2021 (0.1451)	-40.1925 (0.2503)	2.5533 (0.6620)	0.6605 (0.3834)	-2.2520 (-0.1154)
MSN 12	FP	0.9932	-2.9056	-0.1118 (-0.4634)	--	6.9295 (0.4253)	2.3375 (0.9910)	--	0.3087 (-0.5621)
MSN 13	MP	0.7818	16.8940	0.8620 (0.0295)	--	-28.5603 (0.2181)	2.8195 (0.6592)	--	-1.6856 (-0.0822)
MSN 14	FP	0.9910	-0.3473	--	--	--	2.3393 (0.9910)	--	-0.0037 (-0.5621)
MSN 15	MP	0.7466	5.0423	--	--	--	2.9653 (0.6592)	--	0.4322 (-0.0822)

* bracketed values are the correlation coefficients

Table C-5

Model Fitting Results for Snow Tests with Temperature Measurement

Model	Dependant Variable	Multiple Correlation Coefficient	Intercept	Coefficient for Independent Variables and Correlation with Dependant Variable*				
				T _S	T _W	P _S	W	IT
MTS 1	FP	0.9971	- 3.0591	0.0146 (-0.2368)	--	6.8751 (0.5062)	2.2688 (0.9955)	--
MTS 2	IT	0.9776	-36.8185	0.3668 (-0.4870)	--	63.4502 (0.4960)	4.4578 (0.9369)	--
MTS 3	FP	0.9972	- 2.8094	0.0251 (-0.1841)	0.1403 (0.5180)	6.3722 (0.6596)	2.3430 (0.9552)	--
MTS 4	IT	0.9687	-43.0501	-0.3811 (-0.4056)	-0.1338 (0.2141)	76.3543 (0.5874)	4.4639 (0.9289)	--
MTS 5	FP	0.9974	- 4.4523	0.0106 (-0.1841)	0.1352 (0.5180)	9.2860 (0.6596)	2.5134 (0.9552)	-0.0382 (0.8690)
MTS 6	MP	0.9693	98.3641	0.4091 (0.1032)	0.4591 (0.8727)	-190.9102 (0.5123)	3.7728 (0.5507)	--
MTS 7	FP	0.9955	- 0.1065	--	--	--	2.3009 (0.9955)	--
MTS 8	FP	0.9968	- 3.8956	--	--	8.2705 (0.5060)	2.2397 (0.9954)	--
MTS 9	MP	0.9285	9.0102	0.3426 (-0.1032)	0.3652 (0.8721)	--	2.4188 (0.5507)	--
MTS 10	FP	0.9984	0.2092	0.0073 (-0.6282)	0.1352 (0.7423)	--	2.1478 (0.9354)	--
MTS 11	IT	0.9869	- 1.9648	0.0560 (-0.7444)	-0.1359 (0.3085)	--	6.2907 (0.9732)	--

* Bracketed values are the correlation coefficients

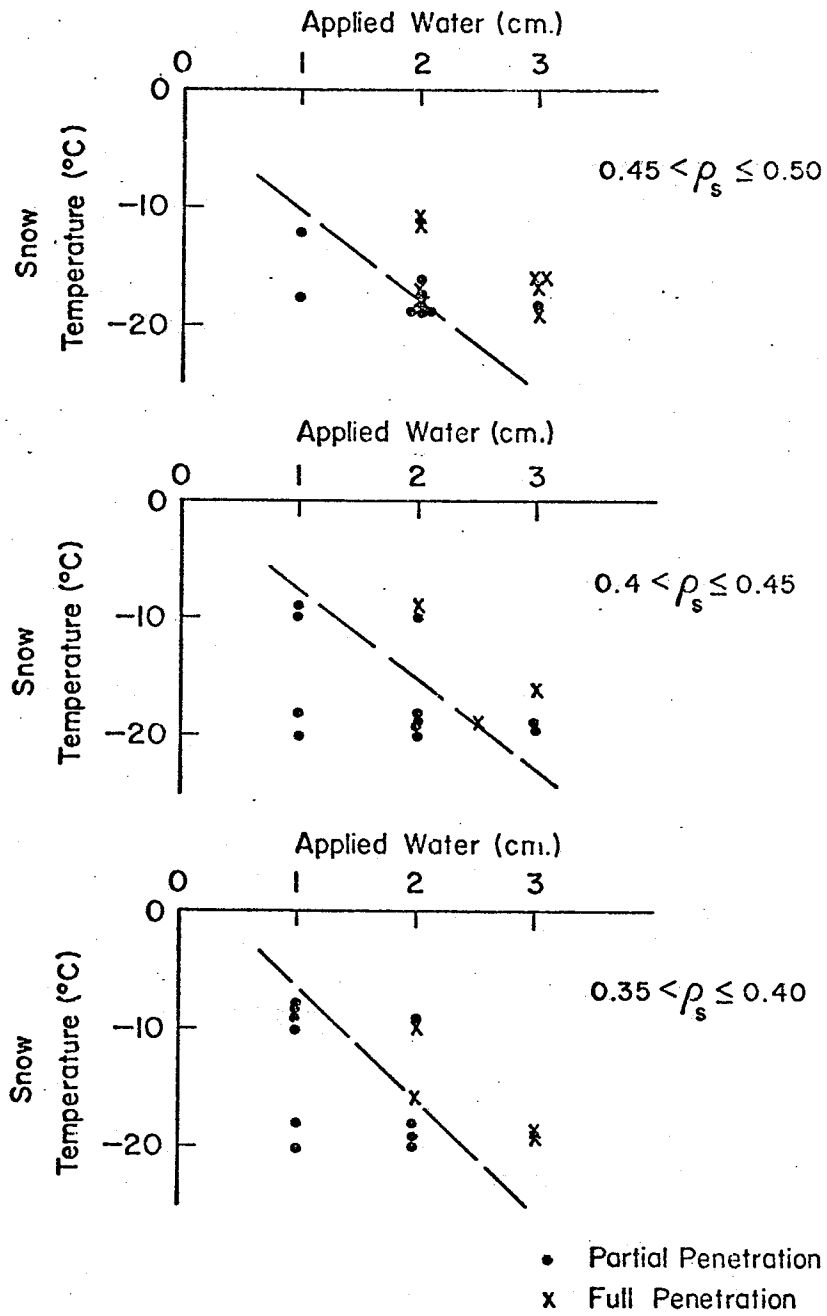


Figure C-1: Incidents of Full Penetration

APPENDIX D

FINITE-DIFFERENCE MODELS

Infiltration
Implicit Finite Difference Formulation

For one dimensional, one phase vertical infiltration

$$\frac{\partial S_w}{\partial t} = - \frac{1}{\phi \mu_w} \frac{\partial}{\partial z} [k_{rw} k_{ow} \left(\frac{\partial p_c}{\partial z} + \rho_w g \right)] \quad (D-1)$$

in terms of capillary pressure

$$\frac{\partial p'_c}{\partial t} = - \frac{1}{\phi \mu_w} \frac{\partial}{\partial z} [k_{rw} k_{ow} \left(\frac{\partial p_c}{\partial z} + \rho_w g \right)] / \frac{\partial S_w}{\partial p_c} \quad (D-2)$$

Expressing this in finite difference form, similar to the development of Giesel [21],

$$\begin{aligned} p_{c_i}^{j+1} - p_{c_i}^j &= \frac{\Delta t}{\phi \mu_w} [(k_{rw} k_{ow})_{i+1/2}^j (p_{c_{i+1}}^j - p_{c_i}^j + \Delta z \rho_w g) \\ &\quad - (k_{rw} k_{ow})_{i-1/2}^j (p_{c_i}^j - p_{c_{i-1}}^j + \Delta z \rho_w g)] / (\Delta z)^2 C_i^j \quad (D-3) \\ &= A_i^j \end{aligned}$$

where

Δt = time increment

Δz = spatial increment

i, j : refer to space and time intervals respectively

$C = S_w / p_c$

$$(k_{rw} k_{ow})_{i+1/2}^j = [(k_{rw} k_{ow})_i^j + (k_{rw} k_{ow})_{i+1}^j] / 2$$

$$(k_{rw} k_{ow})_{i-1/2}^j = [(k_{rw} k_{ow})_i^j + (k_{rw} k_{ow})_{i-1}^j] / 2$$

In Crank-Nicholson form

$$z(p_{c_i}^{j+1} - p_{c_i}^j) = A_i^j + A_i^{j+1}, \quad (D-4)$$

rearranging for Jacobi iteration

$$p_{c_i}^{j+1} = \frac{p_{c_{i-1}}^j + (A_i^j + B_i^{j+1})/2}{1 - (D_i^{j+1}/2)}, \quad (D-5)$$

where

$$B_i^{j+1} = \frac{-\Delta t}{\phi \mu_w} [(k_{rw} k_{ow})_{i+1/2}^{j+1} (p_{c_{i+1}}^{j+1} + \Delta z \rho_w g) - (k_{rw} k_{ow})_{i-1/2}^{j+1} (-p_{c_{i-1}}^{j+1} + \Delta z \rho_w g)] / (\Delta z)^2 C_i^{j+1}, \text{ and } (D-6)$$

$$D_i^{j+1} = \frac{\Delta t}{\phi \mu_w} [(k_{rw} k_{ow})_i^{j+1} / (\Delta z)^2 C_i^{j+1}]. \quad (D-7)$$

For each time step initial values of B_i^{j+1} and D_i^{j+1} are estimated from the current capillary pressures $p_{c_i}^j$ during successive iterations the new estimates of $p_{c_i}^{j+1}$ are used for B_i^{j+1} and D_i^{j+1} calculations. The iteration proceeds until the change in predicted $p_{c_i}^{j+1}$ between iterations is within a specified tolerance. The process is repeated from time step to time step. New saturations and permeabilities are calculated from a given saturation - capillary pressure curve and an estimated relative permeability - saturation relationship.

Infiltration
Explicit Finite Difference Formulation

For one dimensional, one phase vertical infiltration

$$\frac{\partial S_w}{\partial t} = - \frac{1}{\phi \mu_w} \frac{\partial}{\partial z} [k_{rw} k_{ow} \left(\frac{\partial p_c}{\partial z} + \rho_w g \right)]. \quad (D-8)$$

Darcy's law is written as

$$u_w = \frac{k_{ow} k_{rw}}{\mu_w} \left(\frac{\partial p_c}{\partial z} + \rho_w g \right). \quad (D-9)$$

Volumetric flow rate for a basic area of 1 cm^3 is then,

$$q_w = \frac{k_{ow} k_{rw}}{\mu_w} \left(\frac{\partial p_c}{\partial z} + \rho_w g \right). \quad (D-10)$$

Using an approach similar to Phuc [43] flow into, q_i , and out of,

q_o , a finite-difference interval will be defined as

$$q_i = \frac{(k_{ow} k_{rw})_i}{\mu_w} \left[\frac{p_{c_i}^j - p_{c_{i-1}}^j}{\Delta z} + \rho_w g \right], \text{ and} \quad (D-11)$$

$$q_o = \frac{(k_{ow} k_{rw})_i}{\mu_w} \left[\frac{p_{c_{i+1}}^j - p_{c_i}^j}{\Delta z} + \rho_w g \right]. \quad (D-12)$$

Equation (D-8) can now be expressed as

$$\frac{S_w_i^{j+1} - S_w_i^j}{\Delta t} = \frac{1}{\phi \Delta z} (q_i - q_o) \quad (D-13)$$

Rearranging, the explicit finite-difference form for infiltration is

$$S_w_i^{j+1} = S_w_i^j + \frac{\Delta t}{\phi \Delta z} (q_i - q_o). \quad (D-14)$$

New relative permeabilities and capillary pressures will be calculated from the new saturation.

The explicit scheme is stable for $\frac{\Delta t}{(\Delta z)^2} \leq 1/2$

Heat TransferFinite Difference FormulationConduction

One dimensional, transient heat conduction without sources or sinks is defined by

$$\frac{\partial}{\partial x} \left[\alpha \frac{\partial T}{\partial x} \right] = \frac{\partial T}{\partial t} \quad , \quad (D-15)$$

where

T = temperature, °C

t = time, sec

x = spatial coordinate, cm

$\alpha = k/\rho C_p$: thermal diffusivity, cm^2/sec

k = thermal conductivity, $\text{cal}/\text{cm}\cdot\text{sec}\cdot^\circ\text{C}$

$\rho = \text{density}$, g/cm^3

$C_p = \text{specific heat}$ (at constant pressure), $\text{cal}/\text{g}\cdot^\circ\text{C}$.

The finite-difference form of $\frac{\partial T}{\partial t}$ is

$$\frac{\Delta T}{\Delta t} = \frac{T_i^{j+1} - T_i^j}{\Delta t} \quad (D-16)$$

and of $\frac{\partial^2 T}{\partial x^2}$ is

$$\frac{\Delta^2 T}{(\Delta x)^2} = \frac{1}{\Delta x} \left(\frac{T_{i-1}^j - T_i^j}{\Delta x} - \frac{T_i^j - T_{i+1}^j}{\Delta x} \right) \quad (D-17)$$

where

$\Delta x, \Delta t$: spatial and time increments in finite-difference model

i, j : refer to space and time intervals respectively .

Similar to Trupp (53), reorganization into explicit form yields a form suitable for a non-homogeneous, non-isotropic system

$$T_i^{j+1} = F_{i-1,i} T_{i-1} + F_{i,i} T_i + F_{i+1,i} T_{i+1} \quad (D-18)$$

where

$$F_{m,n} = \frac{K_{m,n} \Delta t}{CO_{m,m}}$$

$$K_{m,n} = \frac{K_{m,n} A}{(\Delta x)_{m,n}}$$

$$CO_{m,m} = \frac{A(\Delta x)_{m,m}}{\rho C_p}$$

$(\Delta x)_{m,m}$ = size of interval m

$(\Delta x)_{m,n}$ = distance between nodes m and n

A = cross sectional area

$k_{m,n}$ = lumped thermal conductivity between nodes m and n

The explicit form is convergent for

$$\Delta t \leq \frac{CO_{m,m}}{m+1} \sum_{n=m-1} K_{m,n} \quad (D-19)$$

for the smallest $\frac{CO_{m,m}}{m+1} \sum_{n=m-1} K_{m,n}$ in the finite-difference model.

Excess degree method

The method of "excess degrees" used successfully by Trupp (53) is used here to model the phase change effects in the snow water system. A node which has liquid water present is held at 0°C until sufficient heat has been transferred out of the interval to account for the latent heat of freezing. This technique is particularly simple to incorporate with the afore-mentioned finite difference scheme. During the freezing process, the values of T_i^{j+1} , for the node in consideration, are accumulated until their sum equals the excess degrees required for freezing,

ED_f

$$ED_{\underline{f}} = \frac{L_f S_w \phi V}{C_{Pav}} \quad (^\circ\text{C}) \quad (\text{D-20})$$

where

L_f = latent heat of freezing 79.7, cal/g

S_w = water saturation, dimensionless

ϕ = porosity, dimensionless

V = volume of grid interval, cm^3

C_{Pav} = average heat capacity of grid interval, $\text{cal/g-}^\circ\text{C}$.

Until $ED_{\underline{f}}$ degrees have been accumulated, the T_i^j for the node undergoing freezing is kept constant at 0°C . After the node is totally frozen, the procedure continues allowing the temperature to vary as determined by the finite difference approximation.

APPENDIX E

INFILTRATION SIMULATION

Table E-1

Summary of Infiltration Simulation

Simulation	Snow Porosity	Permeability ($\text{cm}^2 \times 10^6$)	Water (cm^3/cm^2)	Application Time (sec)	Exponent for Relative Permeability	Upper Boundary Condition
CA 1	0.45	3.0	2	1	3.0	Saturated
CA 2	0.45	3.0	2	1	3.0	Saturated
CB 1	0.49	3.0	1	1	3.0	Ponded
CB 2	0.49	3.0	1	1	3.0	Saturated
CB 3	0.56	8.6	1	1	3.0	Ponded
CB 4	0.56	8.6	1	1	3.0	Saturated
CP 1	0.56	8.6	1	1	3.0	Ponded
CP 2	0.50	3.3	1	1	3.0	Ponded
CP 3	0.45	1.5	1	1	3.0	Ponded
CP 4	0.49	3.0	2	2	3.0	Saturated
CP 5	0.56	8.6	2	2	3.0	Saturated
CN 1	0.49	2.8	1	1	4.0	Ponded
CN 2	0.49	2.8	1	1	3.0	Ponded
CN 3	0.49	2.8	1	1	2.5	Ponded

Table E-2

Simulation of Infiltration with Phase Change

Simulation	Snow Porosity		Permeability		Saturation at Freezing	Infiltration Time (sec)
	Initial	Final	Initial ($\text{cm}^2 \times 10^6$)	Final ($\text{cm}^2 \times 10^6$)		
CF 1	0.49	-	2.8	-	-	2.85
CF 2	0.49	0.43	2.8	1.0	0.9	4.25
CF 3	0.56	-	8.6	-	-	1.1
CF 4	0.56	0.51	8.6	3.85	0.9	1.5
CF 5	0.49	0.43	2.8	1.0	0.75	4.75
CF 6	0.49	0.43	2.8	1.0	0.5	5.85
CF 7	0.49	0.43	2.8	1.0	0.1	6.1

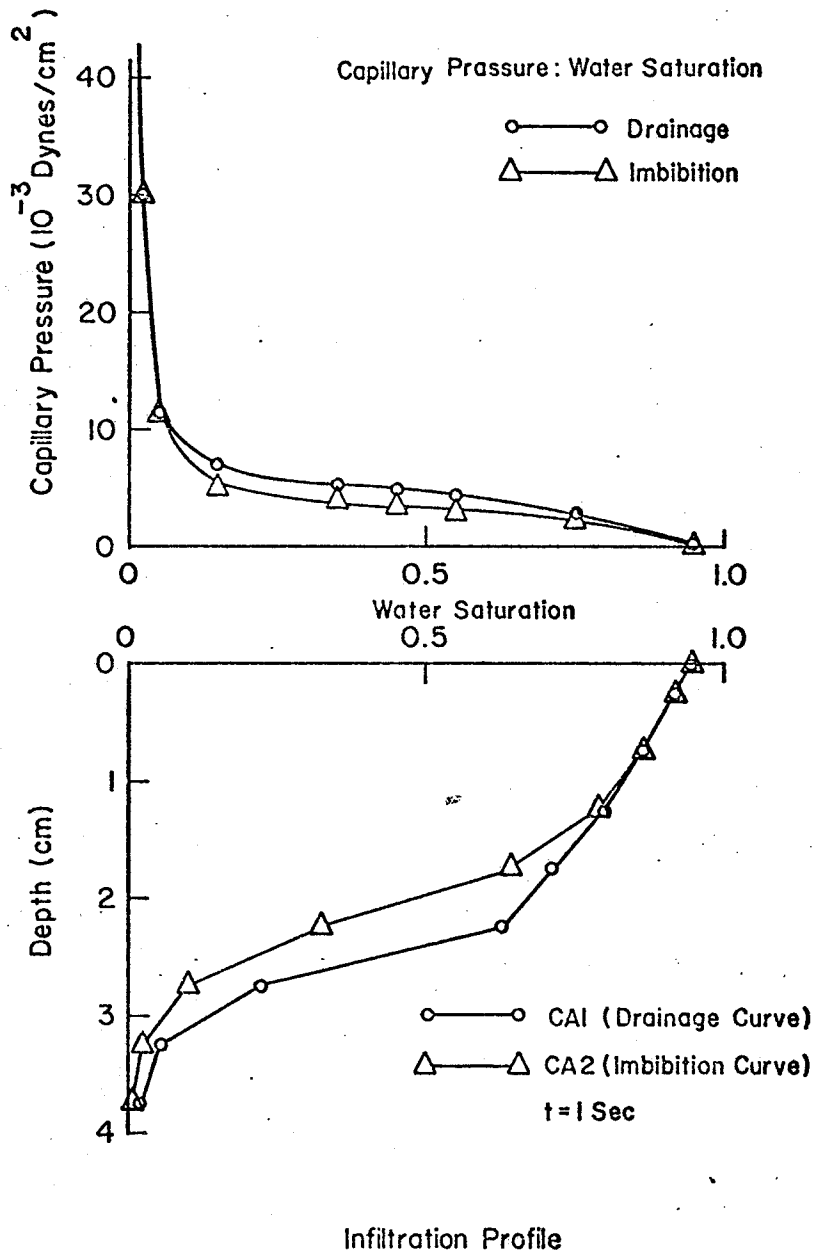


Figure E-1: Infiltration with Drainage and Imbibition Capillary Pressure Curves

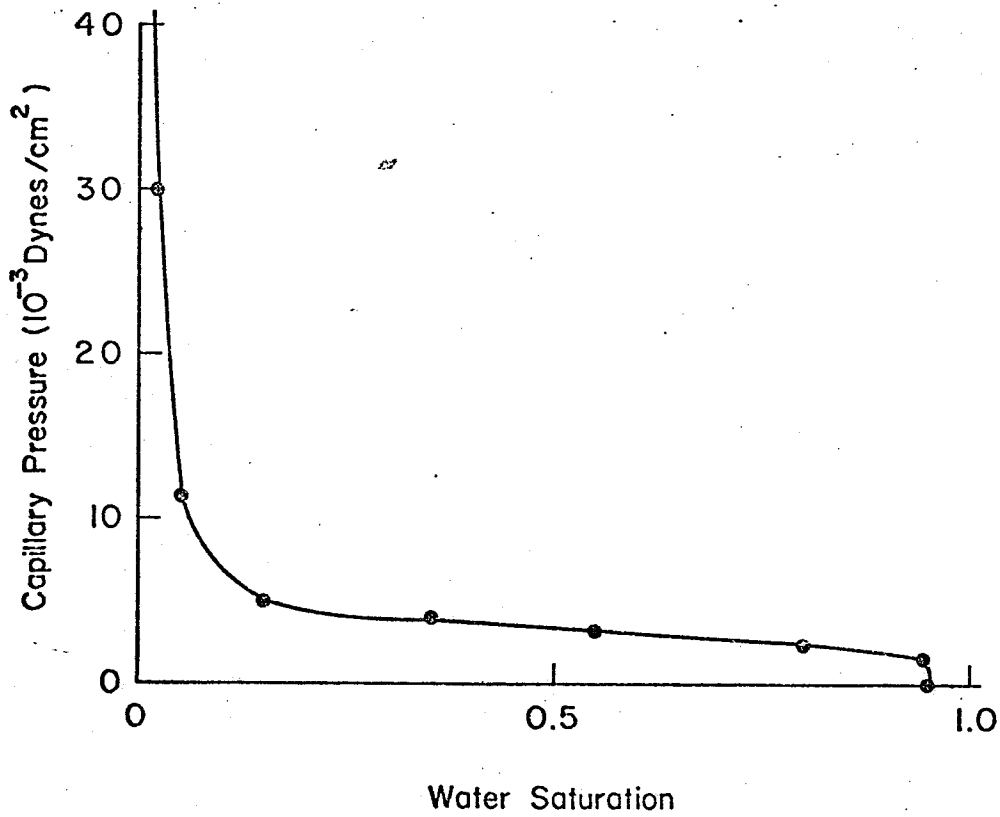


Figure E-2: Capillary Pressure - Water Saturation Curve

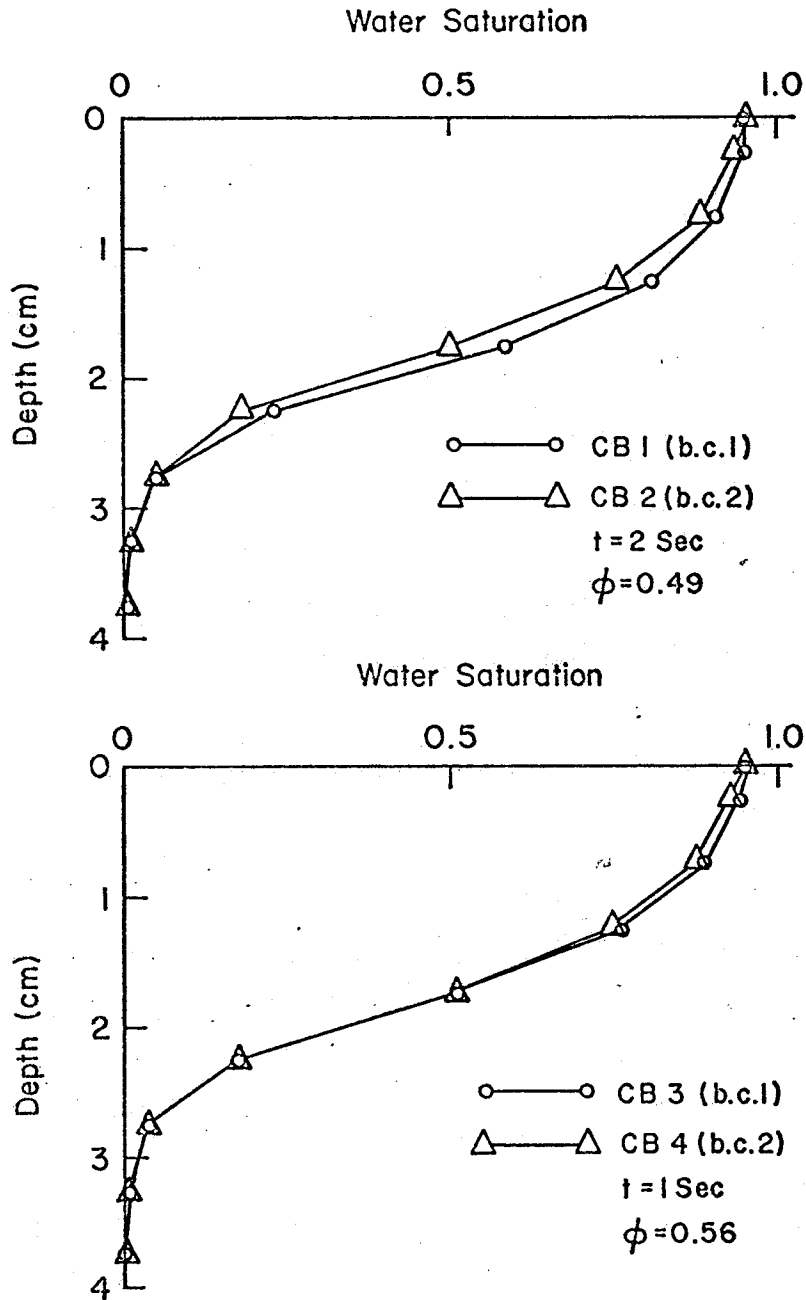


Figure E-3: Water Saturation Profiles

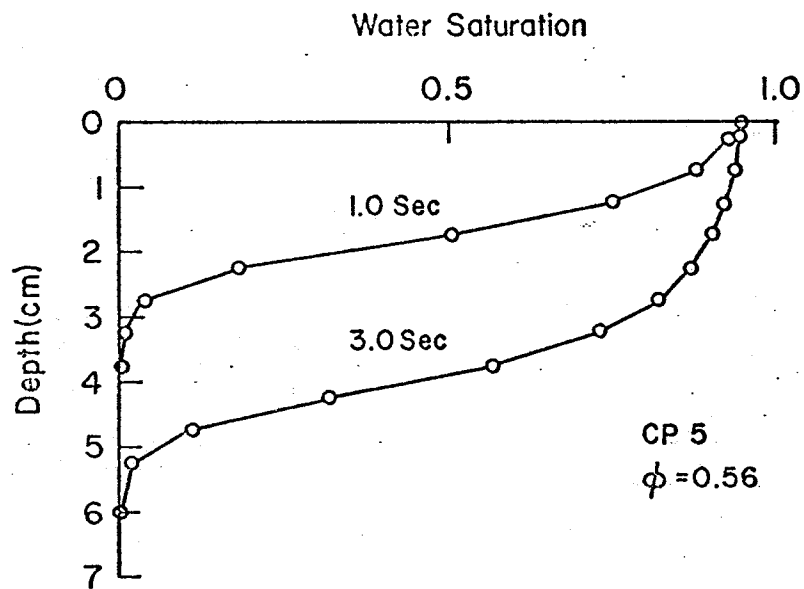
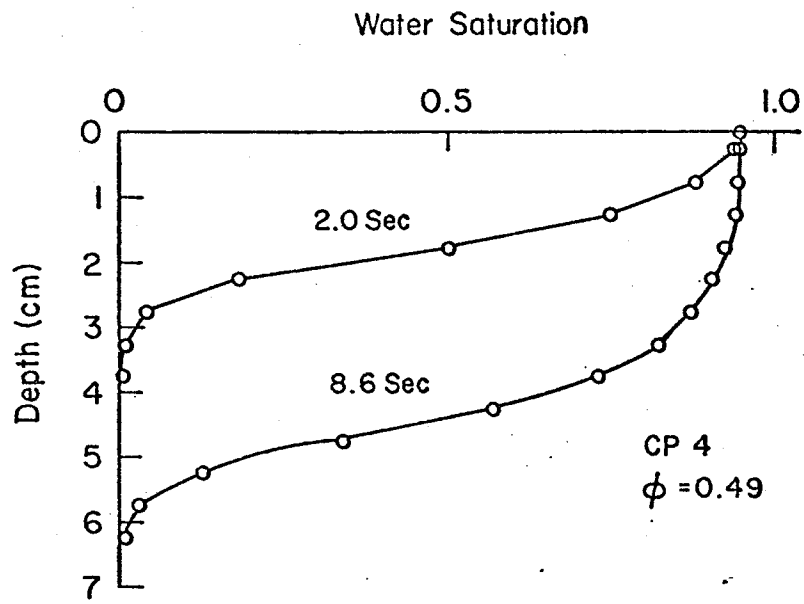


Figure E-4: Water Saturation Profiles

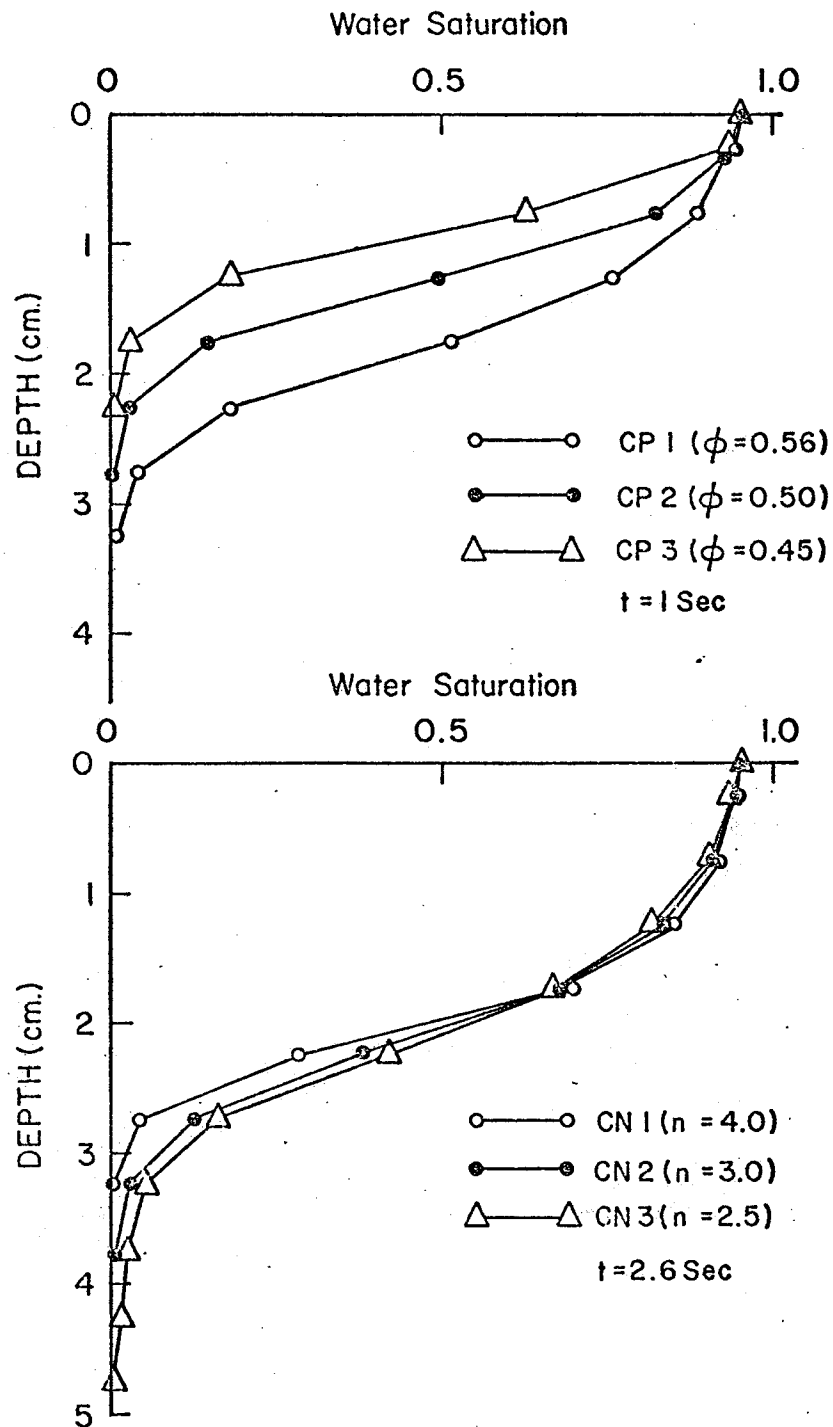


Figure E-5: Water Saturation Profiles

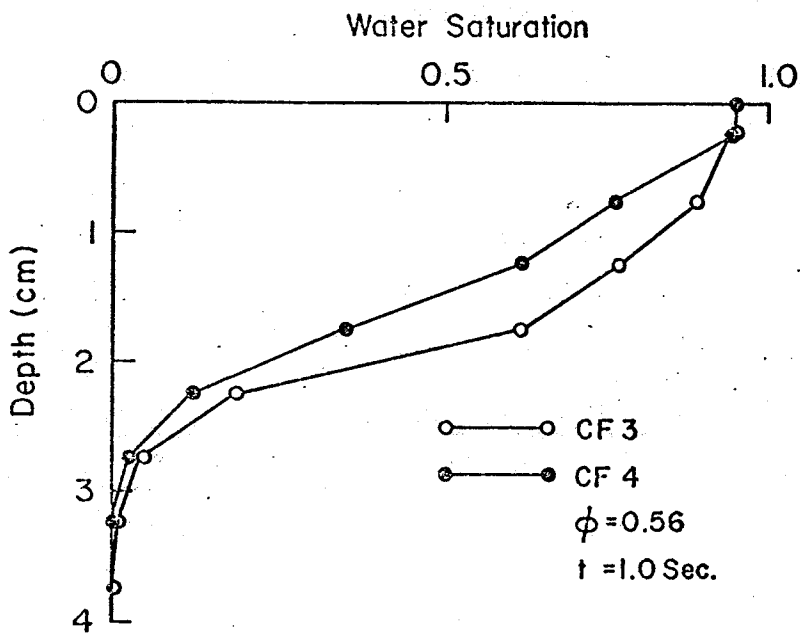
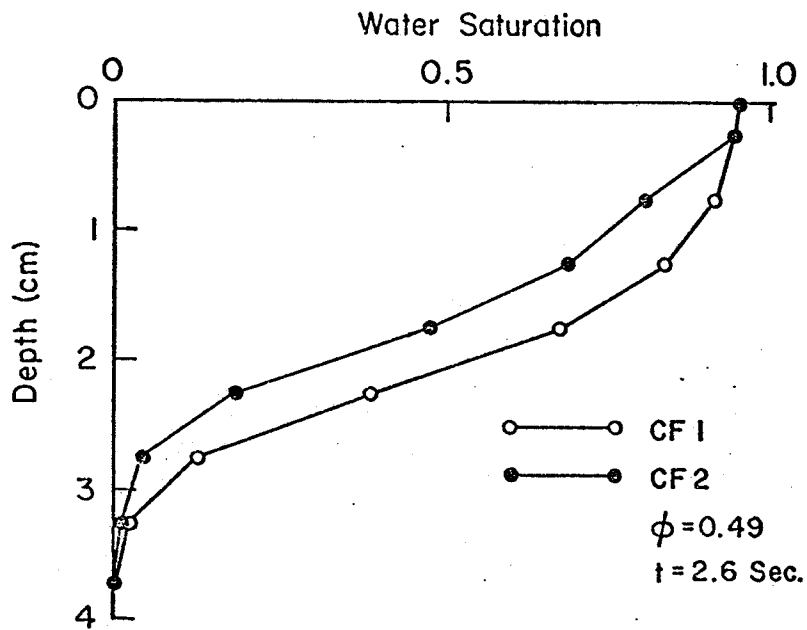


Figure E-6: Water Saturation Profiles

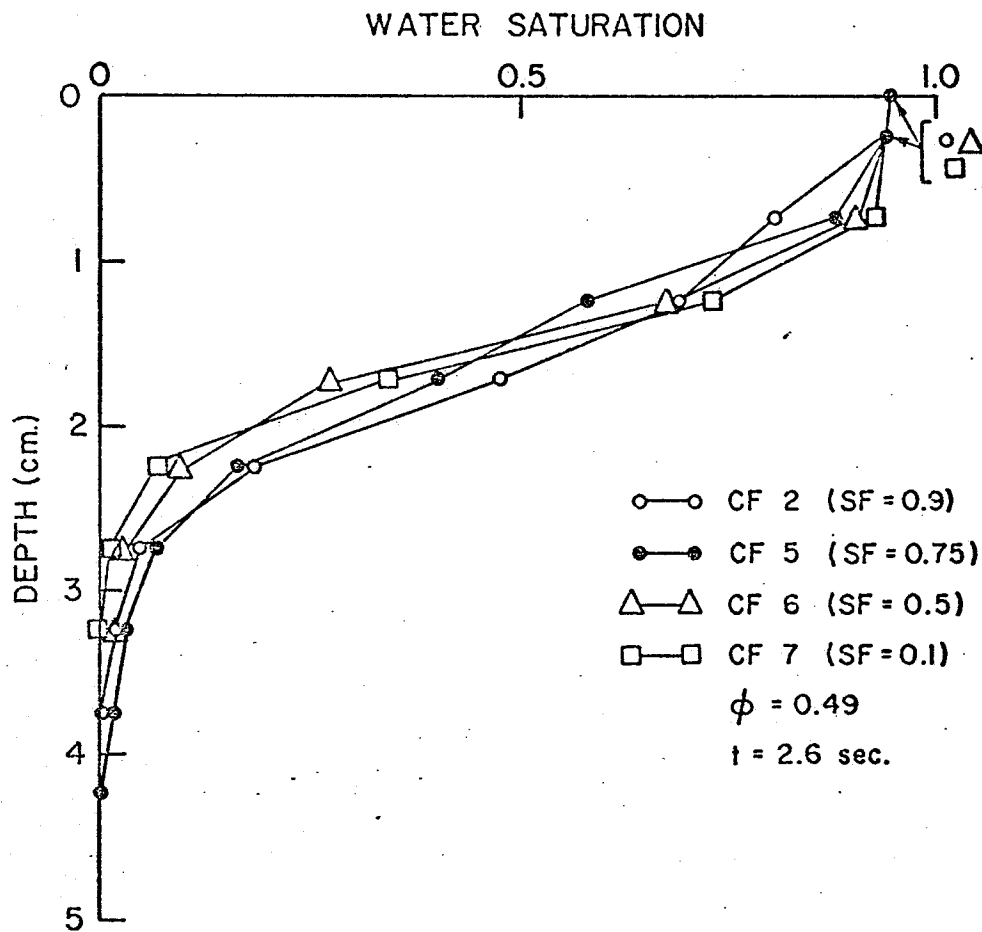


Figure E-7: Water Saturation Profiles

APPENDIX F

ICE-CAP RE-FREEZING

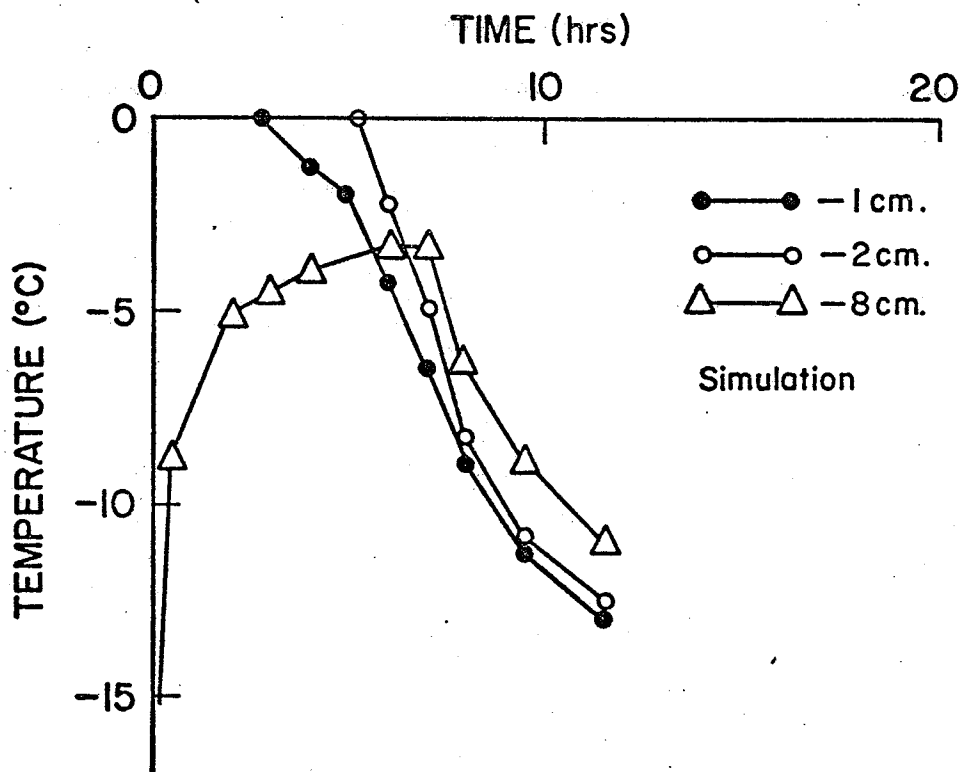
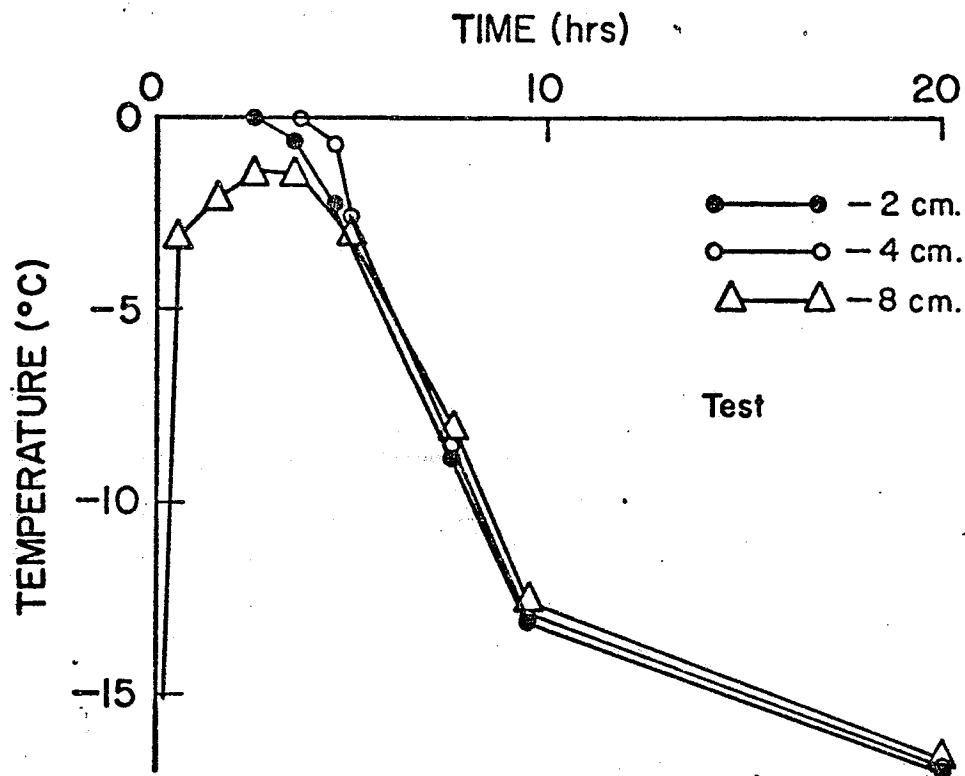


Figure F-1: Re-Freezing Temperatures: Test and Simulation

TABLE F-1

RE-FREEZING SIMULATION TESTS

Simulation	Ambient and Snow Temperature (°C)	Bottom Boundary Temperature (°C)	Water (cm ³ /cm ²)	Penetration (cm)	Time for Re-freezing of Ice-cap Zone (hrs)
RF 1	-18.	-18.	2	4.5	6.35
RF 2	-18.	-18.	3	6.5	8.7
RF 3	-10.	-10.	2	4.5	8.2
RF 4	-10.	-10.	3	6.5	11.95
RF 5	-18.	-10.	2	4.5	6.65